Gas Sensing Properties and Mechanism of WO_3-Based Nanoparticles Sensors for Inflammable Gases

花, 中秋

https://doi.org/10.15017/1470617

出版情報：九州大学, 2014, 博士（工学）, 課程博士
バージョン：
権利関係：全文ファイル公表済

Gas Sensing Properties and Mechanism of WO_3-Based Nanoparticles Sensors for Inflammable Gases

Zhongqiu Hua

Department of Molecular and Material Sciences

Interdisciplinary Graduate School of Engineering Sciences

Kyushu University

July, 2014

CONTENTS

Abstract of the Dissertation

Metal oxide semiconductor (MOS) gas sensors that detect inflammable and toxic gases through changes in the resistance of sensing elements and paly a very important role in a variety of applications. Tungsten trioxide (WO_3) is one of the most investigated materials for MOS gas sensors. Despite for the numerous investigations, the basic sensing mechanism of WO_3 is far from being well understood, especially the sensing of inflammable and reducing gases, for which demonstrate a different sensing process with the conventional MOS gas sensors. On the other hand, investigations on the sensing process of typical inflammable gases (H_2, CO and CH_4) allow us an indirect approach to study the surface oxygen activity and reaction properties with gas molecular. This is beneficial for a better understanding of the surface process of WO_3 during gas sensing. The present dissertation is focused on the basic sensing properties of inflammable gases and their interaction routines with surface adsorbed oxygen and lattice oxygen. In addition, the effect and mechanism of additive Pd on the sensing process are studied.

The WO_3 sensors were prepared from a kind of lamellar-structured nanoparticles by using screen-printing method. The microstructure of neat and Pd-loaded WO_3 nanoparticles and sensor devices have been studied. The resistive response of typical inflammable gases (H_2, CO and CH_4) was investigated. The effects of Pd-loading and humidity on the sensing properties were also discussed. Oxygen adsorption and interaction with WO_3 were studied based on the resistive response under different atmospheres and TPD measurements. The activity of surface lattice oxygen was evaluated through the resistive response and TPR tests

of inflammable gases in the absence of oxygen.

It was found that the resistive response with a designed background allowed us a simple way to investigate the sensing process and mechanism. The oxygen adsorption and interaction with neat WO_3 was really weak, resulting in a small response to inflammable gases. However, Pd-loading enhanced the electronic interaction of oxygen with WO_3 and activated the reaction of surface lattice oxygen. Therefore, Pd-loading not only promoted the sensing response but also changed the basic sensing mechanism of WO_3 sensors.

List of Symbols and Abbreviations

ω: Depletion width

d: Grain size

q: Elementary charge of electron

V_S: The height of the potential barrier

E_C: Conduction band

E_V: Valence band

E_F: Fermi level

E_s: The acceptor states

n_s: Free carrier density

N_d: The donor density

k: Boltzmann constant

T: Temperature

L_D: Debye length

R_g: Sensor resistance in different gaseous ambient

R_0: Sensor resistance in flat band condition

R_{N2}: Sensor resistance in pure N_2

P: Partial pressure or concentration of gas

N_t: Surface charged density

R_{dry}: Sensor resistance in dry condition

R_{wet}: Sensor resistance in wet condition

K_{O2}: Oxygen adsorption constant

CHAPTER 1

1 Introduction

1.1 Metal Oxide Semiconductor Gas Sensors

Gas sensors are developed for the detection of combustible, flammable and toxic gases. They play an important part of many different types of applications such as on oil rigs, manufacture processes, emerging technologies and firefighting [1-4]. Among them, one of the kind's sensors based on metal oxide semiconductor (MOS) known as chemo-resistive gas sensors plays a great role and has been applied for many purposes [3-6]. MOS gas sensors have the property to change the conductivity of sensing material in the presence of reducing and oxidizing gases. The development of MOS gas sensors started from the work of Brattain and Bardeen in the late 1940s [3, 7], who clarified that the resistance of semiconductors was very sensitive to adsorption from the gaseous ambient surrounding it [7-8]. Following up these works, Seiyama et al., demonstrated that the conductivity of thin films of Zinc oxide (ZnO) was very sensitive to the presence of traces of reactive gases in 1962 [5] and similar properties were also observed for Tin dioxide (SnO_2) by Taguchi in 1962 [3, 9]. MOS gas sensors based on SnO_2 was firstly commercialized by Taguchi (Taguchi-type sensors) who established the FIGARO Eng. Company [3, 9]. Nowadays, FIGRAO is still one of the leading companies in MOS gas sensors [3]. Over the past few decades, SnO_2 gas sensors have become predominant in the field of gas alarms used on domestic, commercial and industrial premises [2, 6, 7, 9-10]. Along SnO_2, however, several metal oxides such as Tungsten trioxide

(WO_3), Titanium oxide (TiO_2) and titanium-substituted chromium oxide (CTO) are potential materials for the application of semiconducting gas sensors [11-12]. Table 1 lists the most studied metal oxides as semiconducting gas sensors and their target gases [11]. It is noteworthy that WO_3 is one of the most investigated materials for MOS gas sensors and one of the few materials has been used in commercial devices [13]. It has a good performance in the detection of NO_X [14-15], NH_3 [14], O_3 [16] and H_2S [14].

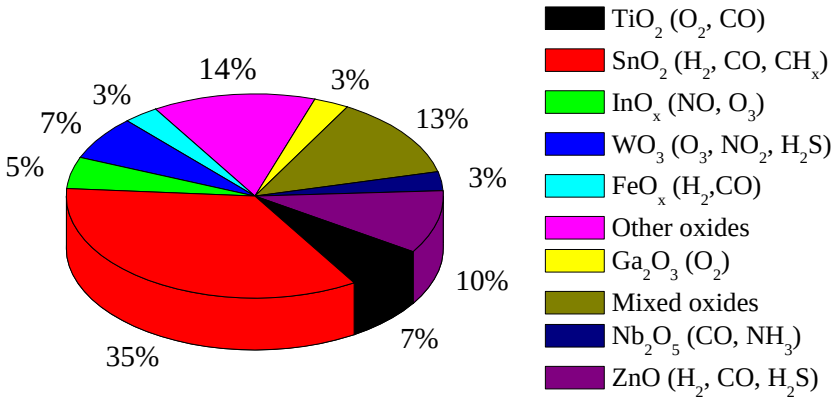

Figure 1-1 a pie chart of relative comparison of metal oxides used for gas sensing applications and their typical detect gases [11].

However, it is unfortunately found that MOS gas sensors always suffer problems of poor selectivity and stability [17-20]. The sensor resistance is sensitive to many gases and the resistance is often not reversible or reproducible when the gaseous ambient is restored to its initial condition [17]. Therefore, numerous efforts have been undertaken to overcome these drawbacks. To enhance the selectivity, various techniques, e.g.: modification of sensing working temperatures, development new sensing material and sensor structures and the application sensor arrays. Nevertheless, the most frequent and simple way to promote the performance is usage of different metallic additives [17, 21-25]. Commonly, noble metals, such as Au [17, 23], Pd [17, 22, 24-25] and Pt [17, 23]

are the most used and effective additives for MOS sensors. Noble additives can modify the gas interaction process with sensors (Receptor function), the conduction process (Transducer function) and the gas diffusion process (Utility factor) [25]. Theoretical investigations on the basic sensing mechanism of MOS are one of the most interesting topics in surface science and semiconductor physics. Nevertheless, a clear understanding of sensing mechanism is really helpful to design high performance MOS gas sensors.

1.2 Basic Sensing Mechanism

Generally, the working principle of MOS sensors can be described as a charge transfer process, which triggers a relative change in the sensor resistance, i.e., sensor signal. This process can be understood from the two basic functions of MOS gas sensors as illustrated in Figure 1-2.

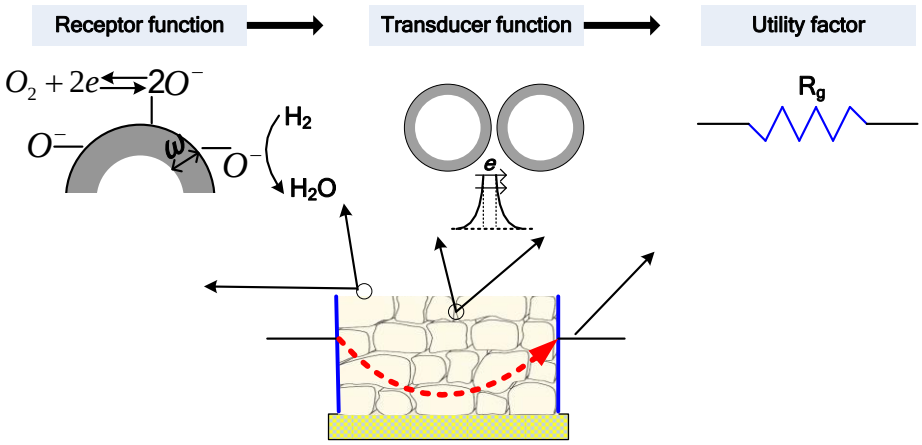

Figure 1-2 schematic representation of the receptor and transducer function of an n-type MOS gas sensor.

Firstly, gas adsorption or reactions on the surface induce a change in the electron trap states [3-4, 7-9]. Then the variation in the trap states leads to a change in the conductivity through the transducer function of sensors. Thus, studies on sensing mechanism of sensors mainly deal with these two aspects, namely, basic

conduction process of oxides and gas adsorption and reaction on the oxide surfaces [3, 9, 26].

1.2.1 Physical conduction process

For a long time, it has been recognized that the transducer function of metal oxide sensors is size and shape dependent [15, 26-27]. A Schottky potential barrier across the contact of metal oxide grain fully control the transducer function of sensors, when the depletion width (ω) is far less than the grain size (d) [28-29]. However, with decreasing the crystal size, the transducer function is changed to a volume depletion model and the sensors become more sensitive [27-29]. When the metal oxide grain is far larger than the depletion layer near the surface, the surface Schottky barrier across each grain boundary dominate the conduction process and the transducer function as schematically illustrated by Fig. 1-3 [4, 6]. The chemisorbed oxygens (O^-) built up the surface potential barriers. In the presence of reactive gases such H_2 and CO, adsorbed oxygen reacts with gas molecules. Consequently, the concentration of O^- is decreased, leading to a reduction in the potential barrier and the sensor resistance. On the contrary, contacting with NO_2 and O_3 introduce new acceptors states and increase the height of potential barrier. As a result, the sensor resistance is increased.

Generally, the electron conduction governed by the Schottky barrier can be described [4, 7, 28]:

$$n_s = N_d \exp(-\frac{qV_s}{kT}) \quad \textbf{(1.1)}$$

Here n_s free carrier density N_d the donor density, V_S the height of the potential barrier and q elementary charge of electron. T and k are the Boltzmann constant and temperature, respectively. The resistance of sensing body, R_g, can be

considered to be inversely proportional to n_s, and represented as:

$$R_g = R_0 \exp(\frac{qV_s}{kT}) \quad \textbf{(1.2)}$$

R_0 is the sensor resistance free of gas interaction (constant) and can be considered as sensors resistance in N_2 (R_{N2}). The Schottky barrier control sensing mechanism is always characterized by power law relationship of sensor resistance with gas concentrations [30], as demonstrated by (3).

$$R_g = cP^n \textbf{or} \ln R_g = c_0 + n \ln P \quad \textbf{(1.3)}$$

Where a, n, c and c_o are constants, and n is the so called power-law exponent. P is the gas partial pressure or concentration.

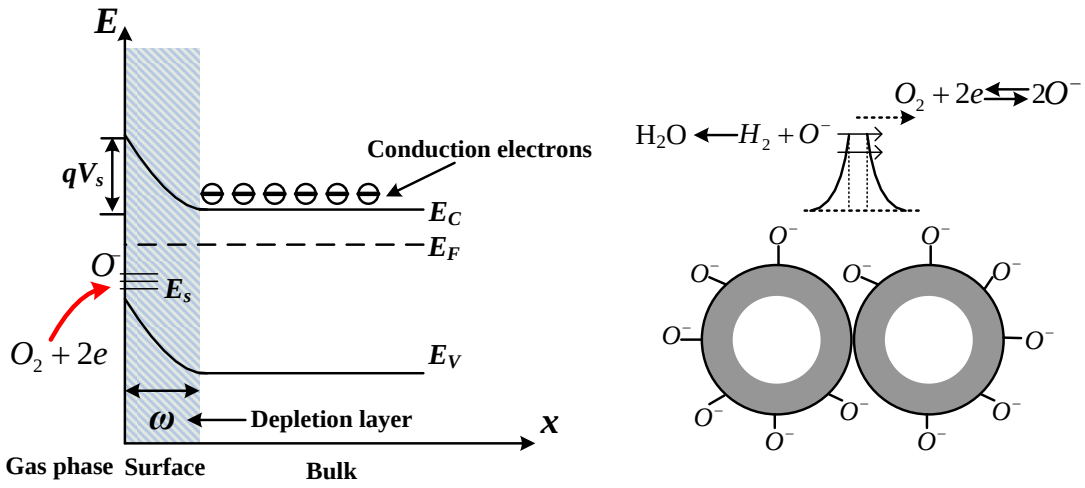

Figure 1-3 (a) Schottky barrier across the grain boundaries for the conduction process, (b) Surface band bending for the *n*-type metal oxide semiconductor. E_C and E_V conduction band and valence band of grain bulk, respectively. E_F Fermi level, E_s the acceptor states formed by the depletive adsorption.

When the size of the metal oxide grains or crystals becomes smaller and comparable with the double of the depletion width (2ω), the sensing properties are known as size and shape dependent [15, 28-29]. Then, the basic sensing mechanism is changed from a Schottky barrier model into a volume depletion model. In the present case, we consider a thin plate semiconductor with a

thickness of 2*a*. For simplicity, oxygen is assumed as the only surface charged species with a density of N_t raised by increasing P_{O2}. Figure 1-4 shows the profiles of the band bending and depletion width with various P_{O2} for a plate nanocrystal. As P_{O2} increasing, surface potential barrier is formed with a depletion width ω(I). Further increasing P_{O2} to P_{O2}(II), the band bending and depletion width are enhanced as shown in the figure. In the state (II), the depletion layer is equal (2ω=2*a*). In other words, the whole crystal is full depleted and there is no place for further depletion. Then the band is bended to state (II). With further increasing P_{O2}, the depletion is fulfilled by a shift down of Fermi level (*pkT*) according to the volume depletion model. However, the profiles of the band bending and depletion width should be kept same state as P_{O2}(II) [28-29]. Therefore, it is obvious that the electron conduction for nanocrystal semiconductor sensors is significantly different from that of large crystals.

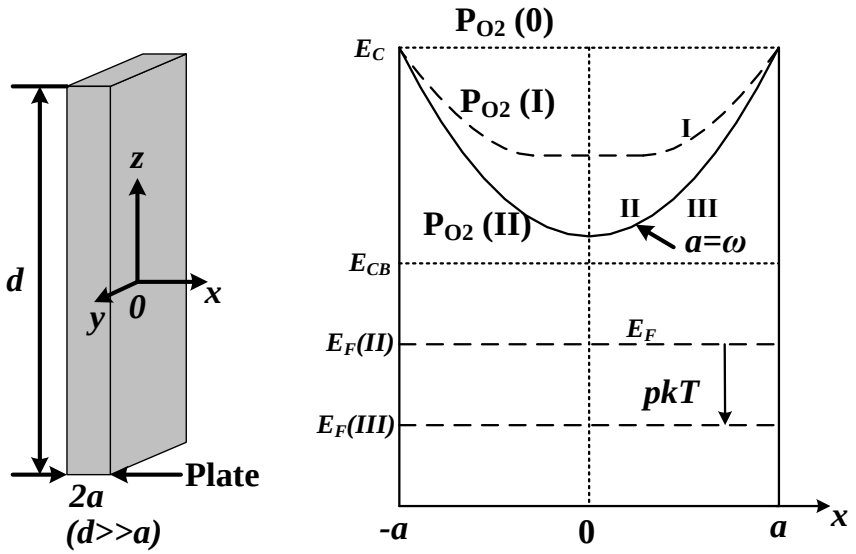

Figure 1-4 plate shape of crystal with lateral size (d) far larger than thickness and the profile of the band bending with P_{O2}.

The electron conduction process in volume depletion model can be

approximately described by the following equations

$$n_s = N_d \exp[-(\frac{n^2}{2} + p)] \quad \textbf{(1.4)}$$

Here, $n=a/L_D$. The sensor resistance is, therefore, can be expressed as:

$$R_g = R_0 N_d \exp(\frac{n^2}{2} + p) \quad \textbf{(1.5)}$$

It is found from (1.5) and (1.6) that the conduction process in volume depletion model is size and shape dependent. Derivation from the above equations, the sensor resistance in volume depletion is linearly depended on P^{α}.

$$\frac{R_g}{R_0} = \frac{1}{a}(k_0 P_{O2}) + 1 \quad \textbf{(1.6) } (\mathbf{O_2^-})$$

$$\frac{R_g}{R_0} = \frac{1}{a}(k_0 P_{O2})^{1/2} + 1 \quad \textbf{(1.7) } (\mathbf{O^-})$$

$$\frac{R_g}{R_0} = \frac{1}{a}(k_0 P_{O2})^{1/4} + 1 \quad \textbf{(1.8) } (\mathbf{O^{2-}})$$

Where the power factor α is strictly equal to 1, 1/2 and 1/4 according to the charged state of adsorbed oxygen (O_2^-, O^- and O^{2-}). For the first time, it was realized that the basic sensing properties of nanosized semiconductor gas sensors can be interpreted by the volume depletion theory.

1.2.2 Gas interaction with sensors

For the receptor function (gas adsorption and reaction), it is really complex and one of the most interesting subjects for surface science. Gas interaction and reaction on the surface of metal oxides is the basic content of sensing mechanism, which trigger the charge transfer process responsible for sensing response. Oxygen chemically adsorbed on the surface plays a basic role in the gas interaction and reaction with reactive gases in air ambient and is responsible for the receptor function of sensors [1, 3, 4, 9]. Therefore, investigations on oxygen

adsorption are one of the effective approaches to clarify the sensing mechanism. One of our tasks of the present study is to reveal the oxygen adsorption and interaction on the surface of WO_3. For a long time, chemical adsorption of oxygen known as ionsorption with a charge transfer from conduction band in the form of superoxide ions (O_2^-), charged atomic oxygen (O^-) and peroxide ions (O^{2-}), respectively [4, 6, 8, 31]. Generally, in the temperature of sensors operation (ca. 200 ºC or above), O^- is believed to be predominated on the surface [31]. It is suggested that oxygen vacancies (V_O) on the surface are the active sites for the chemical adsorption of oxygen [31-35]. Figure 1-5 shows a schematic model for oxygen adsorption on SnO_2 (110) surface with oxygen vacancy sites.

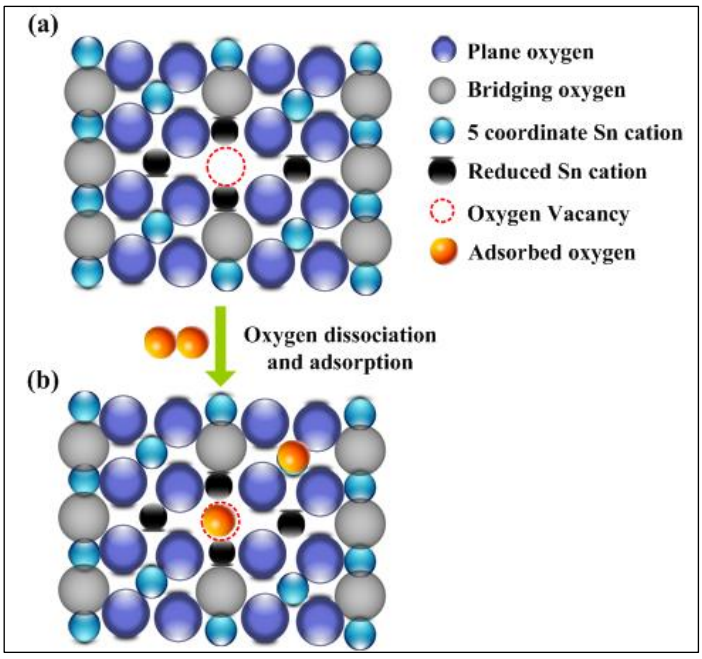

Figure 1-5 schematic model illustrating the dissociation and adsorption process of oxygen on SnO_2 (110) surface.

Oxygen molecules dissociate at an oxygen vacancy site and fill the vacancy sites. And then, the other oxygen atom is singly coordinated to an uncoordinated metal atom [32-33].

As shown in Fig. 1-2, adsorbed oxygens on the surface acting as receptor, react with inflammable gases such as H_2, CO and CH_4 resulting in a reduction in surface potential barrier and a relative change in sensor resistance, i.e., sensor signal. Equation R1 describes the above process

$$A + O^- \xrightarrow{k_1} AO + e \quad \textbf{(R1)}$$

Here, k_1 and k_{-1} are forward and reverse reaction constant, respectively and *A* reducing gas. However, it should be noted that reducing gases could also directly react with surface of metal oxides, such as adsorption and surface redox process [36-40]. Recent studies demonstrated that CO could react with lattice oxygens of sensor surface [36-37]. With an extremely low oxygen ambient or absent of oxygen, Hübner, *et. al.*, found that the sensor resistance of SnO_2 decreased by the presence of CO with the formation of CO_2, however, resistive response was not reversible [37]. Therefore, it is naturally proposed that the surface of SnO_2 could be directly reduced by CO with the additive of Pt [38]. Similar results were also observed for neat WO_3 [36-37]. It was observed that WO_3 surface exhibited a redox reaction in the background with very low oxygen concentration [37]. The resistive response through the direction interaction of reducing gases with metal oxide surface can be expressed by:

$$A + O_L^{2-} + M^{n+} \longrightarrow AO + M^{(n-1)+} + V_O^{\bullet} + e \quad \textbf{(R2)}$$

$$\frac{1}{2}O_2 + M^{(n-1)+} + V_O^{\bullet} + e \longrightarrow O_L^{2-} + M^{n+} \quad \textbf{(R3)}$$

Where *M* stands for the metals listed in Fig. 1-1, O_L is the lattice oxygen on the surface of metal oxides.

Another reaction routine of reactive gases with sensor surface is a direct adsorption behavior. It was observed that with a poor oxygen background, CO

and H_2 could adsorb on the surface of SnO_2 injecting electrons into conduction band [37, 39]. Consequently, a revisable response was observed [39]. Reaction 4 illustrates the adsorption of CO on SnO_2 surface [37, 39]. Where S_D denotes the adsorption site on the surface, such as a single coordinated oxygen anion [39].

$$CO_g + S_D \rightarrow CO_D \rightarrow CO_D^+ + e \quad \textbf{(R4)}$$

Computational results show that H_2 can also chemically adsorb on the fivefold coordinated W atoms on the surface with a charge transfer process [2]. Therefore, it can be concluded that the interaction and reaction of reducing gases with sensor surfaces have three different routines.

Gas sensors operated in the aerial atmosphere are inevitably suffered from problems caused by the presence of humidity [9, 41-44]. Water vapor has a strong effect on the base resistance of sensor; therefore, it hinders the application of MOS sensor as measuring devices such as monitors [43-44]. The resistive response is significantly influenced by the humidity. It is because that the gas interaction and reaction is considerably different from that in a dry condition [41-44]. Thus, clarification of water interaction with metal oxide surface is a very important task. Yamazoe, *et. al.*, reported that water dissociatively adsorbed on the surface of SnO_2 can significantly inhibit O^{2-}, which is really active for gas reaction [43-44]. It was also found that a long term effect of humidity increases the sites for oxygen adsorption [44]. Other researches argued that water chemically adsorbed on the surface acts as donors resulting in a reduction of sensor resistance [41]. Water dissociatively adsorbed on the surface of metal oxides such as SnO_2 and TiO_2 with a similar way to oxygen molecules [45-51]. Figure 1-6 illustrates water dissociation on the (110) surface of TiO_2 and SnO_2.

Oxygen vacancies on the surface are shown to dissociate H_2O molecules. One proton is transferred to the nearby oxygen atom forming hydroxyl group and the rest OH fill the vacancy sites [45-49]. As a result, every oxygen vacancy can form two hydroxyl groups [45-50]. The built up OH groups not only interact with oxygen but also reactive gases [50-51]. Therefore, the sensing process is considerably changed by the presence of water vapor [41-44]. One of tasks of present study is investigation on the humidity effect on the sensing properties of WO_3 gas sensors.

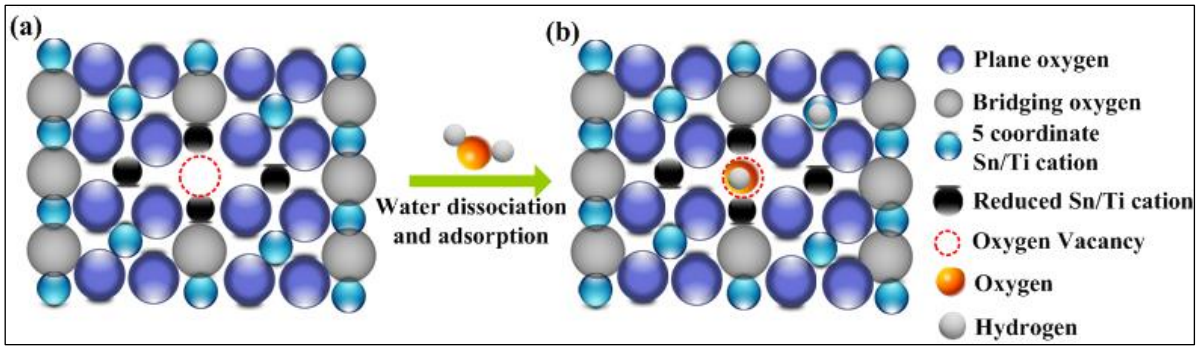

Figure 1-6 water molecules dissociation at oxygen vacancy sites of SnO_2 and TiO_2 surface with formation two OH groups.

Lastly, it should be noted that additives such as Au, Pd and Pt can also significant modify the gas interaction and reaction process [1, 17, 22-25, 52-54]. Au is known for the spill-over effect as schematically illustrated in Fig. 1-7 (a). The spill effect can enhance the adsorption of oxygen and promote the oxidization of reducing gases with chemically adsorbed oxygen [17, 22-25]. The role of Pd is always explained by the Fermi-level control model as shown Fig. 1-7 (b). Pd is convinced appeared as oxidization states and the chemical stoichiometry are sensitive to reducing gases. The change in the oxidation states of Pd is reversible, therefore, it can be considered as additional electron trap states on the surface [53], enhancing the sensing response to reducing gases.

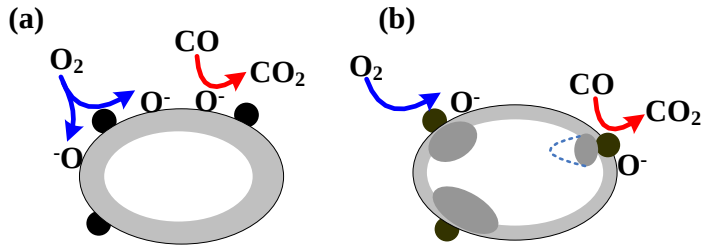

Figure 1-7 mechanism of noble metal additives (a) spill-over, (b) Fermi-level control.

However, recent studies based on the operando spectroscopies have revealed that the chemical state of Pd and Pt on the surface of sensors has no change upon reducing gases [22-25]. Therefore, it is proposed that the dispersed Pd and Pt form clusters with the scale of atom and bond with the metal oxide surface resulting in the shallow surface reconstructions [22-25]. This creates new sites for the adsorption of oxygen and promotes the sensing response.

1.3 Characteristics of WO_3

1.3.1 Bulk properties

WO_3 is one of the most important transition metal oxides and finds a wide variety of applications in catalysis, electrochromic displays and gas sensing [55-57]. It is known that the phase structure and structural distortions of WO_3 are quite complex [14, 58-59]. Full stoichiometric WO_3 adopts a structure derivated from a cubic ReO_3 structure, and can be approximated as a cubic array of corner-shared WO_6 octahedra as shown in Figure 1-8 [58-59]. Various phase structure and structural distortions can be considered from the tilting of the WO_6 octahedra and or the shift of tungsten ions from the centers of the octahedra. These phase structures are temperature-dependent [58-59]. Up to around 1170 K, it experienced at least 5 transitions [60]. From room temperature to 630 K (MOS sensors operating region), monoclinic γ -WO_3 (Lattice constants a=0.7297 nm,

b=0.7539 nm, *c*=0.7688 nm and *β*=90.91) is favored and stable one [36, 61-62]. It is reported that the catalytic and gas sensing properties are phase structure dependent [63]. For example, the oxidized monoclinic WO_3 is more active in photocatalytic behavior than the hexagonal one [64]. However, in the sensing of NO_X and isoprene gases, the hexagonal phase is more sensitive than the monoclinic structure [64]. Normally, in the range of temperature of gas sensor operation (the transition temperature from monoclinic to orthorhombic around 330 ºC), WO_3 has two different crystalline structures [63-64].

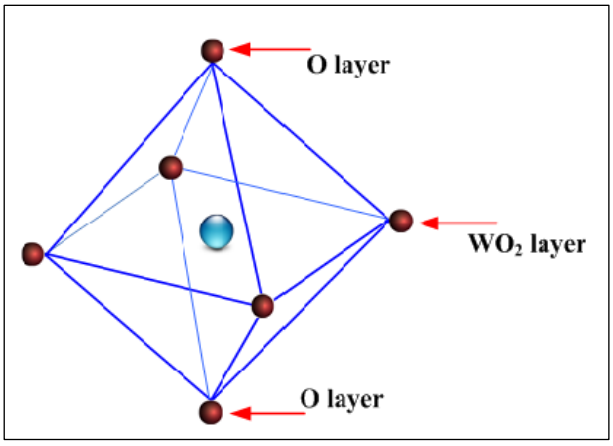

Figure 1-8 WO_6 octahedron of monoclinic WO_3 shown as corner-sharing octahedra.

Stoichiometric monoclinic WO_3 is an insulator at room temperature [64]. However, WO_3 is readily to loss oxygen to form WO_{3-x}. With oxygen deficiency, it is an *n*-type semiconductor with a band-gap of 2.62 or 2.7 eV [64]. Oxygen vacancies are the predominant defect and greatly alter the bulk electronic transport properties by introducing donor states into the bulk band gap [64]. With a strong reduction condition ($x>10^{-4}$), point defects are eliminated by the formation of crystallographic shear (CS) planes along (1*m*0) directions [61-62]. This is realized by changing the corner-shared WO_6 into the edge sharing (WO_4) [59-61].

1.3.2 Surface structure

Fundamental understanding of gas sensing is closely related to the surface structures of WO_3. It is significantly different from SnO_2 that the surface of WO_3 is really active for various catalytic processes; however, SnO_2 surface is chemically inert [61-68]. It is catalytically active for hydrocarbon cracking reactions, hydrotreating reaction, alcohol dehydrogenation, alkane hydrogenation and metathesis [64-67]. WO_3 is potential for acid-catalyzed reactions such as hydroisomerization [64]. In addition, WO_3 can also be used to selectively catalytic reduce NO released from power plants by NH_3 [65-67]. It is well accepted that these catalytic processes are related to the surface active sites, the coordinatively unsaturated sites (cus), i.e., the fivefold W and the single coordinated oxygen anions and surface oxygen vacancies [61, 68-69]. It has been recognized for a long time that oxygen vacancy is the predominant defect on the surface of WO_3 [36-37, 70]. The surface oxygen is readily to loss upon reduction conditions [36-37, 61, 71]. It has been recognized that the oxygen vacancy formation enthalpy decreases and becomes exothermic under poor oxygen containing condition [36]. In other words, thermodynamically, the surface will be reduced spontaneously [36, 61, 70-71]. In addition, surface reduction progress can be significantly changed by different pretreatments such as ion bombardment and electron irradiation [61, 70-71].

The catalytic activity of WO_3 is known as structure-sensitive, because the oxidation state of metal cus (unsaturated sites) and the concentration of terminal oxygen depends on the structure [61, 63, 69]. In addition, Surface reduction also affects the structure and morphology of WO_3 surfaces by eliminating terminal

oxygen, migrating reduced species into the bulk and forming CS planes [61, 63]. It has been reported that monoclinic WO_3 (001) surface has the lowest energy and demonstrates a number of reconstructions depending on treatment conditions [61-63]. The c (2×2) surface as pictured in Figure 1-9 with half of the terminal oxygens are eliminated to produce a stable, charge-neutral surface. Formally, the oxygen atoms cover every other W cation. However, the surface is considered as fully oxidization and all the W ions are in +6 oxidation state [61-63]. With further reduction, WO_3 is susceptible to oxygen loss and forms a serious of reduced surfaces reconstructions such as p (2×1) and (1×1). There is no terminal oxygens left for (1×1) surface, and all W is reduced to 5+ states [60-64]. Figure 1-7 schematically illustrates the reconstructed surface for (001) surface.

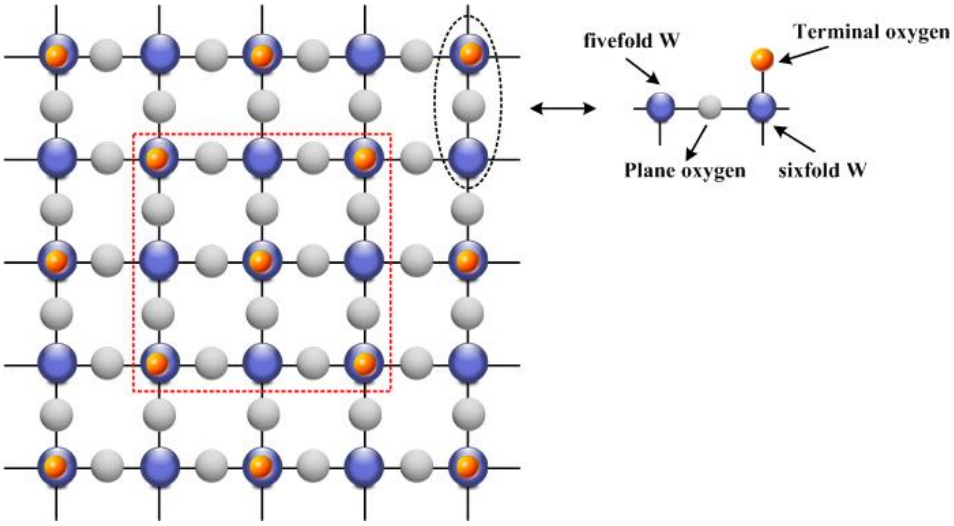

Figure 1-9 model for the c(2×2) reconstruction of WO_3 (001) surface. The blue ball indicates five and six coordinated Tungsten cations (W_{5c}, W_{6c}). The gray ball denotes the in plane oxygens and yellow one is the singly coordinated terminal oxygen.

1.4 WO_3 as Gas Sensors

WO_3 is one of the most studied materials for metal oxide semiconductor gas sensors and it is one of the few materials has been successfully commercialized [13-16, 18, 64]. WO_3 as MOS gas sensor attracted much attention since 1991 or

earlier because of its good performance in NO_2 detection [15]. Even today, most of works about WO_3 still focus on the sensing properties of NO_2. Akiyama, et. al, reported WO_3 fabricated from pyrolyzing ammonium paratungstate at high temperature as NO_x gas sensor in 1991 [13]. Although, the detection ability is very poor from today's opinion, this attempt opens up a new field for the application of WO_3 and developments of MOS gas sensor. Three years later in the same group, WO_3 nanoparticles sensors were prepared and demonstrated a sensing response of 80 to 10 ppm NO_2. This was a great improvement for the detection of NO_2. A prototype NO_2 gas sensor based on WO_3 prepared by pyrolyzing ammonium paratungstate was introduced by Figaro Engineering Inc. in 1995 [13]. Later, sub-ppm sensitivity of WO_3 to NO_2 was reported by X. Wang, *et. al*, in 1997 [72]. Following this work, sensors based on a kind of lamellar-structured WO_3 nanoparticle was prepared in this group [73]. Then sensing response down to 100 ppb of NO_2 was obtained and reported [73]. More recently, a sufficiently high sensitivity to NO_2 at dozens of ppb level was obtained by WO_3 nanoparticles synthesized from an acidification method [74-75]. Therefore, the sensing ability of WO_3 to NO_2 was gradually promoted from dozens of ppm to dozens of ppb during the past 20 years. In addition, WO_3 particularly exhibits a sensitive response to ozone even in the range of ppb, which is possible for atmospheric monitoring [76-77]. The development of WO_3 as O_3 sensor started more than one decade ago [76]. The field measurement shows that ozone instrument based on WO_3 sensors have a lot of potential as a cost-effective alternative to conventional ozone measuring instruments [77]. WO_3 is also very sensitive for H_2S and has been used for commercial H_2S gas sensor

more than 20 years ago [14]. Besides, WO_3 shows a high sensitivity to NH_3 in the level of ppb, which is important for environmental monitoring and health industry (breath marker) [78]. More recently, it is demonstrated that WO_3 has a great potential for commercialized volatile organic compounds (VOCs) gas sensors [79-81]. This is practically useful for noninvasive detection of illnesses through the breath analysis [80] and indoor air quality monitoring [79].

Similarly, to promote the sensing performance, different additives, especially the noble metals (Au, Pd and Pt) have been widely used for WO_3 sensors [54, 79, 81-83]. It was found that Au was quite effective to improve the response of WO_3 to NH_3 and H_2S [78, 84]. Pd and Pt are very useful to improve the sensing response to reducing gases such as H_2, CO [80-81]. Additionally, Pt and Pd are very important for VOCs gas sensing [79, 83]. It is found that Pd and Pt greatly promote the sensitivity of WO_3 to Toluene, ethlybenzene, ethanol and Formaldehyde [79, 83]. They acting as catalysts on sensor surface not only promote the response but also greatly improve the responding and recovery properties [79]. Modifications on the materials morphology such as particle sizes and phase structures can also significantly enhance the sensing performance.

However, WO_3 is always studied as oxidizing gases sensors, which is significantly different from conventional SnO_2 [22, 37-42, 82]. It is reported that WO_3 is not suitable for the detection of typical reducing and inflammable gases such H_2, CO and CH_4 [85]. It is because that the sensing signals considerably drift with time and suffer from a strong effect of humidity [85]. Although, WO_3 has been applied for MOS gas sensors for a long time, nevertheless; the basic sensing mechanism is still far from being well understood [36-37, 82]. This is

obviously an obstacle for the practical application. There are some significant differences in the detection of reducing gases (H_2 and CO) between WO_3 and SnO_2. For the later, the oxidization of reducing gases with surface oxygens are recognized as the sensing mechanism as shown in Fig. 1-3. However, the interactions of reducing gas with the surface of WO_3 are quite complex and the reaction routine depends on the gas atmosphere and material preparations [36-37, 82]. Therefore, the development of WO_3 will be promoted with our continuous efforts on the basic sensing mechanism. In other hand, clarification on the sensing process of WO_3 is obviously beneficial for the deep understanding of MOS gas sensors and its development.

1.5 Motivation and Objectives

Of present knowledge, WO_3 is a promising material for the semiconductor gas sensors. Apparently, the development of WO_3 sensors strongly relies on our understanding about the basic sensing mechanism. Unfortunately, not too much is known about the basic sensing process of WO_3, especially for the inflammable gases such as H_2, CO and hydrocarbons. In addition, the extremely complex surface structure and chemistry of WO_3 make the sensing process difficult to be clarified. To reveal the sensing mechanism, oxygen adsorption behavior on the surface and the way of its reaction with gases and sensor surface should be revealed. The role of Pd additive in the interaction of oxygen and inflammable gases with WO_3 surface is another important aspect concerning the sensing mechanism. For practical applications, the effect of humidity on sensing properties should be investigated and understood. The aim of the present dissertation is to obtain additional insights into the sensing mechanism of WO_3.

The obtained knowledge will be beneficial for the design of semiconductor gas sensors with high performances.

The overall objective of present study will focus on the following 4 aspects:

- The first objective is to investigate the microstructural properties of neat and Pd-loaded WO_3 nanoparticles. Investigations on microstructure and loading state of Pd are beneficial for the better understanding of sensing mechanism.
- The second task is to study the basic sensing behavior of typical inflammable gases for neat and Pd-loaded WO_3 gas sensors. The gas sensing properties are characterized under dry and wet conditions and compared between neat and Pd-loaded WO_3 sensors.
- The third objective is to evaluate the oxygen adsorption behavior and its role in the sensing process of inflammable gases. Oxygen adsorption and interaction with the sensor surface is mainly studied based on the resistive response of oxygen with different background.
- The last objective is to explain the basic sensing process of inflammable gases and the role of Pd-loading. The illustrations of basic sensing process are based on the resistive response of oxygen and TPR measurements with different designed atmospheres.

Finally, based on the above results, a model to illustrate the basic surface process of gas sensing with the presence of Pd additive and humidity will be presented.

1.6 Organization of Dissertation

To the greatest extent possible each chapter of this dissertation is autonomous, dealing with a specific aspect, experimental or theoretical, of

semiconductor gas sensors with WO_3. Figure 1-10 shows the organization of the dissertation.

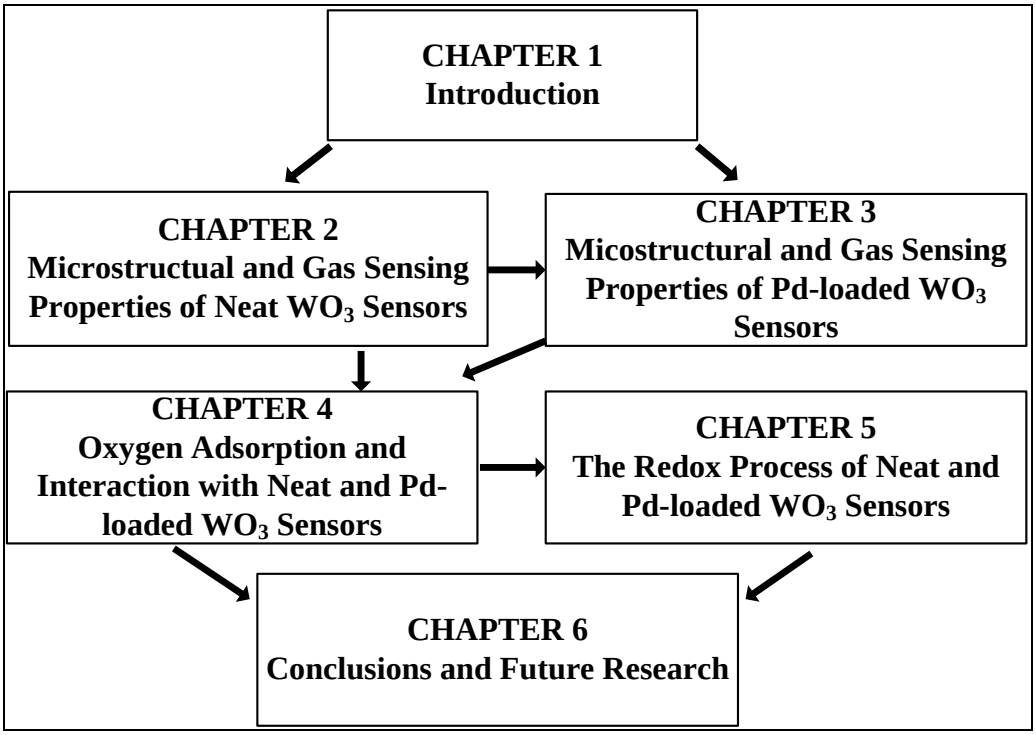

Figure 1-10 outline of thesis.

Chapter 1 composes the background of the present study. The general introductions on the sensing mechanism of metal oxide semiconductor gas sensors are given through two aspects, namely the physical conduction mechanism and gas interaction and reaction process. The basic characteristics of WO_3, especially the surface properties are presented. Finally, the motivation and objectives of the dissertation are introduced.

Chapter 2 and 3 describe the preparations of neat WO_3 nanoparticles from acidification and the procedures of Pd-loading on the surface of WO_3 nanoparticles. The sensor devices and gas sensing setup are introduced. The microstructural properties of neat and Pd-loaded WO_3 nanoparticles with lamellar-structured morphology are analyzed based on electron microscopy. The

sensing properties of typical inflammable gases namely, H_2, CO and CH_4 are investigated for neat and Pd-loaded WO_3 gas sensors under both dry and humid conditions at 350 ºC. The effects of humidity and Pd-loading on the sensing performance are investigated.

Chapter 4 reports the oxygen adsorption properties of neat and Pd-loaded WO_3 gas sensors. Oxygen adsorption is evaluated mainly through the resistive response coupled with the temperature programmed desorption (TPD) measurements. The oxygen resistive response with the presence of inflammable gases is investigated with different partial pressure of oxygen and humidity.

Chapter 5 presents the results temperature programmed reduction (TPR) and gas sensing properties in the absence of oxygen. The surface reducibility interaction of inflammable gases with the surface of WO_3 is analyzed by the TPR measurements. The resistive response of neat and Pd-loaded WO_3 sensors to inflammable gases is characterized in the background in the absence of oxygen.

Chapter 6 summarizes the experimental works related to chapter 2, 3, 4 and 5 to develop a general model of oxygen adsorption and surface process for inflammable gases. Interpretations of the role of Pd and the humidity effect are based on the proposed model. Last part concludes the dissertation with recommendations for future work.

References

[1] N. Yamazoe, Toward innovations of gas sensor technology, Sensors and Actuators B: Chemical 108 (2005): 2-14.

[2] D. Kohl, Function and applications of gas sensors, Journal of Physics D: Applied Physics 34 (2001): R125.

[3] P. K. Clifford, Mechanisms of gas detection by metal oxide surfaces, Diss. Carnegie Mellon University, 1981.

[4] N. Barsan, D. Koziej, and U. Weimar, Metal oxide-based gas sensor research: How to?, Sensors and Actuators B: Chemical 121 (2007): 18-35.

[5] T. Seiyama, A. Kato, K. Fujiishi, M. Nagatani, A New Detector for Gaseous Components Using Semiconductive Thin Films, Analytical Chemistry 34 (1962): 1502-1503.

[6] W. Göpel, S. D. Klaus, SnO_2 sensors: current status and future prospects. Sensors and Actuators B: Chemical 26 (1995): 1-12.

[7] S. R. Morrison, Semiconductor gas sensors, Sensors and Actuators 2 (1982): 329-341.

[8] H. Geistlinger, Electron theory of thin-film gas sensors, Sensors and Actuators B: Chemical 17 (1993): 47-60.

[9] D. E. Williams, Semiconducting oxides as gas-sensitive resistors, Sensors and Actuators B: Chemical 57.1 (1999): 1-16.

[10] C. Pijolat, B. Rivière, M. Kamionka, J.P. Viricelle, P. Breuil, Tin dioxide gas sensor as a tool for atmospheric pollution monitoring: problems and possibilities for improvements, Journal of materials science 38 (2003): 4333-4346.

[11] G. Eranna, B. C. Joshi, D. P. Runthala, R. P. Gupta, Oxide materials for development of integrated gas sensors—a comprehensive review, Critical Reviews in Solid State and Materials Sciences 29 (2004): 111-188.

[12] H. Meixner, U. Lampe, Metal oxide sensors, Sensors and Actuators B: Chemical 33 (1996): 198-202.

[13] T. Inoue, K. Ohtsuka, Y. Yoshida, Y. Matsuura, Y. Kajiyama, Metal oxide semiconductor NO_2 sensor. Sensors and Actuators B: Chemical, 25(1995): 388-391.

[14] I. Jiménez, J. Arbiol, G. Dezanneau, A. Cornet, J.R. Morante, Crystalline structure, defects and gas sensor response to NO_2 and H_2S of tungsten trioxide nanopowders, Sensors and Actuators B: Chemical 93 (2003): 475-485.

[15] J. Tamaki, Z. Zhang, K. Fujimori, M. Akiyama, T. Harada, N. Miura, N. Yamazoe, Grain-size effects in tungsten oxide‐based sensor for nitrogen oxides." Journal of the Electrochemical Society 141 (1994): 2207-2210.

[16] S. R. Utembe, G. M. Hansford, M.G. Sanderson, R. A. Freshwater, K. F. E. Pratt, D. E. Williams, R. L. Jones, An ozone monitoring instrument based on the tungsten trioxide WO_3 semiconductor. Sensors and Actuators B: Chemical, 114(1) (2006): 507-512.

[17] S. R. Morrison. Selectivity in semiconductor gas sensors, Sensors and Actuators, 12(4) (1987): 425-440.

[18] P. Varsani, A. Afonja, D. E. Williams, I. P. Parkin, R. Binions, Zeolite-modified WO_3 gas sensors–Enhanced detection of NO_2, Sensors and Actuators B: Chemical, 160 (2011): 475-482.

[19] D. P. Mann, T. Paraskeva, K. F. E. Pratt, I. P. Parkin, D. E. Williams, Metal oxide semiconductor gas sensors utilizing a Cr-zeolite catalytic layer for improved selectivity. Measurement Science and Technology, 16 (2005): 1193-1200.

[20] M. Ivanovskaya, A. Gurlo, P. Bogdanov, Mechanism of O_3 and NO_2 detection and selectivity of In_2O_3 sensors, Sensors and Actuators B: Chemical 77 (2001): 264-267.

[21] Yamazoe, N, Y. Kurokawa, T. Seiyama. Effects of additives on semiconductor gas sensors, Sensors and Actuators 4 (1983): 283-289.

[22] M. Hübner, N. Barsan, U. Weimar, Influences of Al, Pd and Pt additives on the conduction mechanism as well as the surface and bulk properties of SnO_2 based polycrystalline thick film gas sensors, Sensors and Actuators B: Chemical, 171-172 (2012): 172-180.

[23] M. Hübner, D. Koziej, J. D. Grunwaldt, U. Weimar, N. Barsan, An Au clusters related spill-over sensitization mechanism in SnO_2-based gas sensors identified by operando HERFD-XAS, work function changes, DC resistance and catalytic conversion studies, Phys. Chem. Chem. Phys., 14-38 (2012): 13249-54.

[24] D. Koziej, M. Hübner, N. Barsan, U. Weimar, M. Sikora, J.D. Grunwaldt, Operando X-ray absorption spectroscopy studies on Pd-SnO_2 based sensors, Phys. Chem. Chem. Phys., 11-38 (2009): 8620–8625.

[25] S. Matsushima, T. Maekawa, J. Tamaki, N. Miura, N. Yamazoe, New methods for supporting palladium on a tin oxide gas sensor, Sensors Actuators B: Chemical 9 (1992), 71-78.

[26] N. Yamazoe, K. Shimanoe, New perspectives of gas sensor technology, Sensors and Actuators B: Chemical 138 (2009): 100-107.

[27] C. Xu, J. Tamaki, N. Miura, N. Yamazoe, Grain size effects on gas sensitivity of porous SnO_2-based elements, Sens. Actuators B: Chem., 3 (1991): 147–157.

[28] N. Yamazoe, K. Shimanoe, Roles of shape and size of component crystals in semiconductor gas sensor. (1) Response to oxygen, J. Electrochem. Soc., 155 (4) (2008): J85–J92.

[29] N. Yamazoe, K. Shimanoe, Roles of shape and size of component crystals in semiconductor gas sensor. (2) Response to oxygen, J. Electrochem. Soc., 155 (4) (2008): J93-J98.

[30] N. Yamazoe, K. Shimanoe, Theory of power laws for semiconductor gas sensors, Sensors and Actuators B: Chemical 128 (2008): 566-573.

[31] A. Gurlo, Interplay between O_2 and SnO_2: oxygen ionsorption and spectroscopic evidence for adsorbed oxygen, ChemPhysChem 7 (2006): 2041-2052.

[32] J. Oviedo, M. J. Gillan, First-principles study of the interaction of oxygen with the SnO_2 (110) surface, Surface Science 490 (2001): 221-236.

[33] B. Slater, C. Richard, A. Catlow, D. E. Williams, A. M. Stonehamc, Dissociation of O_2 on the reduced SnO_2 (110) surface, Chemical Communications, 1235(2000): 1235-1236.

[34] P. Scheiber, A. Riss, M. Schmid, P. Varga, U. Diebold, Observation and Destruction of an Elusive Adsorbate with STM:O_2/TiO_2(110), Physical review letters, 105(2010): 216101-1-4.

[35] M. Setvín, U. Aschauer, P. Scheiber, Y. F. Li, W. Hou, M. Schmid, U. Diebold, Reaction of O_2 with Subsurface Oxygen Vacancies on TiO_2 Anatase (101). Science, 341(2013): 988-991.

[36] V. Oison, L. Saadi, C. L. Mauriat, R. Hayn, Mechanism of CO and O_3 sensing on WO_3 surfaces: First principle study. Sensors and Actuators B: Chemical, 160(2011): 505-510.

[37] M. Hübner, C. E. Simion, A. Haensch, N. Barsan, U. Weimar, CO sensing mechanism with WO_3 based gas sensors. Sensors and Actuators B: Chemical, 151(2010): 103-106.

[38] M. Hübner, N. Bârsan, U. Weimar, Influences of Al, Pd and Pt additives on the conduction mechanism as well as the surface and bulk properties of SnO_2 based polycrystalline thick film gas sensors. Sensors and Actuators B: Chemical, 171 (2012): 172-180.

[39] N. Barsan, M. Hübner, U. Weimar, Conduction mechanism in SnO_2 based polycrystalline thick film gas sensors exposed to CO and H_2 in different oxygen backgrounds, Sensors and Actuators B: Chemical, 157(2011): 510-517.

[40] M. Hübner, R. Pavelko, N. Barsan, U. Weimar, Influence of Oxygen Backgrounds on Hydrogen Sensing with SnO_2 Nanomaterials, Sensors and Actuators B: Chemical, 154 (2011): 264-269.

[41] N. Bârsan, U. Weimar, Understanding the fundamental principles of metal oxide based gas sensors; the example of CO sensing with SnO_2 sensors in the presence of humidity,

J. Phys.: Condens. Matter, 15 (2003): R813–R839.

[42] K. Großmann, S. Wicker, U. Weimar, N. Barsan, Impact of Pt additives on the surface reactions between SnO_2, water vapour, CO and H_2; an operando investigation. Physical Chemistry Chemical Physics, 15 (2013): 19151-19158.

[43] N. Yamazoe, K. Suematsu, K. Shimanoe, Extension of receptor function theory to include two types of adsorbed oxygen for oxide semiconductor gas sensors, Sensors and Actuators B: Chemical, 163(2012):128-135.

[44] N. Yamazoe, K. Suematsu, K. Shimanoe, Two types of moisture effects on the receptor function of neat tin oxide gas sensor to oxygen, Sensors and Actuators B: Chemical, 176 (2013): 443-452.

[45] M. Batzill, Surface Science Studies of Gas Sensing Materials: SnO_2, Sensors 6 (2006): 1345-1366.

[46] J. Goniakowski, M. J. Gillan, The adsorption of H_2O on TiO_2 and SnO_2 (110) studied by first-principles calculations, Surface Science 350 (1996): 145-158.

[47] K. P. Hahn, A. Tricoli, G. Santarossa, A. Vargas, A. Baiker, First principles analysis of H_2O adsorption on the (110) surfaces of SnO_2, TiO_2 and their solid solutions. Langmuir, 28(2011):1646-1656.

[48] G. Santarossa, K. Hahn, A. Baiker, Free Energy and Electronic Properties of Water Adsorption on the SnO_2 (110) Surface. Langmuir, 29(2013): 5487-5499.

[49] B. Hammer, S. Wendt, F. Besenbacher, Water adsorption on TiO_2, Topics in Catalysis, 53(2010): 423-430.

[50] Z. Zhang, O. Bondarchuk, Bruce D. Kay, J. M. White, Z. Dohnálek, Imaging Water Dissociation on TiO_2(110): Evidence for Inequivalent Geminate OH Groups, The Journal of Physical Chemistry B, 110 (2006): 21840-21845.

[51] M. A. Henderson, Structural Sensitivity in the Dissociation of Water on TiO_2 Single-Crystal Surfaces, Langmuir 12 (1996): 5093-5098.

[52] S. Matsushima, Y. Teraoka, N. Miura, N. Yamazoe, Electronic Interaction between Metal Additives and Tin Dioxide in Tin Dioxide-Based Gas Sensors, Japanese Journal of Applied Physics, 27(1998): 1798-1802.

[53] N. Yamazoe, K. Shimanoe, Receptor function of small semiconductor crystals with clean and electron-traps dispersed surfaces, Thin Solid Films, 517 (2009): 6148-6155.

[54] M. Penza, C. Martucci, G. Cassano, NO_x gas sensing characteristics of WO_3 thin films activated by noble metals (Pd, Pt, Au) layers, Sensors and Actuators B: chemical, 50 (1998): 52–59.

[55] C. G. Granqvist, G. A. Niklasson, A. Azens, Electrochromics: Fundamentals and energy-related applications of oxide-based devices. Applied Physics A, 89 (2007):

29-35.

[56] E. K. Sichel, J. I. Gittleman, J. Zelez, Electrochromism in the composite material Au-WO_3, Applied Physics Letters, 31 (2008): 109-111.

[57] I. Shiyanovskaya, M. Hepel, E. Tewksburry, Electrochromism in electrodeposited nanocrystalline WO_3 films I. Electrochemical and optical properties, Journal of New Materials for Electrochemical Systems, 3(2000): 241-248.

[58] C. L. Howard, V. Luca, K. S. Knight, High-temperature phase transitions in tungsten trioxide-the last word?. Journal of Physics: Condensed Matter, 14 (2002): 377-387.

[59] J. A. Perri, E. Banks, B. Post, Study of Phase Transitions in WO_3 with a High-Temperature X-Ray Diffractometer. Journal of Applied Physics, 28 (2004): 1272-1275.

[60] C. V. Ramana, S. Utsunomiya, R. C. Ewing, C. M. Julien, U. Becker, Structural Stability and Phase Transitions in WO_3 Thin Films, Journal of Physical Chemistry B, 110 (2006): 10430-10435.

[61] E. I. Altman, U.D. Schwarz, Mechanisms, kinetics, and dynamics of oxidation and reactions on oxide surfaces investigated by scanning probe microscopy. Advanced Materials, 22 (2010): 2854-2869.

[62] F. Wang, C. D. Valentin, G. Pacchioni, DFT Study of Hydrogen Adsorption On the Monoclinic WO3 (001) Surface, The Journal of Physical Chemistry C, 116 (2012): 10672-10679.

[63] I. M. Szilágyi, B. Fórizs, O. Rosseler, et al. WO_3 photocatalysts: Influence of structure and composition, Journal of Catalysis, 294 (2012): 119-127.

[64] L. WANG, Tailored synthesis and characterization of selective metabolite-detecting nanoprobes for handheld breath analysis, Diss. Stony Brook University, 2008.

[65] K. Sayama, H. Hayashi, T. Arai, M. Yanagida, T. Gunji, H. Sugihara, Highly active WO_3 semiconductor photocatalyst prepared from amorphous peroxo-tungstic acid for the degradation of various organic compounds. Applied Catalysis B: Environmental, 94 (2010): 150-157.

[66] A.C.C. Tseung, K.Y. Chen, Hydrogen spill-over effect on Pt/WO_3 anode catalysts, Catalysis Today, 38 (1997): 439-443.

[67] V. K. Yatsimirskii, V. V. Lesnyak, I. N. Gut, O. Y. Boldyreva, Catalytic activity of WO_3 and MoO_3 with Pt and Pd additives in oxidation of hydrogen, Theoretical and Experimental Chemistry, 41(2005): 329-333.

[68] S. M. Kanan, Z. X. Lu, J. K. Juliet, G. Bernhardt, C. P. Tripp, Identification of Surface Sites on Monoclinic WO_3 Powders by Infrared Spectroscopy, Langmuir 18 (2002): 1707-1712.

[69] E. I. Altman, R. E. Tanner, Using scanning tunneling microscopy to characterize adsorbates and reactive intermediates on transition metal oxide surfaces, Catalysis Today 85 (2003): 101-111.

[70] R. D. Bringans, H. Hochst, H. R. Shanks, Defect states on the surface of WO_3, Vacuum, 31 (1981): 473-475.

[71] I.N. Yakovkin, M. Gutowski, Driving force for the WO_3(001) surface relaxation, Surface Science 601 (2007):1481–1488.

[72] X. Wang, G. Sakai, N. Miura, N. Yamazoe, Sub-ppm NO_2 Sensing Characteristics of WO_3 Thin Film Prepared by Sol-Gel Method, Japanese Sensor Newsletter, 11 (1997): 12-18.

[73] Y. G. Choi, G. Sakai, K. Shimanoe, N. Miura, N. Yamazoe, Wet process-prepared thick films of WO_3 for NO_2 sensing, Sensors and Actuators B, 95 (2003): 258-265.

[74] T. Kida, A. Nishiyama, M. Yuasa, K. Shimanoe, N. Yamazoe, Highly sensitive NO_2 sensors using lamellar-structured WO_3 particles prepared by an acidification method, Sensors and Actuators B, 135 (2009): 568-574.

[75] K. Shimanoe, A. Nishiyama, M. Yuasa, T. Kida, N.Yamazoe, Microstructure control of WO_3 film by adding nano-particles of SnO_2 for NO_2 detection in ppb level, Procedia Chemistry, 1(2009): 212-215.

[76] S. R. Aliwell, J.F. Halsall, K. F. E. Pratt, et. al, Ozone sensors based on WO_3: a model for sensor drift and a measurement correction method. Measurement Science and Technology, 12 (2001): 684-690.

[77] S.R. Utembea, G.M. Hansford, M.G. Sanderson, An ozone monitoring instrument based on the tungsten trioxide (WO_3) semiconductor, Sensors and Actuators B, 114 (2006): 507-512.

[78] T. Maekawa, J. Tamaki, N. Miura, N. Yamazoe, Gold-Loaded Tungsten Oxide Sensor for Detection of Ammonia in Air, Chemistry Letters, 4 (1992): 639-642.

[79] K. Kanda, T. Maekawa, Development of a WO_3 thick-film-based sensor for the detection of VOC, Sensors and Actuators B, 108 (2005): 97-101.

[80] M. Righettoni, A. Tricoli, S. E. Pratsinis, Si: WO_3 Sensors for Highly Selective Detection of Acetone for Easy Diagnosis of Diabetes by Breath Analysis, Analytical Chemistry, 82 (2010) 3581-3587.

[81] Z. Hua, M. Yuasa, T. Kida, N. Yamazoe, K. Shimanoe, High sensitive gas sensor based on Pd-loaded WO_3 nanolamellae, Thin Solid Films 548 (2013) 677-682.

[82] Z. Hua, M. Yuasa, T. Kida, N. Yamazoe, K. Shimanoe, H_2 sensing mechanism of Pd-loaded WO_3 nanoparticles gas sensors, Chemistry letters, 2014 (dx.doi.org/10.1246/cl.140396).

[83] J. Zhang, X. G. Liu, M. J. Xu, Pt clusters supported on WO_3 for ethanol detection, Sensors and Actuators B, 147 (2010): 185-190.

[84] T. Maekawa, J. Tamaki, N. Miura, N. Yamazoe, Promoting effects of noble metals on the detection of ammonia by semiconductor gas sensor, Studies in Surface Science and Catalysis, 77 (1993): 421-424.

[85] V. Lantto, P. Romppainen, S. Leppävuori, Response studies of some semiconductor gas sensors under different experimental conditions. Sensors and Actuators, 15(1988): 347-357.

CHARPTER 2

2 Microstructural and Gas Sensing Properties of Neat WO_3 Sensors

In the present chapter, the preparations and characterization of WO_3 nanoparticles have been described for neat WO_3. The WO_3 nanoparticles were prepared by the acidification method and the sensor devices are made by the conventional screen-printing. The gas sensing apparatus was reported and gas sensing properties to inflammable gases (H_2, CO and CH_4) were measured. Sensing properties are characterized under both dry and wet conditions and the humidity effects have been studied.

2.1 Introduction

A kind of lamellar-structured WO_3 nanoparticle has been reported and used for NO_2 sensing for more than one decade in this group [1-3]. The material preparation is quite simple via the acidification of Na_2WO_4; however, the sensors devices fabricated from these nanoparticles are quite sensitive to NO_2, even at dozens of ppb [1-2]. It is suggested that the highly sensitive response is caused by a mesoporous surface structure [2-4] and a volume depletion state due to a very small thickness of the nanoparticles [3-5]. Additionally, this kind of lamellar-structured WO_3 nanoparticles also demonstrates a good sensing performance to VOCs. However, the sensing processes of NO_2 and VOCs are not so clear. Therefore, in order to further understand the sensing mechanism of lamellar-structured WO_3 nanoparticles gas sensors, the sensing properties to

typical inflammable gases (H_2, CO and CH_4) are characterized. It is believed that the simple reaction routines of H_2 and CO with oxygen and sensor surface are beneficial for the clarification of sensing process of WO_3; therefore, it allows us an indirect method to study surface characteristics of WO_3 as a sensing material.

2.2 Experimental Details

2.2.1 Synthesis of WO_3 nanoparticles

The lamellar-structured WO_3 nanoparticles are synthesized from an acidification method. The preparation process has been introduced by our previous reports [1-3]. A typical preparation procedure is illustrated in Fig. 2-1.

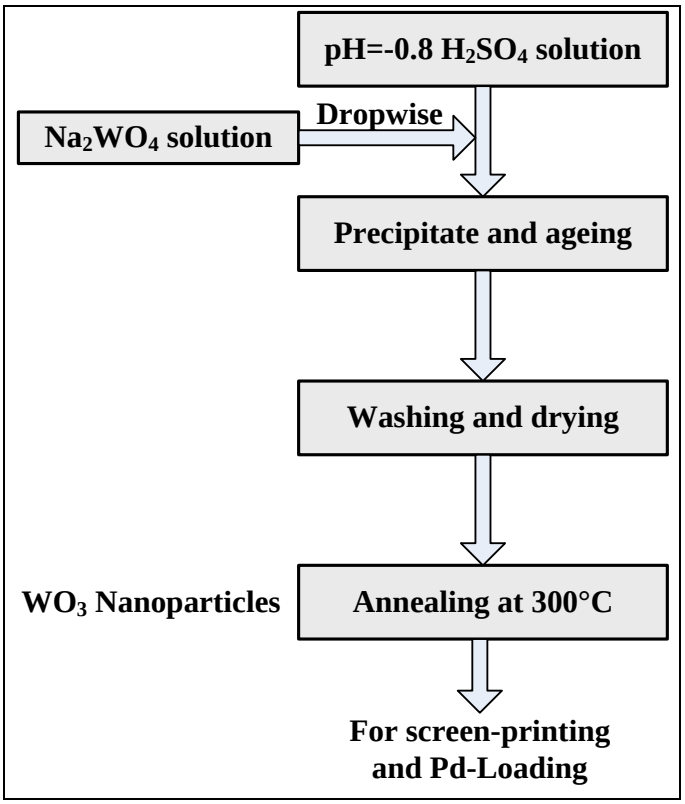

Figure 2-1 preparation of WO_3 nanoparticles through the acidification method.

Firstly, Na_2WO_4 was dissolved by distilled water and added into a strong acid solution drop by drop under vigorous stirring. The two solutions were mixed so as to set the molar ratio of Na^+/H^+ at 10. The pH of the acidic solution was

controlled with H_2SO_4 at -0.8. A yellow gel (crystalline $WO_3 \cdot 2H_2O$) appeared immediately when mixing the two solutions. The gel was aged for 24 h at 30ºC and then washed thoroughly with distilled water by centrifugation for several times. After drying at 40ºC, the final powders were obtained and calcined at 300ºC in air for 2 h for the materials characterizations and fabrication of sensor device fabrication.

2.2.2 Characterization of materials

Various characterization techniques were used to obtain the structural, morphological, physical and chemical information of materials to understand the sensing process. The phase structure was characterized by the powder X-ray diffraction carried out by a RINT 2100 (Rigaku, Japan) with $Cu_{k\alpha}$ radiation (40 kV, 40 mA) with a 2θ range from 10º to 80º at a speed of 1º min^{-1}. The crystalline sizes obtained from XRD peaks are calculated from the relation

$$D = 0.9\lambda / B\cos\theta \quad \textbf{(2.1)}$$

Where D denotes mean crystalline size, B represents full width at half maximum of the peak, λ is the wavelength of the X-ray (0.15418 nm), and θ is the center angle of the peak.

FE-SEM micrographs were obtained using a JSM-6340, JEOL. Both the morphology of the nanoparticle powders and the sensor surface were analyzed. Transmission electron microscopy (TEM), high resolution TEM (HRTEM) and high annular dark field scanning TEM (HADDF-STEM) were performed on a Tecnai-F20 (FEI, US) equipped with an X-ray energy-dispersive spectroscopy (EDS) at an accelerating voltage of 200 kV. The sample powders were dispersed into ethanol solution forming a suspension, and then ultrasonically agitated for

one hour. After agitation, the suspension was dropped on to coated copper TEM grids. In the case of sensor devices, the powders were collected from the sensor substrates and then made TEM samples. The BET surface area and microspore structure were analyzed by the by liquid nitrogen sorption (BELSOEP-mini, Japan). Sample powders were grinded and weighted at 0.2 g for each BET test.

2.2.3 Characterization of sensing properties

The sensor devices were prepared by the conventional screen-printing technique [2]. For sensors fabrication, the obtained WO_3 nanoparticles powders were mixed with water to form a homogeneous paste. The resulting paste was then screen-printed by a mesh on an alumina substrate equipped with a pair of comb-type Au microelectrodes (line width: 180 μm; distance between lines: 90 μm; sensing layer area: 64 mm^2).

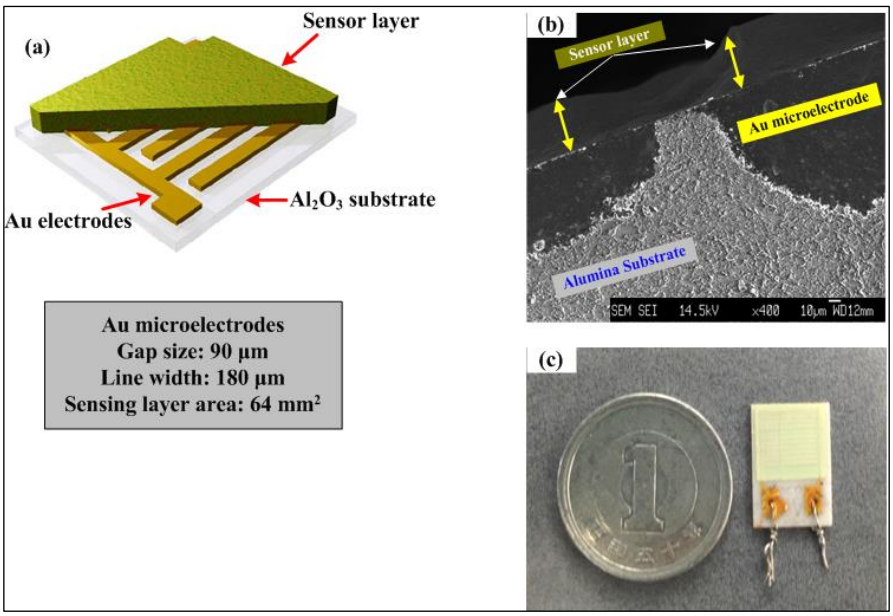

Figure 2-2 (a) the configuration of the sensor device, (b) FE-SEM image of cross structure and (c) the photograph of a fabricated WO_3 sensor.

Then the deposited film was annealed at 400ºC for 2 h, which was a low temperature to control the sublimation and maintain the nanostructure. The

sensing film was aged at operating temperatures (300 and 350 ºC) for 12 h before the sensing measurements. Figure 2-2 shows the configuration, microstructure and photograph of the sensor devices.

WO_3 sensors were characterized towards O_2, H_2, CO and CH_4 balanced with air or N_2 at 300 and 350 ºC, respectively. Different humidity was obtained by flowing gas into a water bubble and the humidity was monitored by commercial humidity sensor (TR-77Ui) with a grantee acutance of relative humidity from 0.1% to 99%. The total flow rate was adjusted at 100 cm^3 min^{-1} and be precisely controlled by the mass flow controller (MFC). The sensor response was defined as the ratio of R_a/R_g in the presence of inflammable gases.

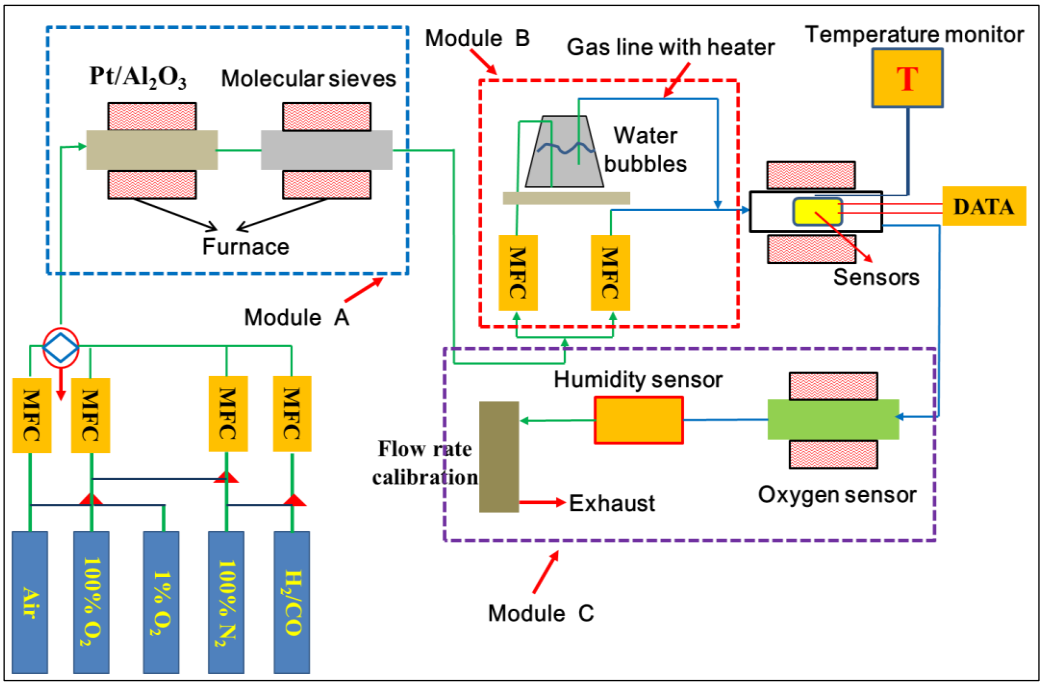

Figure 2-3 experimental set-ups for the gas sensing properties characterizations. (According to the functional, the set-up is consisted by three different parts. Module A: Gas purifying, Module B: Humidity modulation and Module C: Exhaust monitor).

The gas sensing properties were measured by means of a conventional gas flow apparatus equipped with an electrical furnace. For oxygen adsorption study, the gas was flowed into a gas home-made purifying apparatus consisted by a

catalyst (5% Pt/Al_2O_3) and molecules sieves absorbance (5A 1/16). This procedure can effectively remove the contaminated gases (extremely low concentration of H_2O, CO and CH_x) in oxygen and nitrogen gas cylinders. A schematic illustration of the experimental set-up is represented in Fig. 2-3.

2.3 Results and Discussions

2.3.1 Materials characterizations

The phase structures of WO_3 nanoparticle powders are characterized by the X-ray diffraction as shown in Fig. 2-4. The XRD patterns suggested a monoclinic WO_3 phase (JCPDS 43-1035) for sample powders sintered at 300 ºC and 400 ºC. By sintering at 400 ºC for 2 h in air, the crystalline size determined from the peak (200), (020) and (002) are 25.6 nm, 20.3 nm and 13.9 nm, respectively.

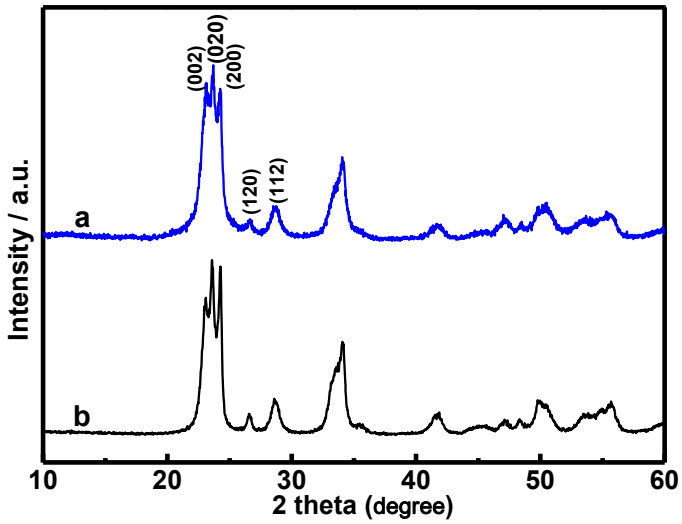

Figure 2-4 XRD patterns of WO_3 nanoparticles powders calcined at (a) 300 ºC and (b) 400 ºC for 2 h in air.

The sample nanoparticles powders and surface morphology of the sensor devices were analyzed by FE-SEM. Figure 2-5 represents the FE-SEM images of nanoparticle and sensor devices. Apparently, the sample powder consists of a numerous of irregular planar-like particles. And these particles loosely and

randomly stacked together, resulting in a large mesoporous structure. This is important for the gas diffusion process, which is one of the reasons for the highly sensitive response to NO_2 [1, 4]. From the insert high magnification SEM images, it is estimated that the lateral size is around 100-200 nm with a thickness 10-30 nm. The sample powders demonstrated a surface area *ca*. 19 m^2/g with a pore volume around 4.5 cm^3/g.

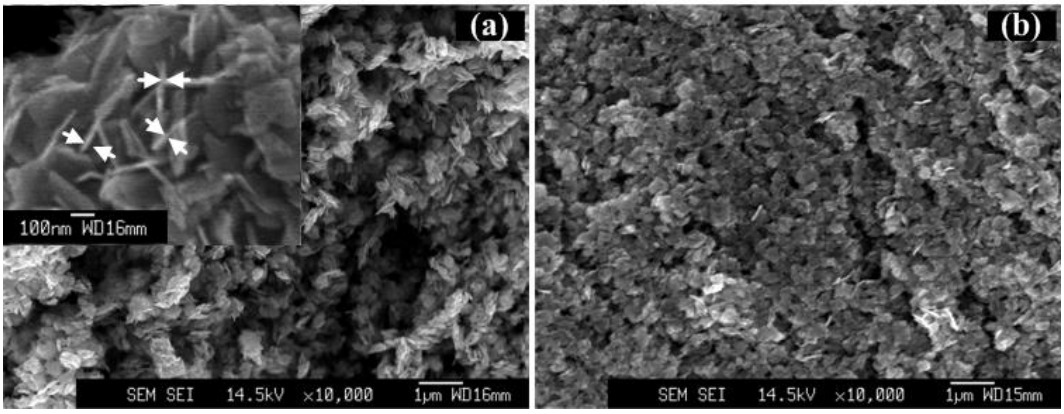

Figure 2-5 FE-SEM images of (a) the fabricated WO_3 nanoparticles powders and (b) the prepared sensor layer calcined at 400 ºC for 2 h in air atmosphere.

Further characterizations on the morphology of the nanoparticles were performed by TEM. Figure 2-6 shows the typical TEM images of the prepared WO_3 nanoparticles. One can easily find that the nanoparticles have a highly irregular shape with a broad distribution in lateral size ranging from dozens of nm up to several hundreds of nm. By counting from TEM images, the lateral size was estimated around 200 nm. HRTEM images and the fast Fourier transform (FFT) pattern of the pure WO_3 nanoparticle were represented in Fig. 2-6 (b). The interplanar spacings marked in the figure are 0.364 nm and 0.376 nm, which were corresponded to (020) and (200) faces of monoclinic WO_3, respectively. The FFT pattern can be clearly indexed. From these results, it can be concluded that the fabricated nanoparticle was single crystalline and thickness growth was

in (002) direction [3].

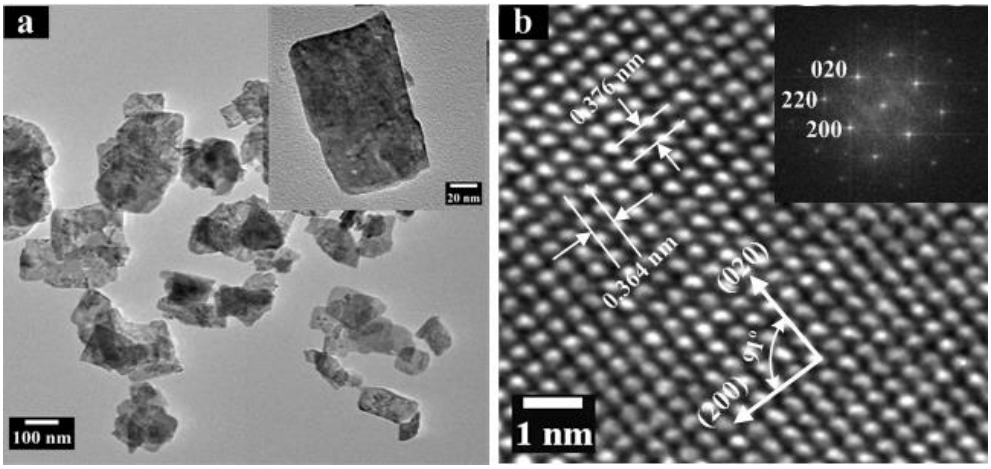

Figure 2-6 (a) a typical TEM image of WO_3 nanoparticles and (b) HRTEM insert with FFT pattern.

It was found that the thickness of WO_3 nanoparticles determined from the HRTEM in Fig. 2-7, was around 10 nm, much smaller than the results observed from SEM images. However, the value was comparable with the crystal size estimated from the peak (002) of XRD pattern.

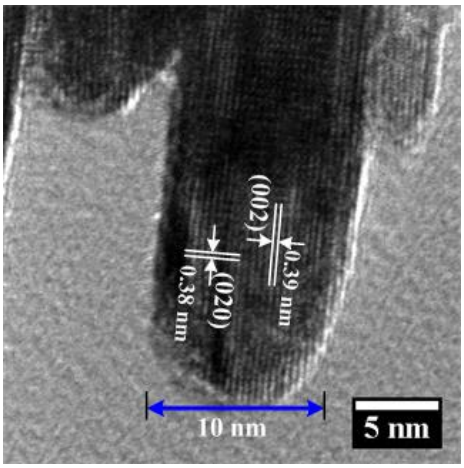

Figure 2-7 HRTEM of WO_3 nanoparticles.

This was consistent with our proposal that the thickness is in (002) planes. It should be noted that TEM results demonstrated an inhibition of growth in (002) planes, however, there was no preferred peak for XRD pattern. Combining TEM results with the SEM images, we believed that it was because of a randomly

stacking of WO_3 nanoparticles, which made similar possibilities of exposing to X-ray diffraction for different faces.

Lastly, the short-term stability of the microstructure of the synthesized WO_3 nanoparticles was investigated based on electron microscopy results. Figure 2-8 (a) presents the SEM image of the surface of a completely new WO_3 sensor device before any sensing test. Figure 2-8 (b) shows the corresponding TEM image of newly fabricated WO_3 nanoparticles.

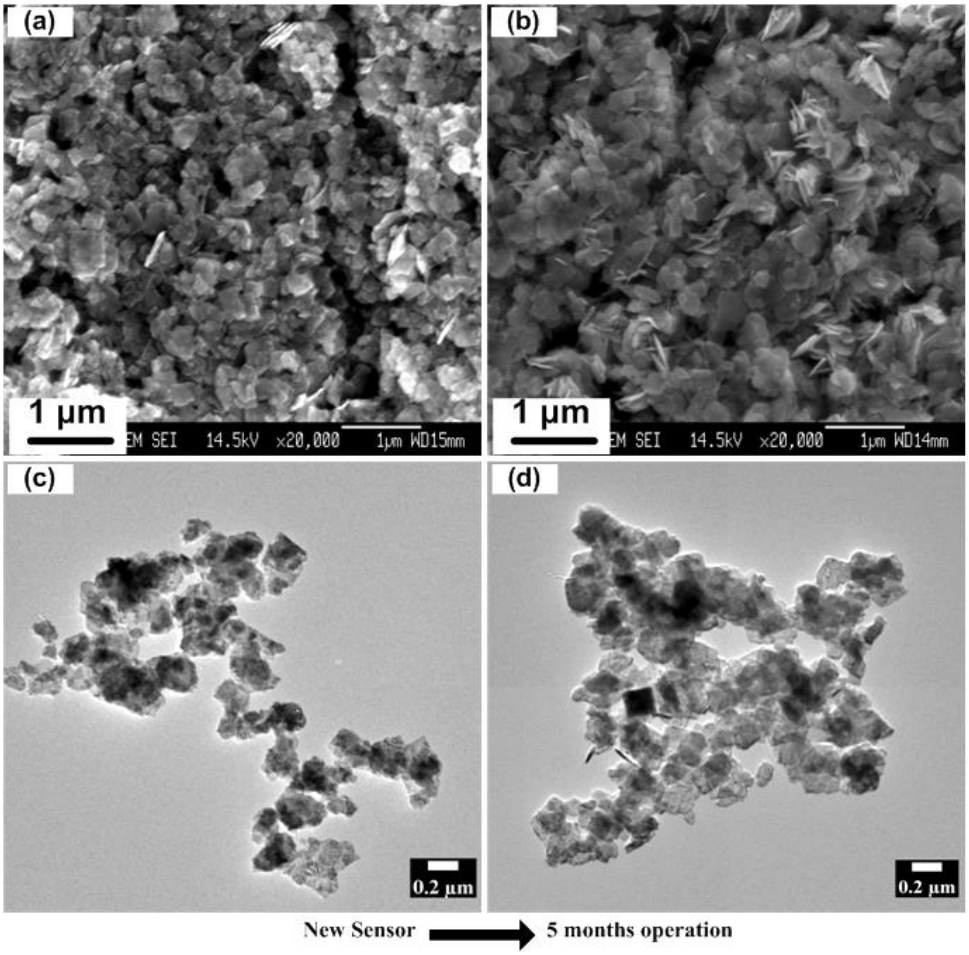

Figure 2-8 SEM (a), TEM (b) images of a new WO_3 sensor and (c) SEM, (d) TEM images of the same sensor after 5 months of continuous operation.

After 5 months of continuous operation at temperature ranging from 250 to 350 ºC and hundreds hours of sintering at 400 ºC, the same sensor was analyzed by FE-SEM and TEM again as shown in Fig. 2-8 (c) and (d). For TEM

characterization, a small amount of powders was scratched from the substrate and made a TEM sample similar as that of powder sample. It was quite clear that there was no visible difference in either the morphology or size after a continuous operation, indicating a good stability of its nanostructure. This is also confirmed by the results of BET measurements. Figure 2-9 shows the BET surface area and pore volume of neat WO_3 nanoparticle powders as a function of sintering times at 350 ºC in air atmosphere. It was found that surface area and pore volume slightly decreased at the first five days. With further increasing the sintering times to 15 days, the reduction in surface area and pore volume was very small almost in the range of error. This demonstrated a good stability of nanostructure for WO_3.

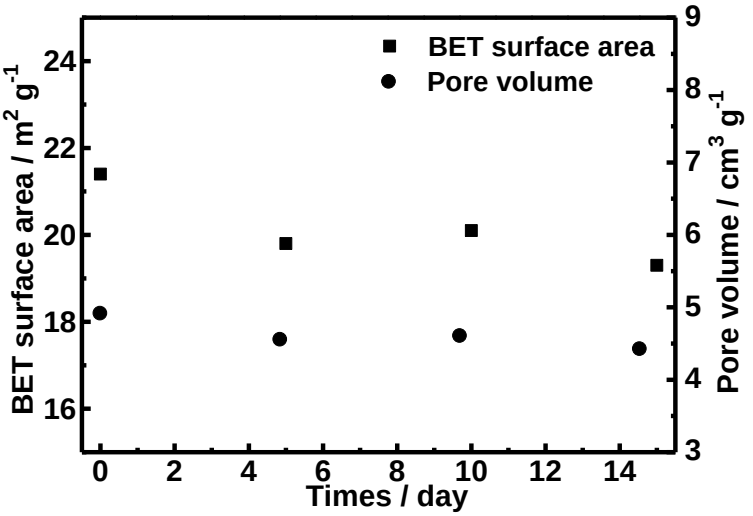

Fig 2-9 BET surface area and pore volume of WO_3 nanoparticle powders as a function of sintering times at 350 ºC in air.

2.3.2 Sensing results

The sensing properties of WO_3 nanoparticle gas sensor to inflammable gases namely, H_2, CO and CH_4 were measured under dry and humid conditions. For simplicity, sensing properties under wet condition were only characterized at 350

ºC. Firstly, sensing response to hydrogen at small and large concentration region was tested, respectively. The sensing response is defined by R_a/R_g, where R_a and R_g is the sensor resistance in air and reducing gas (H_2, CO and CH_4) respectively. Figure 2-10 presents the sensing response to a low concentration of H_2 at 300 ºC and 350 ºC.

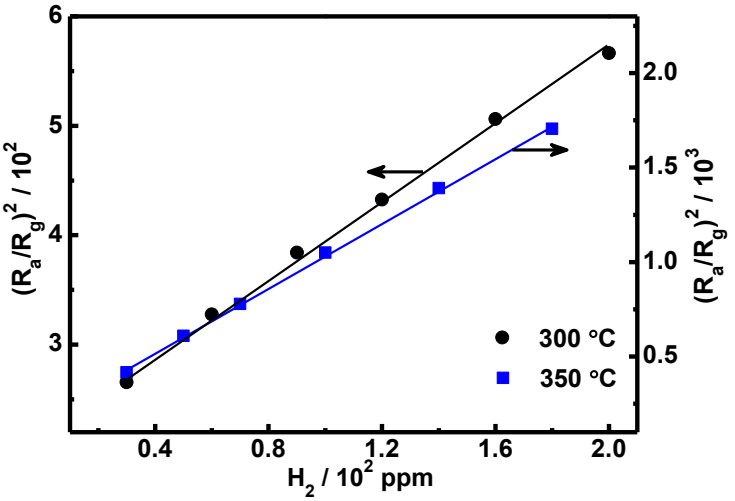

Figure 2-10 $(R_a/R_g)^2$ as a function of P_{H2} ranging from 30 ppm to 200 ppm at 300 ºC and 350 ºC for WO_3 nanoparticle gas sensor.

It was found the sensor response was slightly increased with increasing temperatures and the square of the sensor response has a good linearity with P_{H2} at 300 ºC and 350 ºC. According to the volume depletion theory [5-6], the sensor response can be expressed by:

$$\left(\frac{R_a}{R_g}\right)^2 = 1 + \frac{c}{aN_d} P_{H2} \quad \textbf{(2.1)}$$

This indicates that surface reaction of H_2 can be described by (2.1):

$$H_2 + O^- \underset{k_{11}}{\overset{k_{-11}}{\rightleftharpoons}} H_2O + e \quad \textbf{(R2.1)}$$

In other words, the sensor response was due to the oxidation of H_2 by adsorbed

O^-. Figure 2-11 shows the sensor response to H_2 at a high concentration. It was found that sensor response was increased with H_2 concentration and the linear relationship is clearly evidenced, indicating the same surface reaction as (R2.2).

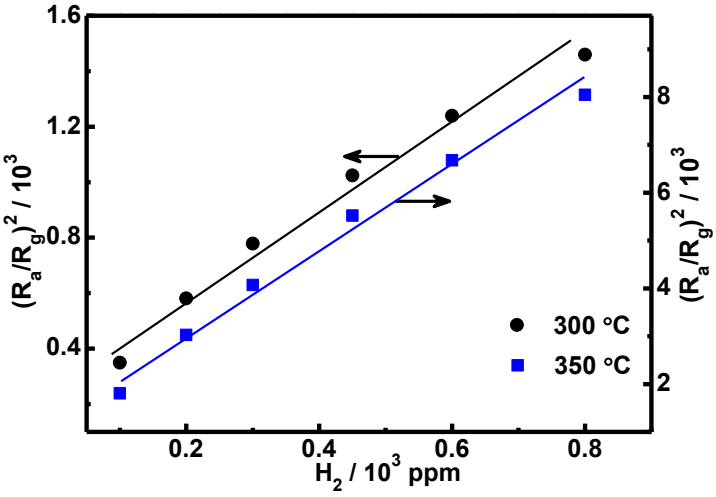

Figure 2-11 $(R_a/R_g)^2$ as a function of P_{H2} ranging from 100 ppm to 800 ppm at 300 ºC and 350 ºC for WO_3 gas sensor.

The sensing properties of CO were also examined for WO_3 nanoparticle gas sensors. Figure 2-12 shows the square of sensor response as a function of CO concentration.

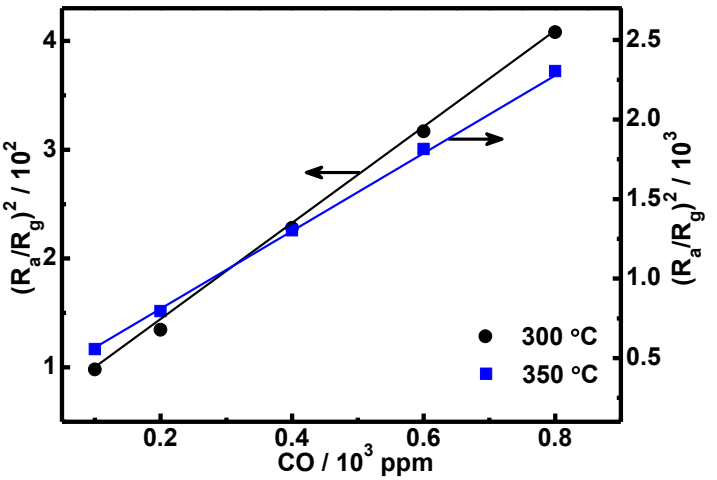

Figure 2-12 $(R_a/R_g)^2$ plotting with P_{CO} at 300 ºC and 350 ºC for WO_3 sensor.

It was obvious that the sensor response was increased with temperatures and

$(R_a/R_g)^2$ demonstrated a linear dependence on P_{CO} at both temperatures. Therefore, it can be concluded that the sensing response of CO was due to the following reaction:

$$CO + O^- \underset{k_{11}}{\overset{k_{-11}}{\rightleftharpoons}} CO_2 + e \quad \textbf{(R2.3)}$$

Sensing response to CH_4 was measured. However, it was found that the recovery speed was quite slow and the sensor response was not repeatable at 300 ºC. Thus, the sensing test was only carried out at 350 ºC. Figure 2-13 shows the sensor response of CH_4 as a function of concentration.

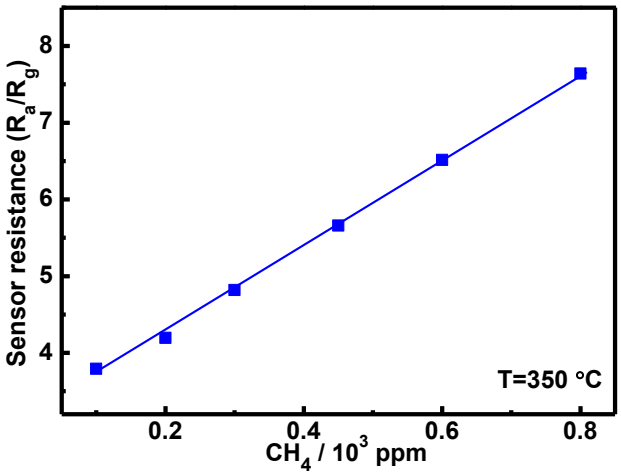

Figure 2-13 sensor response as a function of CH_4 concentration at 350 ºC for WO_3 nanoparticles gas sensor.

It was found that WO_3 sensor responded to CH_4, nevertheless, the response was much smaller than that for H_2 and CO. The sensor response of 200 ppm CH_4 was just around 6.9, whereas, it was accounted for more than 55 and 7.3 for H_2 and CO at the same concentration, respectively. It is well accepted that the oxidation of CH_4 was quite complex [7-8]. Thus, in present case, it was quite difficult to propose the reaction routines for the sensing response of CH_4. However, it is believed that the reaction of CH_4 arises from to the surface adsorbed oxygen.

In order to study the effect of water vapor, the sensing responses to inflammable gases were measured under different humidity. Figure 2-14 (a) shows the sensor response as function of H_2 concentration under wet condition. It was observed that the sensor response was greatly reduced with the presence of water vapor. Taking 1 VOL.% humidity for example, the sensor response was decreased down to only 1.3 for 200 ppm H_2, 40 times smaller than that of dry condition. Figure 2-14 (b) presents the dependence of sensor response on humidity for WO_3 sensor. It was quite obvious that sensor response was greatly reduced with a little humidity and slightly decreased with further increasing humidity up to 3 VOL.%. The deterioration of sensor response can be ascribed to the water poisoning effect [2-3, 5, 9].

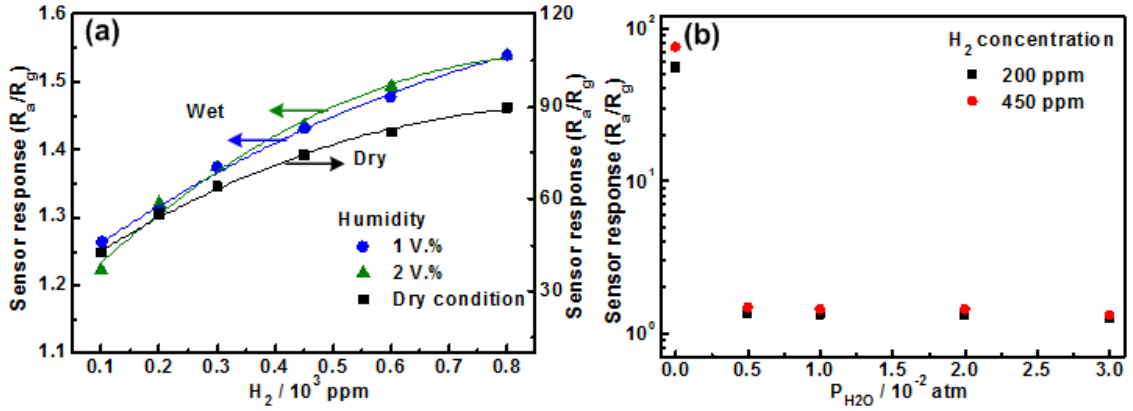

Figure 2-14 (a) sensing response as a function of H_2 concentration with presence of water vapor at 350 ºC and (b) the dependence of sensor response on humidity for 200 ppm and 450 ppm H_2 at 350 ºC.

The water poisoning effect was also evidenced for CO and CH_4 sensing. Figure 2-15 (a) shows the sensing response of CO as a function of concentration with presence of humidity. Similarly, the sensor response was degenerated by humidity and much smaller than that of dry condition. Obviously, the sensor response decreased with increasing humidity as shown in Fig. 2-15 (b).

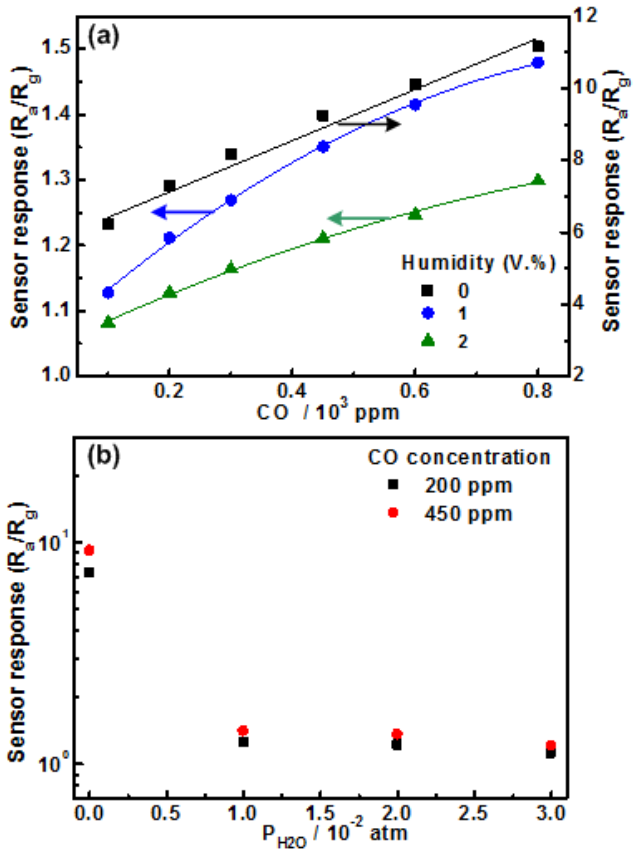

Figure 2-15 (a) sensing response as a function of CO concentration with presence of water vapor at 350 ºC and (b) the dependence of sensor response on humidity for 200 ppm and 450 ppm CO at 350 ºC.

Figure 2-16 (a) shows the sensor response of CH_4 under those wet condition. It was found that the sensing results were similar with those of H_2 and CO for which the sensor response was greatly reduced by water vapor. However, the sensor response to CH_4 was so slight with a small concentration of water vapor, comparing with that of H_2 and CO. The sensor response to 450 ppm CH_4 was just 1.2 with 0.5 VOL.% humidity. By increasing humidity, the sensor response was further decreased as shown in Fig. 2-16 (b). Therefore, it can be concluded that water vapor significant reduced the sensor response of WO_3 sensor to inflammable gases.

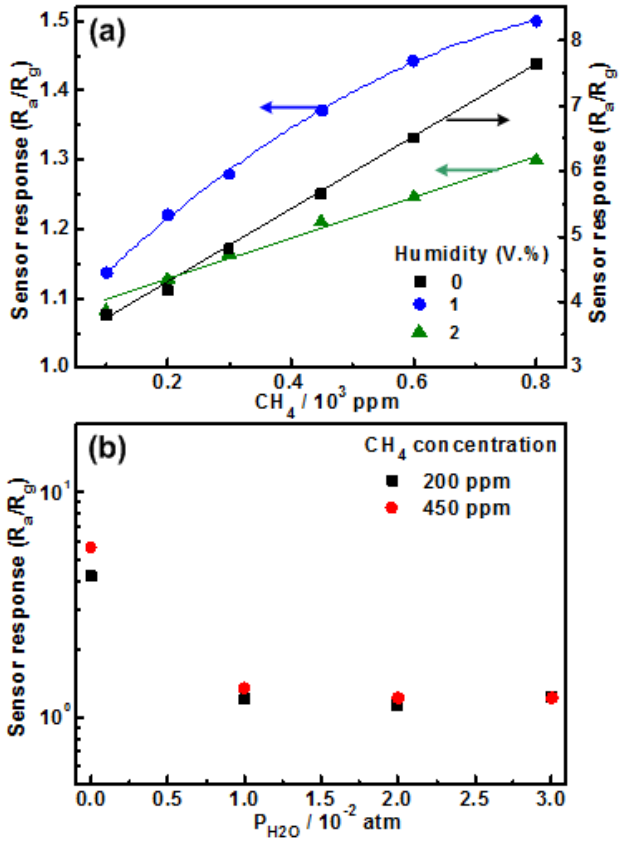

Figure 2-16 (a) sensing response as a function of CH_4 concentration with presence of water vapor at 350 ºC and (b) the dependence of sensor response on humidity for 200 ppm and 450 ppm H_2 at 350 ºC.

2.4 Conclusions

In this chapter, the preparation of materials and sensors devices was introduced. Then the structural and sensing properties of WO_3 nanoparticles gas sensors were investigated. The main conclusions are listed below.

- The fabricated WO_3 nanoparticles demonstrated a two dimensional nanostructure with a highly irregular lamellar shape. The lateral size ranged broadly from dozens to several hundred nm with a thickness just around 10 nm. The prepared WO_3 nanoparticle has a single crystalline quality (Monoclinic, JCPDS 43-1035) and the thickness was in (002) direction.
- Sensor devices made by the scree-printing technique demonstrated a

mesoporous structure with a thickness *ca*. 30 μm. WO_3 sensors showed a sensor response to inflammable gases in a sequence of H_2, CO and CH_4, in addition, the sensor response was increased around 2 times with increasing temperature from 300 to 350 ºC.

- Sensor response was greatly reduced by the presence of humidity. More specifically, with 0.5 VOL.%, the sensor response to H_2 was decreased by around 30 times, just around 1.3. However, the sensor response was almost kept the same with further increasing the humidity. The reduction of sensor response with humidity was so slight, and the variation of response was within 2 for all of three gases from 0.5 to 3 VOL.%.

References

[1] T. Kida, A. Nishiyama, M. Yuasa, K. Shimanoe, N. Yamazoe, Highly sensitive NO_2 sensors using lamellar-structured WO_3 particles prepared by an acidification method, Sensors and Actuators B, 135 (2009): 568-574.

[2] K. Shimanoe, A. Nishiyama, M. Yuasa, T. Kida, N.Yamazoe, Microstructure control of WO_3 film by adding nano-particles of SnO_2 for NO_2 detection in ppb level, Procedia Chemistry, 1 (2009): 212-215.

[3] Z. Hua, M. Yuasa, T. Kida, N. Yamazoe, K. Shimanoe, High sensitive gas sensor based on Pd-loaded WO_3 nanolamellae, Thin Solid Films, 548 (2013) 677-682.

[4] T. Kida, A. Nishiyama, Z. Hua, K. Suematsu, M. Yuasa, K. Shimanoe, WO_3 Nanolamella Gas Sensor: Porosity Control Using SnO_2 Nanoparticles for Enhanced NO_2 Sensing, Langmuir, 30 (2014): 2571-2579.

[5] N. Yamazoe, K. Suematsu, K. Shimanoe, Extension of receptor function theory to include two types of adsorbed oxygen for oxide semiconductor gas sensors, Sensors and Actuators B: Chemical, 163 (2012):128-135.

[6] N. Yamazoe, K. Shimanoe, Roles of shape and size of component crystals in semiconductor gas sensor. (2) Response to NO_2 and H_2, J. Electrochem. Soc., 155 (2008): J93-J98.

[7] M. Boulova, A. Gaskov, G. Lucazeau, Tungsten oxide reactivity versus CH_4, CO and NO_2 molecules studied by Raman spectroscopy. Sensors and Actuators B: Chemical, 81 (2001): 99-106.

[8] D. Dissanayake, M. P. Rosynek, K. C.C. Kharas, J. H. Lunsford, Partial oxidation of methane to carbon monoxide and hydrogen over a Ni/Al_2O_3 catalyst, Journal of Catalysis, 132 (1991): 117-127.

[9] Z. Hua, M. Yuasa, T. Kida, N. Yamazoe, K. Shimanoe, H_2 sensing mechanism of Pd-loaded WO_3 nanoparticles gas sensors, Chemistry letters, 2014 (dx.doi.org/10.1246/cl.140396).

CHAPTER 3

3 Microstructural and Sensing Properties of Pd-loaded WO_3 Sensors

In this chapter, the preparation for Pd-loaded WO_3 nanoparticles was described. Then, the microstructural and sensing properties of Pd-loaded WO_3 nanoparticles were investigated and compared with those of neat WO_3 nanoparticles. The loading states of Pd on the surface were analyzed based on electron microscopy. Lastly, the effects of Pd-loading and humidity on the sensing response of inflammable gases for WO_3 gas sensors were studied.

3.1 Introduction

For a long time, it has been recognized that the introduction of different additives is one of most effective ways to enhance the sensing performance of MOS gas sensors. However, the promotion mechanism is not well understood by now and it is still one of the interesting subjects in MOS sensors [1-4]. Generally, it is believed that the role of additives in gas sensing can be explained by the spill-over [2], Fermi-level control [3] and surface reconstruction [3-4] as shown in Fig. 1-7. It is found that Au and Pt are very effective additives for WO_3 sensor and has been used in the sensing of NH_3 and H_2S [5-6]. The promotion mechanism is explained by the enhanced interaction of gas by the presence of Au [5]. However, in the case of inflammable gases, noble metal additives, such as Pd is most used [1-3]. There are various methods to introduce metal additives; nevertheless, the conventional incipient wetness impregnation method is

extensively used in SnO_2 gas sensors due to its technique simplicity [1-4]. This method composes a process of impregnating the metal oxide support into a metal precursor dispersed in an aqueous solution and a dry process. However, it does not seem to be an effective way for WO_3, which has a really high acidic surface with a point of zero charge (PZC) below 0.5 [7]. Hence, it is not suitable for the loading of Pd by the conventional impregnation method. In this study, a modified impregnation method was used for the loading process of Pd. The loading state of Pd and its effect on sensing performance were investigated.

3.2 Experimental Details

3.2.1 Synthesis of Pd-loaded WO_3 nanoparticles

Pd was loaded on the surface of WO_3 nanoparticles through a modified impregnation process. The WO_3 support powder was prepared from an acidification method as described in chapter 2.1. In the present study, due to the highly acidic surface of WO_3 as demonstrated in Fig. 3-1, we proposed a modified impregnation routine based on the electroastic adsorption mechanism.

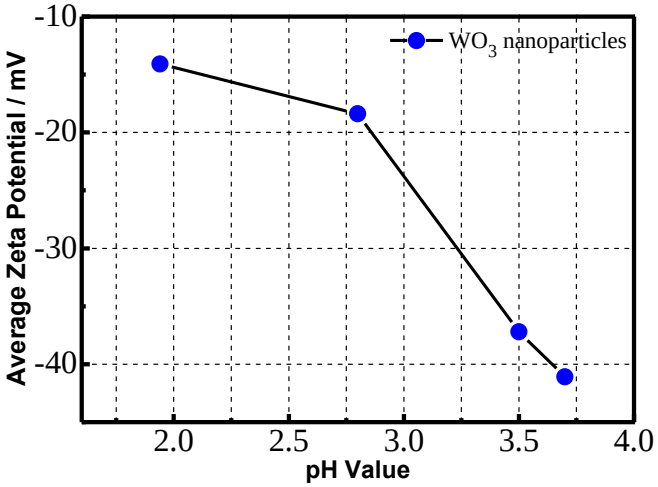

Figure 3-1 Zeta potential as function of pH value for WO_3 nanoparticles.

Figure 3-2 schematically shows the mechanism of electrostatic adsorption.

Above the PZC, the surface become protonated and positively charged [8-9]. When the pH is below PZC, the surface of metal oxide is deprotonated and thus negatively charged [8-9].

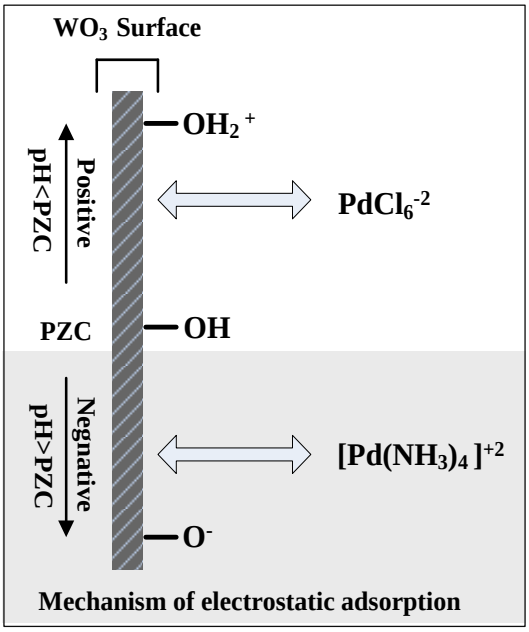

Figure 3-2 mechanism for electrostatic adsorption of Pd species on the charged surface of metal oxide.

Without controlling the pH, the surface tends to become neutral and the metal deposition process is ineffective and become a physical deposition process, resulting in a board distribution of size and large particles during the drying process [8-10]. For a long time, it has been reported that WO_3 has really a low value of PZC, therefore, in practical; it is very difficult to be positively charged [7]. This is the reason that the traditional wetness impregnation process is not effective. The main species for Pd is in $[PdCl_6]^{2-}$, which cannot be adsorbed on a negatively charged surface [8-9].

In the present study, a modified impregnation process was applied by adjusting pH value with ammonia solution. In the base condition, the $[PdCl_6]^{2-}$ were transformed into $[(NH_3)_4Pd]^{2+}$, therefore, it could be effectively deposited

on the surface of WO_3 [8-10]. In a typical process, 1 g of a WO_3 support powder obtained from the calcination of WO_3•$2H_2O$ at 300ºC for 2 h was dispersed in an aqueous solution of H_2PdCl_4 containing the designed Pd loading amount 0.12%, 0.5% and 0.74% by weight percent. Hereafter, it was referred as 0.12 Pd/WO_3, 0.5 Pd/WO_3 and 0.74 Pd/WO_3, respectively. The starting solution's pH was around 3. The suspension was stirred for 4 h and aged at room temperature for 1 h and then 30 mL ammonia solution (1 M, pH=10) was added and stirred. The solids were washed with 0.5 L distilled water for two times by filtration. After drying at 80ºC for 12 h in air, Pd-loaded WO_3 powders were obtained. Figure 3-3 shows a typical procedure of preparing Pd-loaded WO_3 nanoparticles.

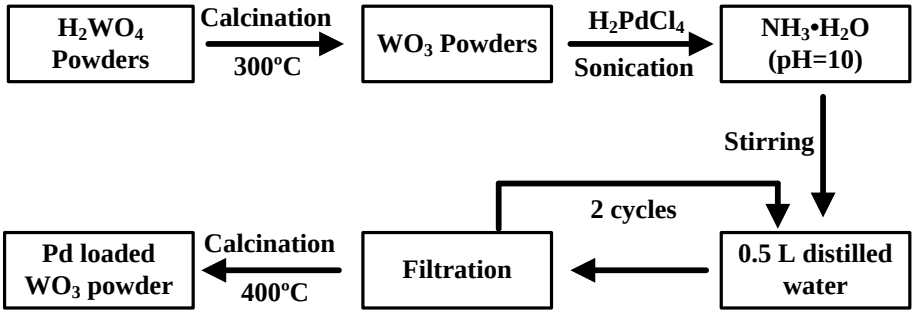

Figure 3-3 the process for the deposition of Pd on WO_3 surface.

3.2.2 Characterization Techniques

The loading amount of Pd was determined by an inductively coupled plasma atom emission spectroscopy (ICP-AES; SPS1700 HVR, Seiko instruments, Japan). The sample powders with and without calcination were dissolved into aqua regia and agitated for 24 h for a good dissolution of Pd. The microstructural properties were characterized by XRD, FE-SEM and TEM using the same procedure as that of neat WO_3 nanoparticles. The sensor devices were prepared by the scree-printing and the sensing properties were tested by the same sensing apparatus and the exactly same way as that in Chapter 2.

3.3 Results and Discussion

3.3.1 Materials characterizations

The phase structures of Pd-loaded WO_3 nanoparticle powders are characterized by X-ray diffraction as shown in Fig. 3-4. All samples exhibited the same pattern corresponding with the monoclinic WO_3 (JCPDS 43-1035) and there were no visible changes with Pd-loading. No peaks corresponding to either metallic or oxidized Pd could be detected. This could be due to the small loading amount for the detection of XRD or the fine dispersion of Pd on the surface.

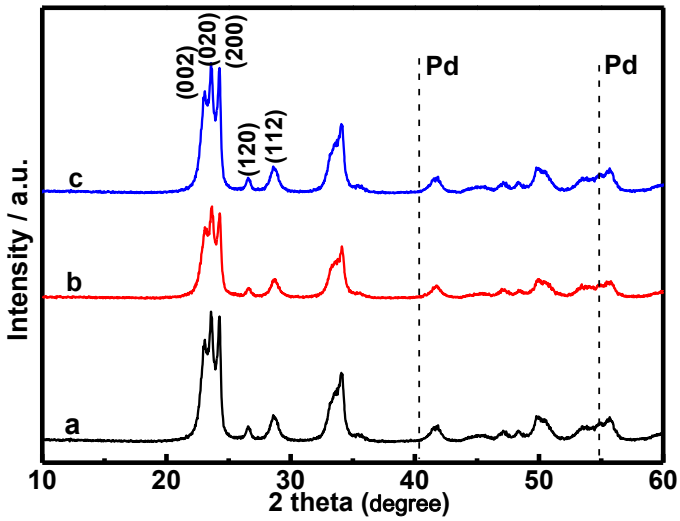

Figure 3-4 XRD patterns of (a) neat, (b) 0.12 and (c) 0.74 wt.% Pd-loaded WO_3.

To decide the loading amount, ICP-AES experiments were carried out. Figure 3-5 shows the deposition amount of Pd as a function of the concentration of the precursor solution. It is quite obvious that after two times of washing treatment, only a very few amount of Pd can be detected, which is consistent with the above XRD observations. Most of the Pd was lost due to the treatment of filtering. The loading amount took a maximum value of 0.74 wt.% at the concentration of 1.5×10^{-3} M for the precursor. A further increase in the precursor concentration; however, resulted in a decrease in the loading amount.

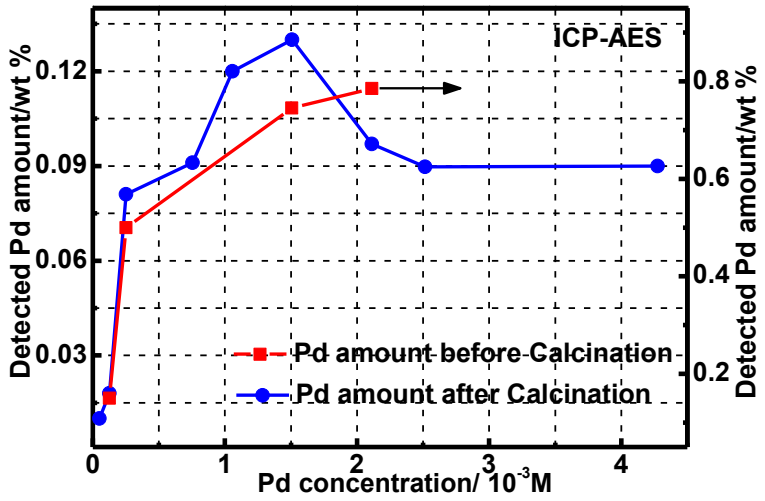

Figure 3-5 Pd-loading amounts as a function of the precursor's concentration.

It was believed that a relatively low detected amount can be ascribed to the small surface area of WO_3 support (25.8 m^2/g calcined at 300 ºC.). During the washing treatment, most of Pd species remaining in the solutions were removed to prevent the precipitation of Pd forming large particles (cluster). Additionally, ammonia treatment was also effective to eliminate the chlorine residues after impregnation [27]. It was found that after a sintering at 400 ºC for 2 h in air, the loading amount detected by ICP-AES significantly decreased comparing with that before sintering. This suggested that Pd on the surface was not completely dissolved into the aura regia by the present method, which could be one of reasons for the low detected amount.

Figure 3-6 shows the FE-SEM images of neat and Pd-loaded WO_3 nanoparticles. Apparently, the nanoparticles powders were consisted of a numerous of irregular planar-like particles. These particles are loosely and randomly stacked together, resulting in a large mesoporous structure, resulting in a good diffusion process of gas molecules [11].

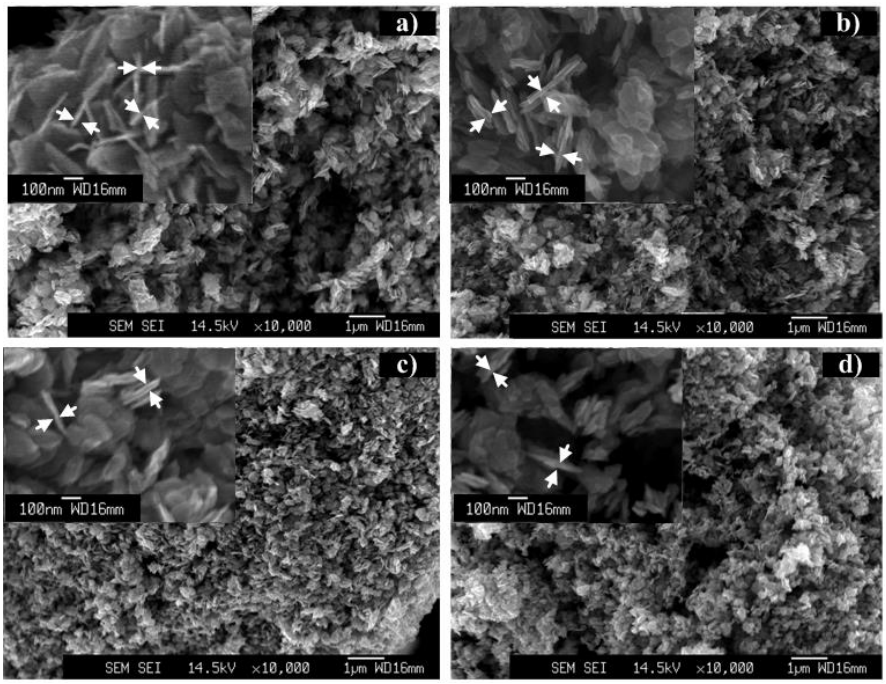

Figure 3-6 FE-SEM images of WO_3 nanoparticles with (a) 0, (b) 0.15, (0.5) and (d) 0.74 wt.% of Pd-loading (The inset is a corresponding high magnification image).

It was estimated from the inset high magnification SEM images that the lateral size is around 100-200 nm with a thickness 10-30 nm. It seemed that the particle size was reduced by Pd-loading because a slight part of WO_3 was dissolved by the ammonium solution during the washing treatments [12]. However, there were no obvious changes for the surface area and pore structure.

Table 3-1 BET surface area and pore volume of neat and Pd-loaded WO_3.

Loading amount (wt.%)	**BET surface area (m^2g^{-1})**	**Pore volume (m^3g^{-1})**
0	19	4.4
0.15	21	4.3
0.5	19	4.9
0.74	21	4.8

Table 3-1 summarizes the BET surface area and pore volume as a function of Pd loading amount for WO_3 nanoparticle powders. All the samples demonstrate a similar value of surface area *ca*. 19 m^2/g with a pore volume around 4.5 cm^3/g.

The morphology of the nanoparticles and the loading state of Pd were further analyzed by TEM. Figure 3-7 shows typical TEM images of the fabricated nanoparticles. One could easily find that the Pd-loaded WO_3 nanoparticles also demonstrated a highly irregular shape similar with neat WO_3.

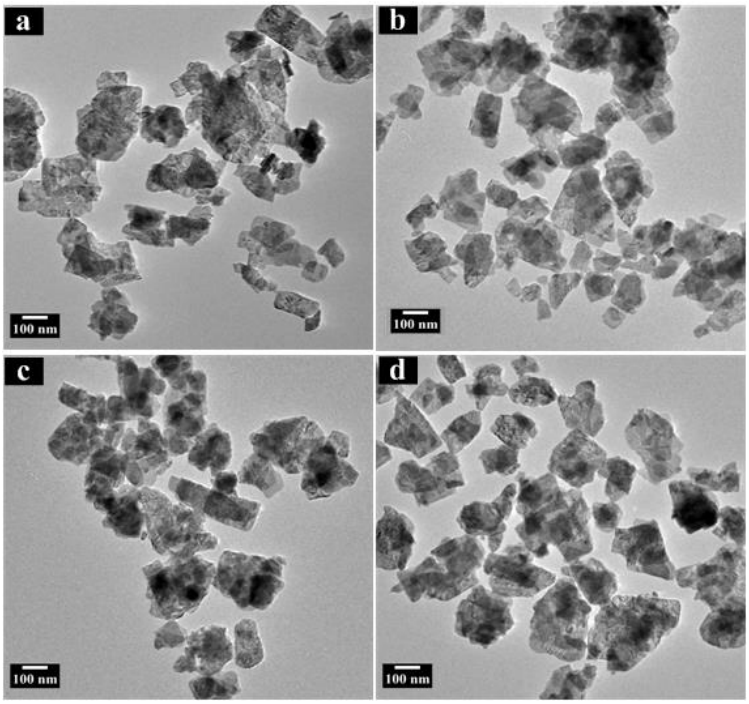

Figure 3-7 TEM images of WO_3 nanoparticles with (a) 0, (b) 0.15, (0.5) and (d) 0.74 wt.% of Pd-loading.

No significant changes in either size or shape were distinguished with Pd-loading. In addition, it was really difficult to observe the presence of Pd from the TEM images due to the small loading amount or the small size.

To study the loading state of Pd, HRTEM, HADDF-STEM and EDX mapping were carried. Figure 3-8 is the HRTEM images of 0.74 Pd-WO_3.

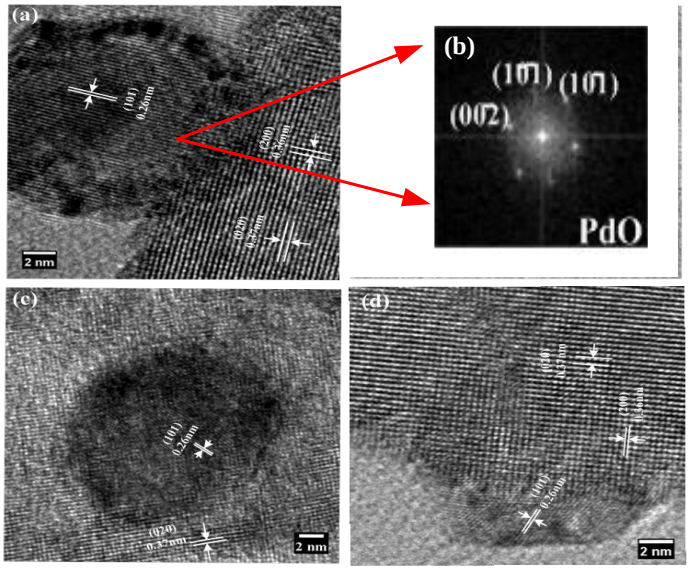

Figure 3-8 HRTEM of 0.5 Pd-loaded WO_3 and the corresponding FFT pattern.

The appearance of Pd can be easily observed. However, it was very difficult to detect the presence of Pd for the lowest Pd-loading samples, i.e., 0.15 Pd/WO_3. The measured lattice spacing for the particles attached on the surface of WO_3 was in good agreement with (101) plane of tetragonal PdO (JCPDS 03-0515). This was consistent with the FFT pattern indexed in Figure 2-13 (d). Additionally, it was found that the number of the particles detected was quite small and the particle size range from 2 nm to about 15 nm. In the present case, we could not detect the metallic form of Pd, which is consistent with other reports that Pd is really oxidized in air.

Figure 3-9 shows a typical STEM image of 0.74 Pd-loaded WO_3 nanoparticles. It was found that STEM was really effective to reveal the deposition of Pd. The white points in the image clearly showed the size and position of Pd and confirmed by the EDX mapping. However, the number of particles was quite small number with broad distribution in size.

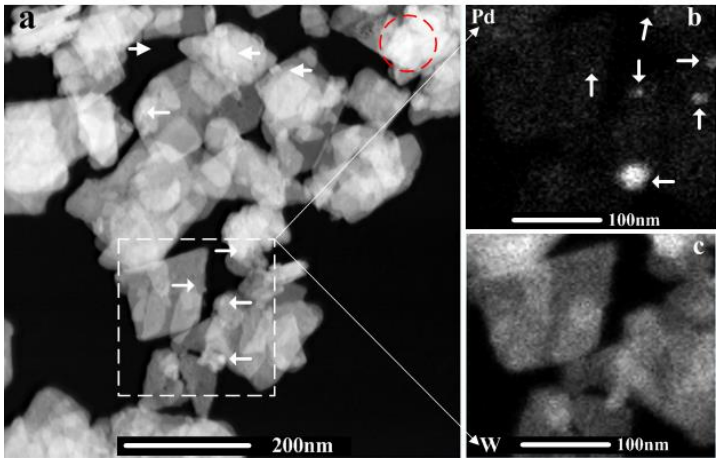

Figure 3-9 HAADF-STEM (a), EDX mapping of Pd (b) and W (c) of the 0.74 Pd-WO_3 nanoparticles.

Figure 3-10 shows the EDX spectra of the white points appeared on the surface of WO_3 nanoparticles, which clearly demonstrated the efficiency of STEM to observe the small and rare Pd nanoparticles. Also these images confirmed that the present modified impregnation method was really effective for the loading process of Pd [12].

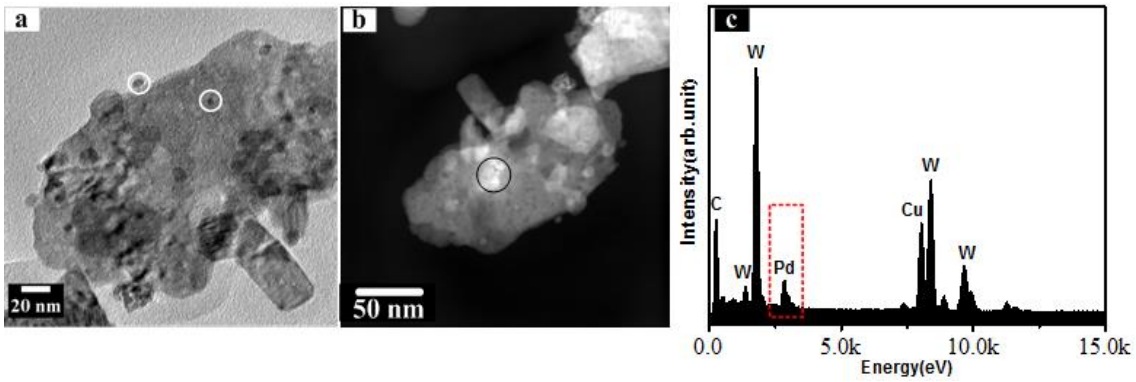

Figure 3-10 (a) TEM, (b) HADDF-STEM and (c) EDX spectra of 0.74 Pd-WO_3.

Here, we would like to stress that Pd particles in large size have been observed on the surface; nevertheless, the number is quite small. According to ICP-AES results, it is reasonable to propose that there is a distribution of Pd on surface with size at an atomic scale beyond the limit of the electron microscopy [12]. For a long time, it has been accepted that the catalyst on surface in small size is much

more effective for catalytic and sensing process [13-14].

3.3.2 Sensing results

Sensing properties of Pd-WO_3 gas sensors for inflammable gases (H_2, CO and CH_4) were measured and compared with the neat WO_3 sensors. Figure 3-11 shows the square of sensor response of hydrogen in a small concentration ranging from 30 ppm to 200 ppm.

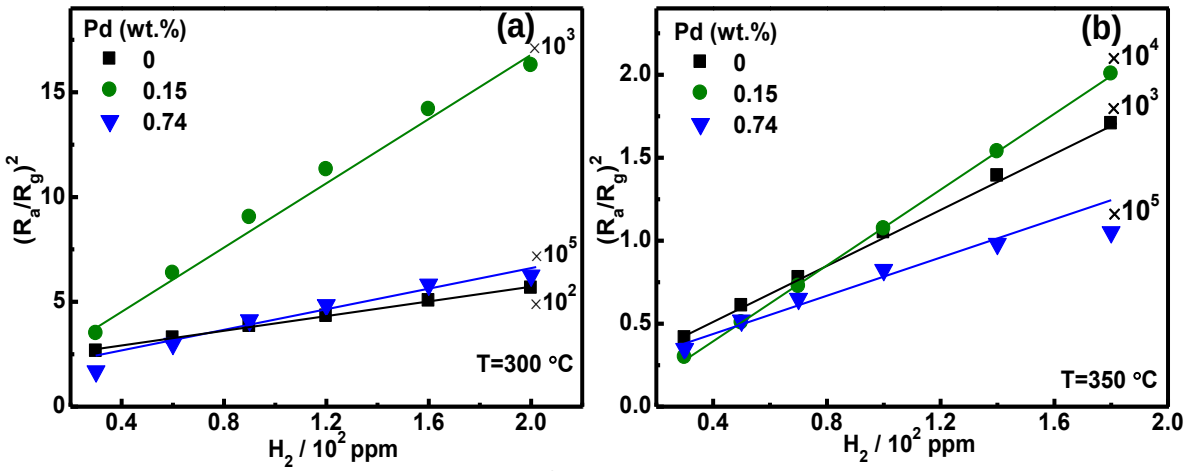

Figure 3-11 The linear plot of $(R_a/R_g)^2$ with of P_{H2} at (a) 300 ºC and (b) 350 ºC.

It could be seen that Pd-loading significantly promoted the sensing response and a linear fit of $(R_a/R_g)^2$ with P_{H2} was evidenced for all of sensors, indicating a reaction of H_2 with O^- on the surface. Figure 3-12 shows the plot of $(R_a/R_g)^2$ with P_{H2} at a concentration region. Interestingly, it was found that the sensor response was greatly improved, however, the linearity of $(R_a/R_g)^2$ with P_{H2} was lost for 0.5 and 0.74 wt.% Pd-loaded WO_3 gas sensors. However, for neat and 0.15 wt.% Pd-loaded WO_3 sensors, the linearity was clearly evidenced for all of concentrations and temperatures. It was believed that the degenerated linearity was caused a catalytic combustion of H_2 on the surface, leading to a reduction of gas diffusion [2, 12-13]. Additionally, the catalytic of H_2 on the surface resulted in a poisoning effect of water vapor and decrease of sensor response [2, 14-16].

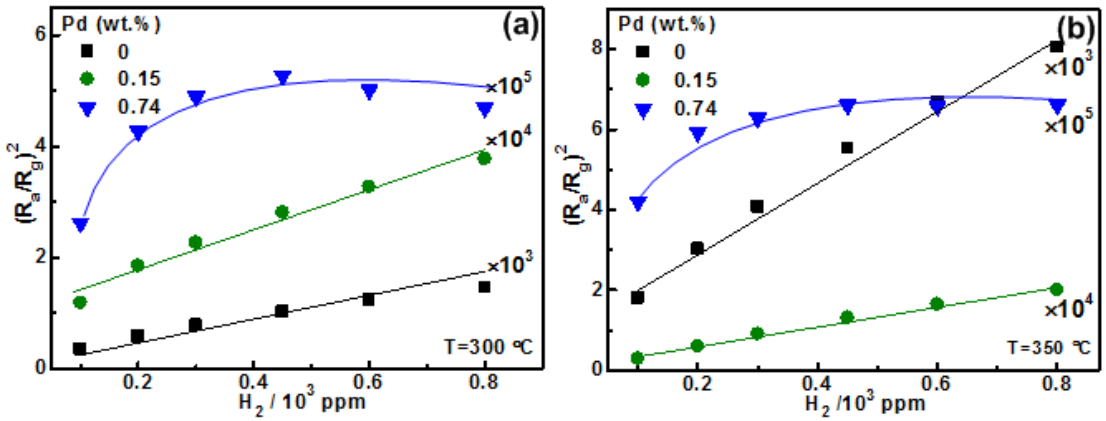

Figure 3-12 $(R_a/R_g)^2$ as a function of P_{H2} at (a) 300 ºC and (b) 350 ºC.

Figure 3-13 shows the square of sensor response as a function of CO. It could be observed that the sensor response was obviously promoted by Pd-loading at both temperatures. At 300 ºC, the sensor response of neat WO_3 was only 11.6 for 200 ppm CO; however, it was rise up to 388 with 0.5 wt.% of Pd-loading. However, it was found that the sensor response was decreased with increasing temperature for Pd-loaded WO_3 gas sensors. The sensor response of 0.5 Pd-WO_3 was decreased from 388 at 300 ºC to 243 at 350 ºC for 200 ppm CO. In contrast, the neat WO_3 sensor demonstrated an increase of sensor response with rising temperature from 300 ºC to 350 ºC. It was also observed that a linearity of $(R_a/R_g)^2$ with P_{CO} was evidenced for neat WO_3 at both temperatures, however, Pd-loaded WO_3 sensors exhibited a linearity below 600 ppm. Further increasing CO concentration, the linear relationship was lost. It was proposed that such a behavior could be caused a different sensing mechanism, which will be discussed in detail in chapter 4.

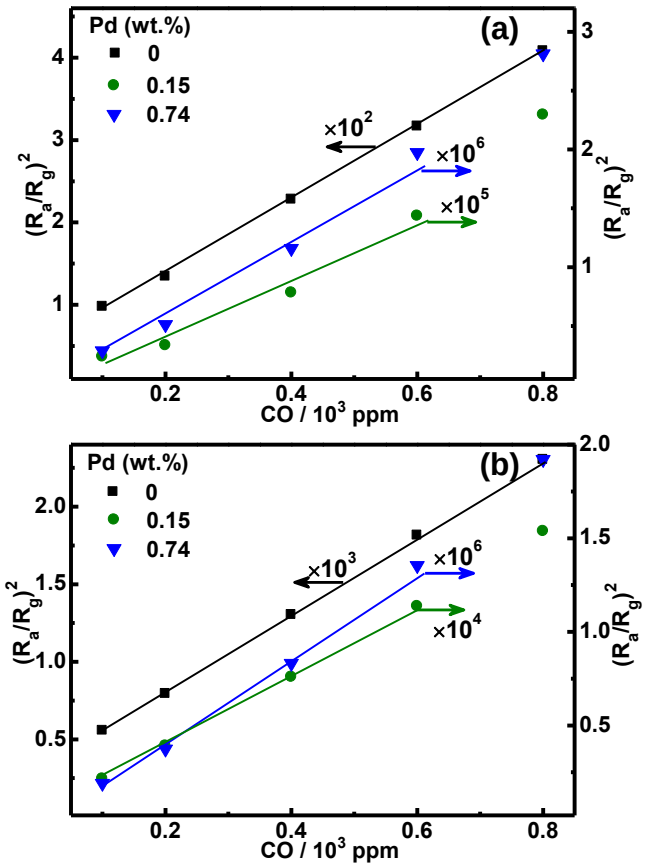

Figure 3-13 $(R_a/R_g)^2$ as a function of CO concentration at (a) 300 ºC and (b) 350 ºC.

Figure 3-14 represents the sensor response as a function of concentration of CH_4. It was found that the sensing response to CH_4 was also obviously improved by Pd-loading. A response of 6.9 to 200 ppm CH_4 was obtained for neat WO_3 sensor at 350 ºC; however, it was increased to 55.3 with 0.5 wt.%. The sensor response of CH_4 was much smaller than that of H_2 and CO for both neat and Pd-loaded WO_3 sensors at the same temperature and concentration. It was suggested such a difference in sensor response could be due to a different sensing mechanism between CH_4 and CO, H_2. This will be explained in next chapter.

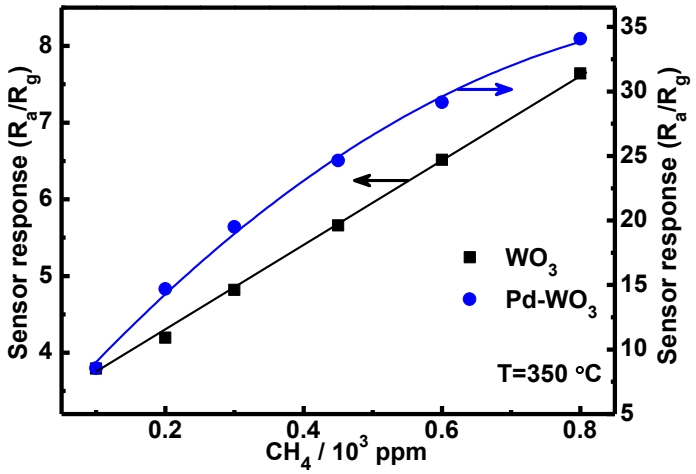

Figure 3-14 Sensor response as a function CH_4 concentration for neat and Pd-loaded WO_3 gas sensors at 350 ºC.

The sensing properties of Pd-loaded sensors in wet condition were also investigated. For simplicity reason, only 0.5 Pd-WO_3 sensor was used and its sensing properties were compared with the neat WO_3 sensor. Figure 3-15 (a) shows the sensing response of H_2 for neat and 0.5 Pd-WO_3 sensors under 1 VOL.% and 2 VOL.% humidity condition.

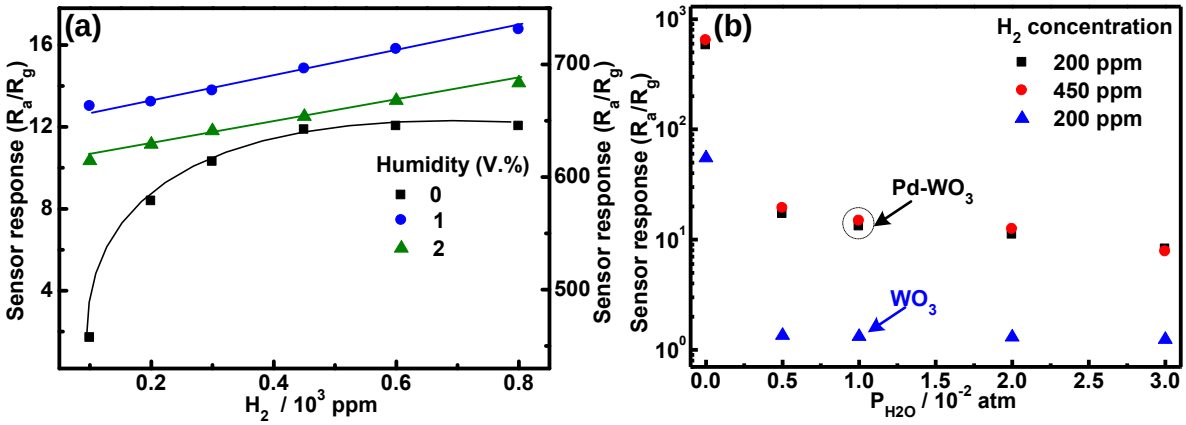

Figure 3-15 sensor response of 0.5 Pd-WO_3 as a function of H_2 concentration with presence of water vapor at 350 ºC.

It was quite clear that the sensor response was greatly decreased with the presence of water vapor at 350 ºC. With 1 VOL.% of humidity, the sensor response of 0.5 Pd-loaded WO_3 was decreased from 579 in dry down to only 13 for 200 ppm H_2. The sensor response was further reduced with increasing

humidity; however, the reduction became much moderate. In addition, there was no saturation in the sensing response up to 800 ppm. Figure 3-15 (b) shows the dependence of sensor response on humidity at 350 ºC for 200 and 450 ppm H_2. It can be seen that the sensor response is significantly deteriorated with increasing humidity; however, Pd-loaded WO_3 sensor still showed a much higher sensor response, which was around 6 times of neat sensor in wet condition.

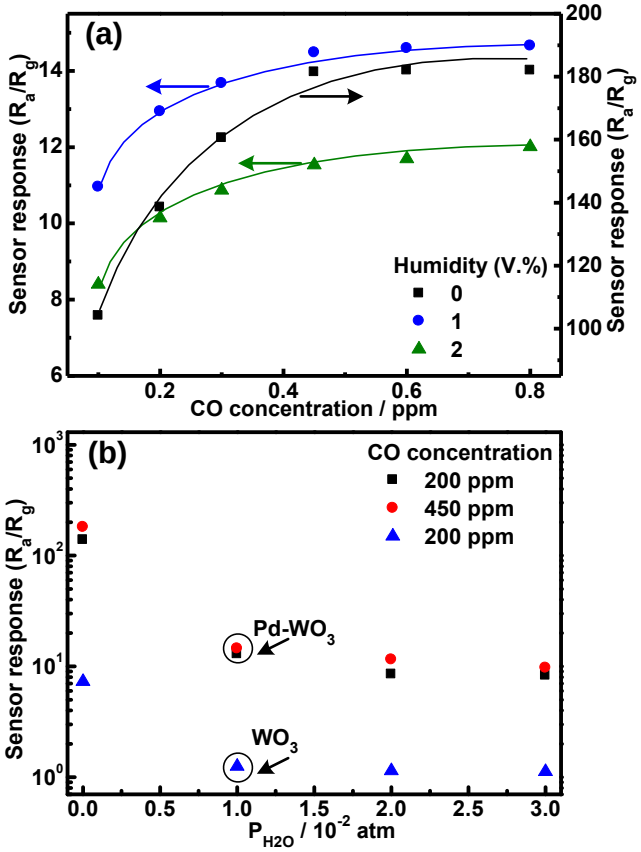

Figure 3-16 sensor response to 200 and 450 ppm CO for both Pd-loaded and neat WO_3 sensors as a function of humidity at 350 ºC.

The sensing properties of CO in the presence of humidity were also investigated. Figure 3-16 (a) shows the sensor response of CO for Pd-loaded WO_3 sensor with 1 VOL.% and 2 VOL.% humidity at 350 ºC. Comparing with the dry condition, the sensor response was obviously reduced by around 10 times. Additionally, it was found that the sensor response in wet condition was much

closed with that of H_2; however, in dry atmosphere, the sensor response for H_2 was much larger than that of CO. Figure 3-16 (b) shows the sensor response to 200 and 450 ppm CO as a function of humidity. It was quite obvious that the sensing response for CO was significantly degenerated by water poisoning effect.

Similarly, the sensor response to CH_4 with presence of humidity was also greatly reduced comparing that of dry condition. Figure 3-17 (a) represents the sensor response as a function of CH_4 concentration with 1 and 2 VOL.% humidity. Obviously, the sensing response was greatly reduced by water vapor and all the sensing response was less than 2.

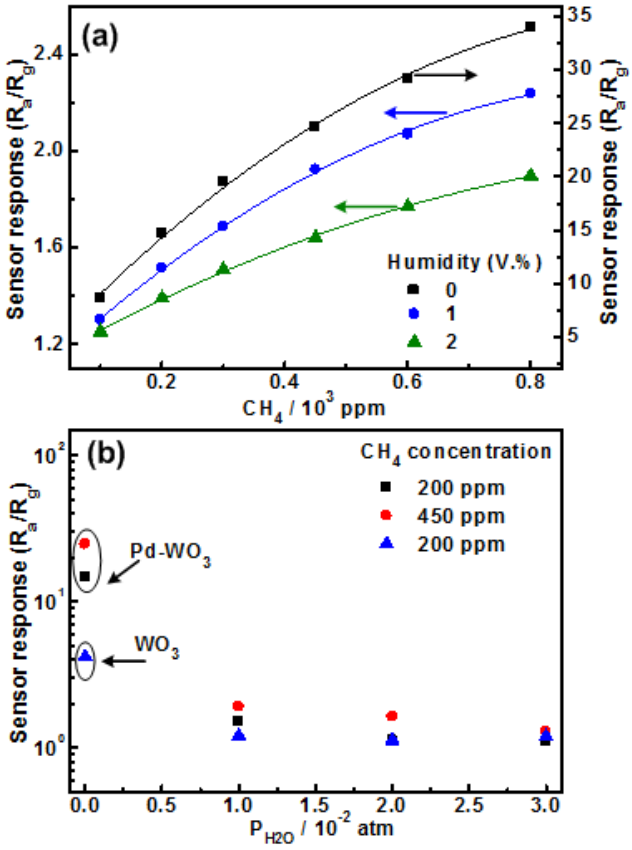

Figure 3-17 sensor response of 0.5 Pd-WO_3 as a function of CH_4 concentration with presence of water vapor at 350 ºC.

Figure 3-17 (b) shows the dependence of humidity on the sensor response of CH_4. One could easily observe that the sensor response to CH_4 in wet condition was

extremely small and almost neglectable for both neat and Pd-loaded WO_3 sensors.

3.4 Conclusions

The main results and conclusion of Pd-loading on the microstructural and sensing properties of WO_3 nanoparticles gas sensors are listed below.

- The highly acidic surface of WO_3 is not suitable for a conventional impregnation of Pd. Pd has loaded on the surface of nanoparticles by the modified impregnation method; however, the loading amount was quite low after filtration due to a small surface area of WO_3 support.
- Pd nanoparticle was evidenced on the surface with a broad distribution of particle size ranging from around 2 to 20 nm; nevertheless, the number of detected nanoparticles was relatively small. The large Pd nanoparticle was in oxidized state evidenced by HRTEM. There was no obvious difference on the shape and size of WO_3 nanoparticles with Pd-loading.
- Comparing with the neat WO_3 sensor, it was found that the sensing response of inflammable gases was greatly promoted with Pd-loading with a sequence of H_2, CO and CH_4. Under dry condition, Pd-loaded WO_3 sensor showed a much larger response to H_2, which were more than 2 orders of that of neat WO_3 sensor.
- The sensor response of Pd-loaded significantly decreased with the presence of humidity, with 1VOL.% humidity, the sensor response was reduced more than 10 times for all the three inflammable gases. However, the Pd-loaded WO_3 still showed a much higher sensor response than that of neat WO_3 with wet background.

References

[1] J. Kappler, N. Barsan, U. Weimar, A. Dieguez, J. L. Alay, A. Romano-Rodriguez, W. Göpel, Correlation between XPS, Raman and TEM measurements and the gas sensitivity of Pt and Pd doped SnO_2 based gas sensors. Fresenius' journal of analytical chemistry, 361 (1998): 110-114.

[2] S. Matsushima, T. Maekawa, J. Tamaki, N. Miura, N. Yamazoe, New methods for supporting palladium on a tin oxide gas sensor, Sensors Actuators B: Chemical 9 (1992), 71-78.

[3] D. Koziej, M. Hübner, N. Barsan, U. Weimar, M. Sikora, J.D. Grunwaldt, Operando X-ray absorption spectroscopy studies on Pd-SnO_2 based sensors, Phys. Chem. Chem. Phys., 11-38 (2009): 8620–8625.

[4] M. Hübner, D. Koziej, M. Bauer, N. Barsan, K. Kvashnina, M. D. Rossell, J. D. Grunwaldt, The Structure and Behavior of Platinum in SnO_2-Based Sensors under Working Conditions, Angewandte Chemie International Edition, 50 (2011): 2841-2844.

[5] M. Ando, S. Suto, T. Suzuki, T. Tsuchida, C. Nakayama, N. Miura, N. Yamazoe, H_2S and CH_3SH Sensor Using a Thick Film of Gold-Loaded Tungsten Oxide, Chemistry Letters, 2 (1994): 335-338.

[6] T. Maekawa, J. Tamaki, N. Miura, N. Yamazoe, Promoting effects of noble metals on the detection of ammonia by semiconductor gas sensor, Studies in Surface Science and Catalysis, 77 (1993) 421-424.

[7] S. Ivanova, C. Petit, V. Pitchon, A new preparation method for the formation of gold nanoparticles on an oxide support, Appl. Catal. A, 267 (2004): 191-201.

[8] M. Schreier, J. R. Regalbuto, A fundamental study of Pt tetraammine impregnation of silica 1. The electrostatic nature of platinum adsorption, Journal of Catalysis 225 (2004): 190-202.

[9] J. R. Regalbuto, A. Navada, S. Shadid, M. L. Bricker, Q. Chen, An Experimental Verification of the Physical Nature of Pt Adsorption onto Alumina, Journal of Catalysis, 184 (1999): 335-348.

[10] J. T. Miller, M. Schreier, A. Jeremy Kropf, J. R. Regalbuto, A fundamental study of Pt tetraammine impregnation of silica 2. The effect of method of preparation, loading, and calcination temperature on (reduced) particle size, Journal of Catalysis, 225 (2004): 203-212.

[11] T. Kida, A. Nishiyama, Z. Hua, K. Suematsu, M. Yuasa, K. Shimanoe, WO_3 Nanolamella Gas Sensor: Porosity Control Using SnO_2 Nanoparticles for Enhanced

NO_2 Sensing, Langmuir, 30 (2014): 2571-2579.

[12] Z. Hua, M. Yuasa, T. Kida, N. Yamazoe, K. Shimanoe, High sensitive gas sensor based on Pd-loaded WO_3 nanolamellae, Thin Solid Films, 548 (2013) 677-682.

[13] M. Hübner, N. Bârsan, U. Weimar, Influences of Al, Pd and Pt additives on the conduction mechanism as well as the surface and bulk properties of SnO_2 based polycrystalline thick film gas sensors. Sensors and Actuators B: Chemical, 171 (2012): 172-180.

[14] J. M. McAleer, J.T. Moseley, J. O. Norris, D. E. Williams, B. C. Tofield, Tin dioxide gas sensors. Part 2.-The role of surface additives, Journal of the Chemical Society, Faraday Transactions, 184 (1988): 441-457.

[15] Z. Hua, M. Yuasa, T. Kida, N. Yamazoe, K. Shimanoe, H_2 sensing mechanism of Pd-loaded WO_3 nanoparticles gas sensors, Chemistry letters, 2014 (dx.doi.org/10.1246/cl.140396).

[16] N. Yamazoe, K. Suematsu, K. Shimanoe, Extension of receptor function theory to include two types of adsorbed oxygen for oxide semiconductor gas sensors, Sensors and Actuators B: Chemical, 163 (2012):128-135.

CHAPTER 4

4 Oxygen Adsorption and Interaction with Neat and Pd-loaded WO_3 Sensors

In this chapter, the surface process of gas sensing for inflammable gases was studied based on the adsorption and interaction properties of oxygen with WO_3. The adsorption and interaction of oxygen was mainly investigated through the resistive response of oxygen coupled with TPD measurements. The oxygen adsorption properties were found no difference with Pd-loading, which was really weak. However, it was revealed that the interaction of oxygen with sensor surface in the presence of inflammable gases was significantly different with Pd-loading and gas atmospheres. Thus, it was suggested that Pd-loading not only promoted the sensing response but also changed the sensing mechanism. In addition, the sensing mechanism was also different with partial pressure of oxygen and inflammable gases.

4.1 Introduction

According to the introduction part, oxygen adsorbed on the surface of MOS sensors plays a vital role in the sensing process to inflammable gases. It reacts with gas molecules as receptor function, in other hand, the adsorbed oxygen leading to a surface barrier severs as transducer function [1-3]. Therefore, the study of oxygen adsorption and interaction is one of effective approaches to clarify the sensing mechanism of inflammable gases. In present study, the oxygen adsorption properties were investigated by the resistive response and TPD

measurements [4]. However, it should be stressed that the surface adsorbed oxygen is not the only resources of sensing response of reducing gases. It was suggested that the surface lattice oxygen can also react with reducing gas molecules, leading to a sensing response [4-7]. Thus, the role of adsorbed oxygen in sensing process of inflammable gases should be clarified. One of the effective and simple approaches is the resistive response properties of oxygen in the presence of inflammable gases [4]. In this chapter, the resistive properties of oxygen were studied in the presence of inflammable gases (H_2, CO and CH_4) with different partial pressure of oxygen (P_{O2}).

4.2 Experimental Details

Temperature programmed desorption (TPD) performed in a flow of He (50 mL min^{-1}) at a ramping rate of 10 ºC min^{-1} (BEL-CAT, BEL Japan) up to 500 ºC. The sample powders (0.1 g) were packed in a tubular quartz reactor and heat-treated at 400 ºC for 30 min in a flow of air. After cooling down to 50 ºC in air and the TCD (thermal conductivity detector) and mass spectrometer (MS, GDS30102 PFEIFFER VACUUM) were stabilized for 3 h in He before the TPD measurements. The desorbed gases were continuously monitored by the MS. Figure 4-1 shows the procedure for the treatment and measurements of TPD.

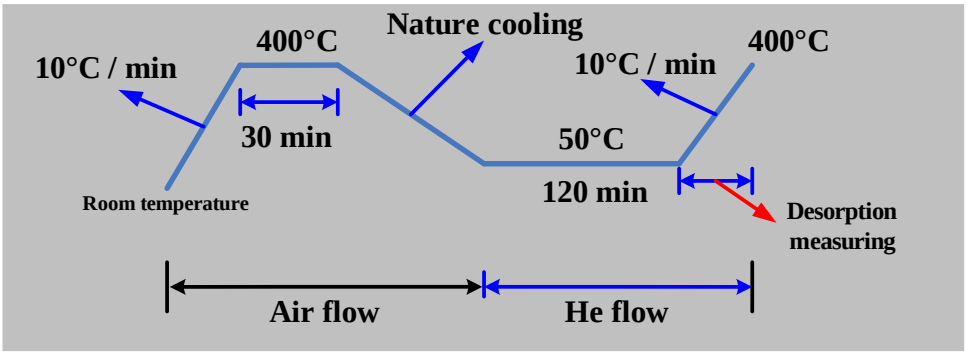

Figure 4-1 the procedures of pretreatments and measurements of oxygen TPD for neat and 0.5 Pd-loaded WO_3 nanoparticles powders.

For the resistive sensing measurements, the sensor fabrication and testing were same as the previous chapters. However, only neat and 0.5 Pd-loaded WO_3 sensors were studied in this chapter for the sake of simplicity (hereafter the loaded WO_3 referred as Pd-WO_3). The dependence of sensor resistance on P_{O2} with the presence of inflammable gases was measured by fixing the concentration of different inflammable gases and control the partial pressure of oxygen balanced with pure N_2. The partial pressure of oxygen (P_{O2}) was continuously monitored by a home-made oxygen sensor as shown in Fig. 2-3.

4.3 Results and Discussion

4.3.1 Oxygen adsorption behavior

As discussed in the introduction part, oxygen resistive responses allow us a probe to study the basic interaction process of oxygen with WO_3 surface. Based on the volume depletion theory proposed by N. Yamazoe, et. al., a linear plot of sensor resistance with $(P_{O2})^{\alpha}$ not only reveals the adsorption species but also the adsorption strength [2-3]. Therefore, in the present study, the oxygen resistive responses were used for the investigation of oxygen adsorption. The sensor resistance was measured with different partial pressure of oxygen at 300 and 350 ^{o}C. Different P_{O2} was obtained by mixing oxygen with N_2 and calibrated with our home-made oxygen sensor from 0.05 to 1 atm. For each P_{O2}, the sensor resistance was stabilized for 90 min to reach a quasi-equilibrium state and recorded as shown in Figure 4-2. However, a complete equilibrium state of resistance cannot be obtained even several hours later. For each test, two same samples were investigated to ensure a reliability of date.

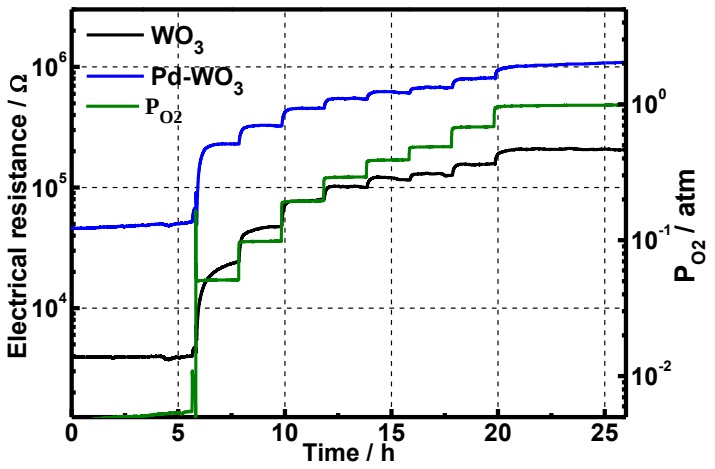

Figure 4-2 a typical transient of sensor resistance for neat and Pd-WO_3 for oxygen adsorption study at 350 ºC.

The linear plot of sensor resistance with P_{O2} is clearly evidenced at 350 ºC for both sensors as shown in Fig. 4-3 (a). According to equation 1.6-1.7, it was suggested that superoxide ion (O_2^-) was the form of oxygen adsorption for both pure and Pd-loaded WO_3 sensors.

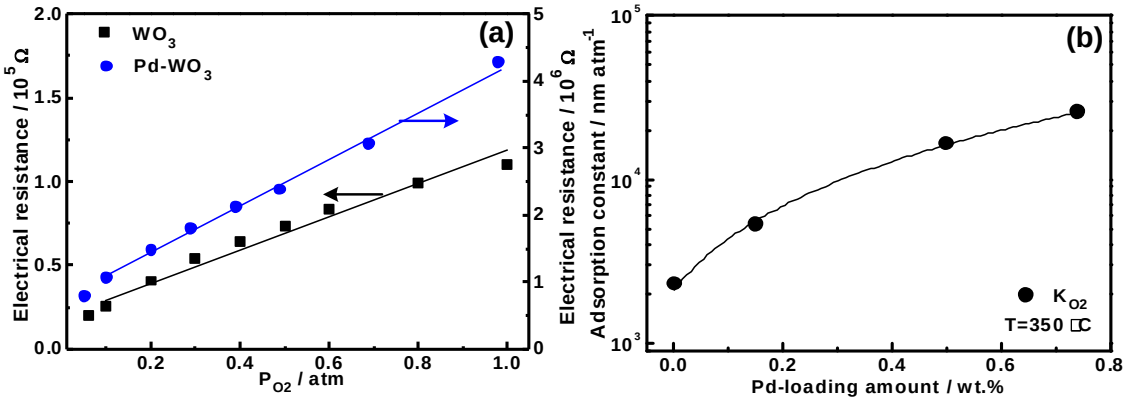

Figure 4-3 (a) the linear dependence of sensor resistance of neat and Pd-WO_3 on P_{O2} and (b) the calculated oxygen adsorption constant (k_{O2}) as a function of the amounts of Pd-loading at 350 ºC.

The sensor resistance was greatly increased more than one order with Pd-loading, indicating a good electronic interaction of PdO with metal oxide i.e. the P-N junction [8-9]. It was suggested that Pd-loading has no changes on the species of adsorption [4].

According to the linear fit in Figure 4-3 (a), the oxygen adsorption on the

surface can be described by:

$$O_2 + e \underset{k_{-1}}{\overset{k_1}{\Leftrightarrow}} O_2^- \qquad \textbf{(R4.1)}$$

Where, k_{01} and k_{-01} are the reaction constant for forward and reverse reaction, respectively. The adsorption strength expressed by the reaction constant K_{O2} ($K_{O2}=k_{01}/k_{-01}$) in R4.1 can be roughly estimated from the linear fit based on equation 1.7. Then adsorption constant can be written in terms of fit slope (k_α) as $k_\alpha=(K_{O2}\cdot a)$, where a=5 nm, the half thickness determined from HRTEM image in Fig. 2-7. However, to precisely determine the slope, R_0 should be obtained. It has been reported that the flat band resistance can be considered as sensor resistance in N_2 (R_{N2}) [2-3, 5]. Consequently, the calculated K_{O2} was obtained and shown in Fig. 4-3 (b). It was quite obvious that the adsorption constant was significantly increased with the loading amount. In other words, the electronic interaction of oxygen with WO_3 surface has been enhanced by Pd-loading through the P-N junction effect [8-9]. In addition, it was proposed that Pd-loading could promote the oxidization states of sensor surface, which could also explain the enhanced interaction of oxygen with WO_3 surface [4].

The oxygen adsorption properties in wet condition were also investigated based on the resistive response. Figure 4-4 shows the sensing resistance in oxygen (R_{O2}) as a function of P_{O2} with 1 VOL.% and 2 VOL.% humidity. It seems that the plot of R_g with P_{O2} was linear similar with dry conditions indicating that oxygen adsorbed on the surface was superoxide ion (O_2^-) [1]. However, it should be point out that such a conclusion only be valid at a deep depletion state of WO_3 nanoparticles. Due to the block effect of water vapor for oxygen adsorption, the linear plot was used at high partial pressure of oxygen to

guarantee a deep depletion state (volume depletion).

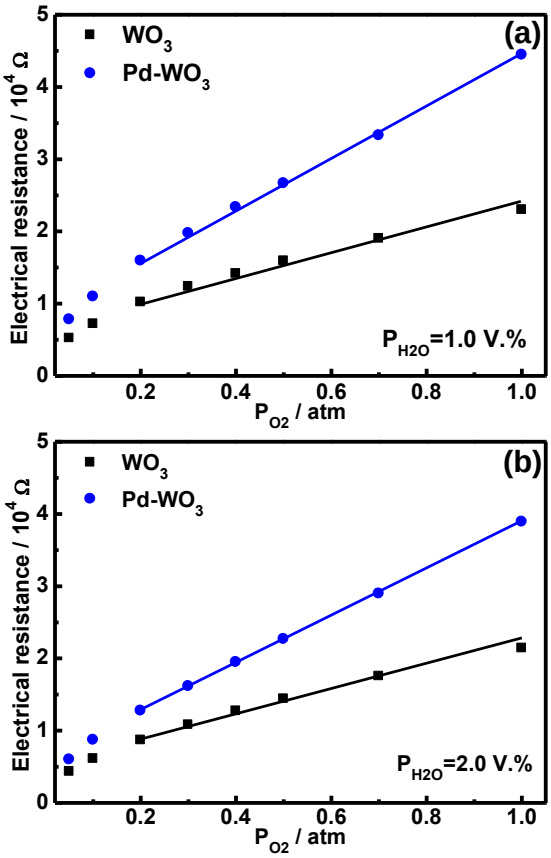

Figure 4-4 linear plot of R_{O2} with P_{O2} in the presence of (a) 1 VOL.% and (b) 2 VOL.% humidity at 350 ºC.

The adsorption constants were obtained by the linear fit of R_{O2} with P_{O2} in different humid atmospheres as shown in Fig. 4-2, and the calculation procedure is same as that under dry condition. It was quite clear that the adsorption constants were significantly decreased with increasing humidity. In other words, the electronic interaction of oxygen with WO_3 surface was reduced by water vapor. It was proposed that oxygen adsorption was blocked by the chemical dissociation of water molecules on WO_3 surface [4, 10]. In addition, the effect of Pd-loading on sensor resistance was not obvious comparing that for dry condition. The sensing resistance of Pd-WO_3 sensor was just about 2 times higher than that of neat WO_3 sensor. In contrast, the sensor resistance of Pd-WO_3 was one order

of neat WO_3 sensor under dry condition. In other words, the interaction of Pd with WO_3 was reduced by water vapor. This was also evidenced by the adsorption constants as shown in Fig. 4-5. This could be caused by the blocking of water vapor for oxygen adsorption, which could give a different chemical state of Pd with that in dry condition.

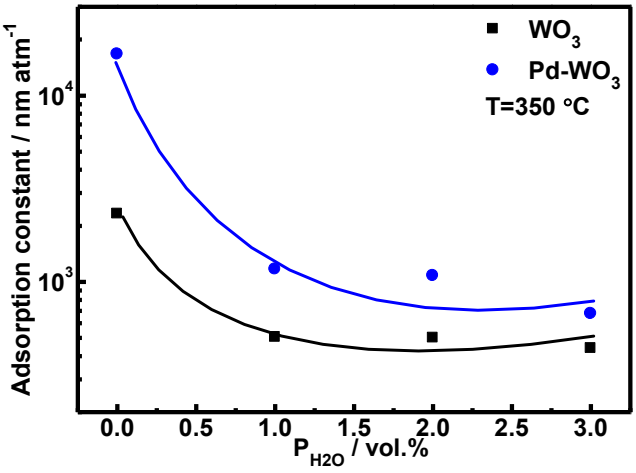

Figure 4-5 oxygen adsorption constant as a function of humidity for neat and Pd-WO3 sensors at 350 ºC.

To further study the oxygen adsorption properties, O_2-TPD experiments were carried out on nanoparticles powders. Figure 4-6 shows the TCD and mass spectra of oxygen desorption for neat and Pd-loaded WO_3 nanoparticles powders. There was only one peak observed around 200 ºC in the spectra. The MS suggests that oxygen desorption peak at 213 ºC, indicating the adsorption oxygen in O_2^- form [11] and no difference with Pd-loading. Therefore, it was proposed that the changes of TCD peaks were mainly associated with desorption of water adsorbed on the sample holder and gas lines. In addition, it was found that oxygen desorption peak was relatively low revealing a small amount of oxygen adsorption. The adsorption amount was calculated from the mass spectroscopy and found no increase with Pd-loading as illustrated in Table 3-1. This conclusion

is highly consistent with our previous result that the oxygen adsorption is really weak on WO_3 [12]. However, we want to stress that the precise analysis of oxygen desorption amount is suffered from a large desorption of water. Actually, in the present case, water is the main desorption species and the amount is much larger than the oxygen.

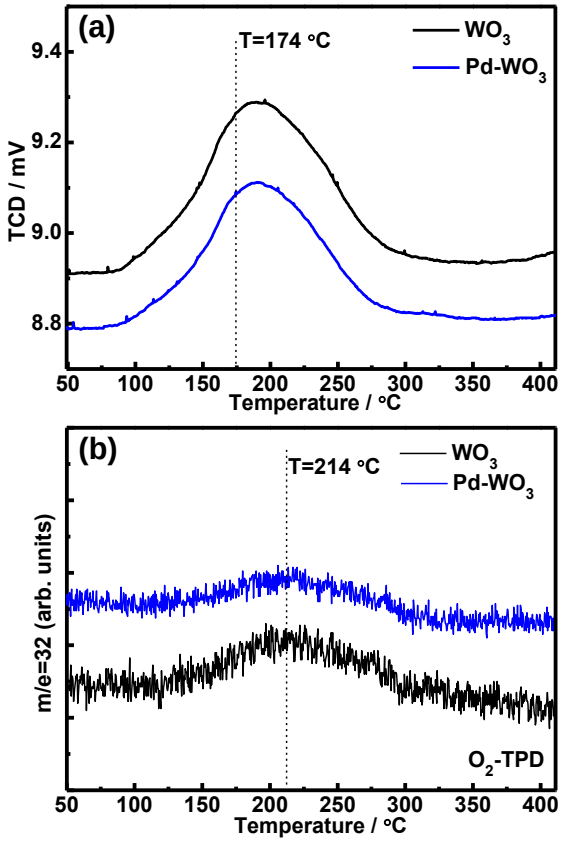

Figure 4-6 TCD spectra and Mass spectroscopy of oxygen desorption obtained on neat and Pd-WO_3 nanoparticles powders.

In order to clarify the role of Pd in oxygen adsorption behavior, O_2-TPD was also investigated with different calcined temperatures. Figure 4-7 presents TCD and mass spectroscopy of neat and Pd-loaded WO_3 nanoparticles calcined at 500 ºC for 2h. From the mass spectroscopy, there was no effects on the oxygen desorption peak and amount with different sintering temperatures. It was believed that the shift of TCD spectra was also caused by desorption of water.

Table 3-1 O_2 desorption amount with different Pd-loading.

Loading amount (wt.%)	Adsorption constant (nm^2 atm^{-1})	O_2 desorption amount (10^{-5} mol g^{-1})
0	19.2	1.2
0.15	21.3	1.0
0.5	18.8	0.8
0.74	20.9	1.0

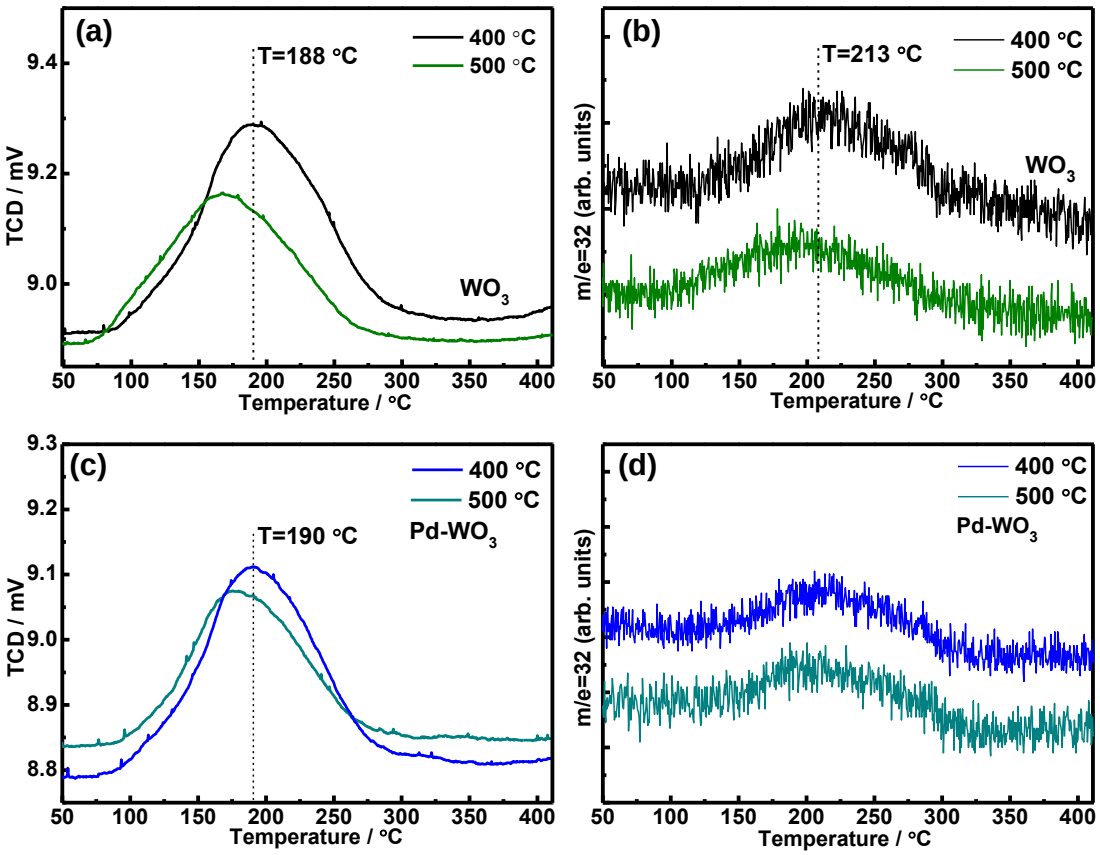

Figure 4-7 TCD spectra and Mass spectroscopy of oxygen-TPD measurements for (a-b) neat and (c-d) Pd-loaded WO_3 nanoparticles calcined at 400 and 500 ºC.

Based on the results of oxygen adsorption, it can be concluded that Pd-loading not changes the adsorbed species; however, promotes the electronic interaction of oxygen with WO_3 surface. In other words, the sensing response to oxygen was enhanced, which was evidenced by the increase of adsorption constant. However, O_2-TPD results demonstrated that oxygen adsorption amount

was relatively small for both neat and Pd-loaded WO_3 and there was no increase in adsorption amount with Pd-loading. Therefore, it was proposed that the enhanced electronic interaction was due to the P-N junction of oxidized Pd with WO_3 surface. Additionally, it was also suggested that with increasing partial pressure of oxygen, oxidization state of Pd could be promoted, leading to expanding of space charge layer, which can also enhance the electronic interaction. With presence of water vapor, it was found the oxygen adsorption was blocked for both neat and Pd-WO_3 sensors. The adsorption constant was greatly decreased around one order for neat and Pd-loaded WO_3 sensors.

4.3.2 Oxygen resistive response with inflammable gases

It is known that sensing response of inflammable gases can be caused by the oxidization of gas molecules with either the surface adsorbed oxygen or lattice oxygen. However, it is found that the oxidization of gas molecules with adsorbed oxygen should be highly oxygen-dependent. In other words, sensing process should depend on the concentration of oxygen. On the contrary, sensing response based on the surface redox, i.e., lattice oxygen should weakly depend on the partial pressure of oxygen [4]. Based on the reaction R1.1, the sensor resistance in the presence of oxygen should be sensitive to P_{O2}. Taking H_2 for an example, the dependence of sensing resistance on P_{O2} in the presence of H_2 can be derived based on the volume depletion theory.

$$H_2 + O^- \xrightarrow{k_{11}} H_2O + e \qquad \textbf{(R4.2)}$$

This reaction reduces the concentration of O^-; however, it is supplied by the adsorption of oxygen. The density of $[O^-]$ can be determined by [2-3]:

$$\frac{d[O^-]}{dt} = k_1 P_{O2}[e_S] - k_{-1}[O^-]^2 - k_{11} P_{H2}[O^-] \qquad \textbf{(4.1)}$$

There are three different cases according to the concentration of hydrogen and oxygen, respectively.

Case I

The concentration of H_2 is relatively small such as the level of several ppm and P_{O2} is relatively high. Sensor is working on the volume depletion state. The reduction of $[O^-]$ is quite small comparing with its large concentration on surface and then the last term in 4.1 can be neglected. Therefore, the sensor resistance in oxygen can be written by 1.7, and keep the same expression as that without H_2.

$$\frac{R_g}{R_0} = \frac{1}{a}(K_{O2} P_{O2})^{1/2} + 1 \qquad \textbf{(4.2)}$$

Case II

The concentration of H_2 is large or P_{O2} is not very high to ignore the term of $k_{11}P_{H2}[O-]$. However, the volume depletion is still valid. At steady state, $d[O-]/dt=0$, then we can obtain

$$(K_{O2} P_{O2})^{1/2}[e_S] = [O^-]\left\{1 + \left(\frac{cP_{H2}}{[O^-]}\right)\right\}^{1/2} \qquad \textbf{(4.3)}$$

According to volume depletion theory, the density of [O-] can be expressed

$$[O^-] = \frac{N_d - [e_S]}{a} = \frac{N_d}{a} \qquad \textbf{(4.4)}$$

By using $R_{O2}/R_0=N_d/[e_S]$, sensing resistance in oxygen for case II is written as

$$\frac{R_{O2}}{R_0} = a\left\{1 + \frac{caP_{H2}}{N_d}\right\}^{-1/2}(K_{O2} P_{O2})^{1/2} = A_0(K_{O2} P_{O2})^{1/2} + 1 \qquad \textbf{(4.5)}$$

Where, A_0 is constant smaller than 1 and related with the concentration of H_2. Thus, it can be seen that the linear relationship is still valid in this case;

nevertheless, the slope is $A_0(K_{O2})^{1/2}$. Actually the slope should be smaller than that of absent of H_2 and decrease with increasing H_2 concentration.

Case III

In this case, P_{H2} is very large or P_{O2} is quite small. The volume depletion state is not suitable. In other words, 4.4 is not valid. $[O^-]$ is represented as

$$[O^-] = \frac{N_d}{a} - [e_S] \qquad \textbf{(4.6)}$$

Then R_g is expressed as:

$$\frac{R_{O2}}{R_0} = \left\{1 + \frac{cP_{H2}}{[O^-]}\right\}^{-\frac{1}{2}} \bullet \left(\frac{1}{a} - \frac{[O^-]}{N_d}\right)^{-1} \bullet (K_{O2}P_{O2})^{\frac{1}{2}} = A_0(P_{O2}) \bullet (K_{O2}P_{O2})^{\frac{1}{2}} + 1 \quad \textbf{(4.7)}$$

In the last case, R_{O2} should be increased with P_{O2}; however, the linear relationship is not valid. The slope with $(P_{O2})^{1/2}$ is a function of P_{O2} until A_0 $(P_{O2})=A_0=1$. Therefore, it can be concluded that sensing resistance based on R4.2 should be oxygen-dependent in all of conditions. However, sensing response based on the lattice oxygen should be less oxygen-dependent, which will discussed latter. It can allow us a probe to clarify the sensing process of inflammable gases and the role of Pd-loading. In the rest part, the oxygen resistive responses with the presence of reducing gases were explored.

Figure 4-8 shows the dependence of sensing resistance, R_g on P_{O2} with presence of 50, 200 and 450 ppm H_2 at 350 ºC.

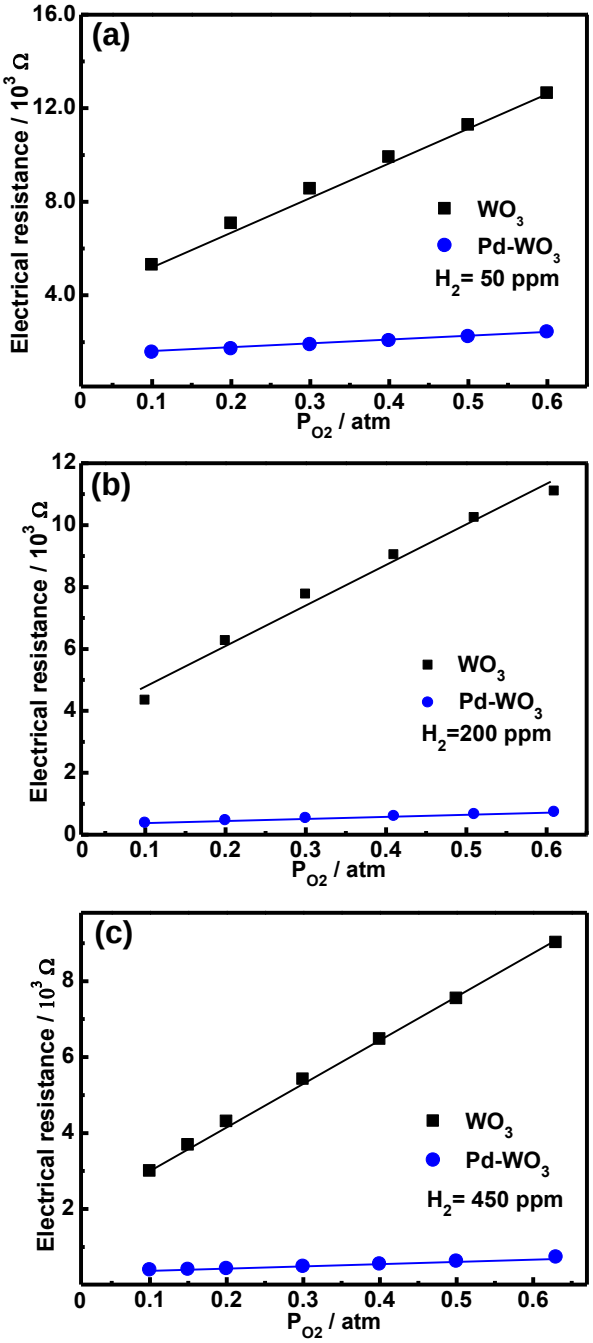

Figure 4-8 resistive response of oxygen with presence of (a) 50, (b) 200 and (c) 450 ppm H_2 at 350 ºC.

It is obvious that neat and Pd-loaded WO_3 sensors demonstrate a quite different resistive response with P_{O2}. With the presence of H_2, sensing resistance of neat WO_3 significantly increased with P_{O2}; however, Pd-loaded sensor showed a relatively weak dependence on oxygen with the presence of H_2. In addition, it

was found that with increasing the concentration of H_2, such a difference became more apparent.

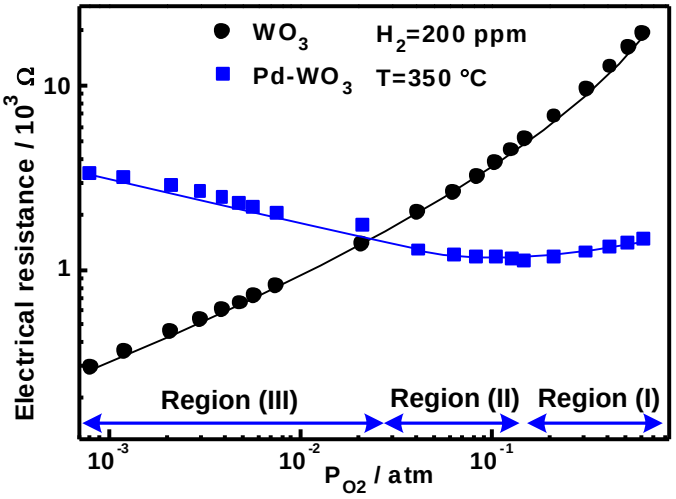

Figure 4-9 resistive response of oxygen with presence of 200 ppm H_2 at P_{O2} ranging from 0.8×10^{-3} to 0.6 atm at 350 ºC.

Therefore, it was suggested that Pd-WO_3 sensor has a different sensing mechanism with neat WO_3 sensor. The surface lattice oxygen could take part in the sensing process of H_2 with Pd-loading.

To confirm this proposal, the oxygen resistive response with the presence of H_2 was studied from an extremely low to a high region of P_{O2}. It is because that at low partial pressure of oxygen, the surface redox process should be much easier [6]. Figure 4-9 shows the resistive response to P_{O2} with 200 ppm H_2. One can easily note that Pd-loaded WO_3 sensor demonstrated a different resistive behavior with neat WO_3 sensor and the resistive response could be divided into three different regions namely, region (I), region (II) and region (III) from a low P_{O2} to a high P_{O2}.Pd-loaded WO_3 sensor almost had no response to the variation of P_{O2} at low partial pressure. Even a slight decrease of R_g was observed with increasing P_{O2} from around 1000 to 6000 ppm. This could not be understood from the reaction with surface adsorbed oxygen. In contrast, pure WO_3

demonstrated a sensitive response to oxygen at all region of P_{O2}. This result was well consistent with our prediction that with increasing P_{H2} or decreasing P_{O2}, the surface redox behavior became more obvious for Pd-loaded WO_3 sensor. It was, therefore, concluded that Pd-loading not only promoted the sensing response but also significantly modified the sensing process of WO_3.

To explain this difference, it is surmised that sensing response to H_2 can be created not only by the reaction with the adsorbed oxygen but also a direct reaction with lattice oxygen of WO_3 surface. In other words, surface redox process took part in the sensing process for Pd-loaded sensors. WO_3 surface is ready to be reduced with the formation of oxygen vacancies (V_O) [6-7]. Decreasing oxygen partial pressure or with the presence of reducing gases, the formation enthalpy of oxygen vacancy decreases and becomes exothermic [4, 6]. Therefore, it was suggested that in the case of reducing gases sensing, the surface reduction of WO_3 should be taken into considerations even in normal air atmosphere [4, 6]. Based on the surface redox reaction, a revisable sensing response to H_2 can be described by the following reactions:

$$H_2 + O_L^{2-} + W^{6+} \longrightarrow H_2O + W^{5+} + V_O^{\bullet} + e \qquad \textbf{(R4.3)}$$

$$\frac{1}{2}O_2 + W^{5+} + V_O^{\bullet} + e \longrightarrow O_b^{2-} + W^{6+} \qquad \textbf{(R4.4)}$$

Surface lattice oxygen is eliminated by H_2 with formation of oxygen vacancies ($V^{\bullet}_O$) and W^{5+} ions near Pd sites R4.3 and resulted in a decrease in the electrical resistance of sensor. After removing H_2, the generated vacancies are reoxidized by oxygen and then sensor resistance is recovered. In the small amount of P_{O2}, reaction R4.3 is easy to progress rather than reaction R4.4, leading to the low electrical resistance. In addition, it seems that reactivity of oxygen adsorbed on

WO_3 surface is very low as shown in Fig. 4-8 and Fig. 4-9. With increasing P_{O2}, reaction R4.4 progresses to the right side and then the electrical resistance gradually increases. Therefore, reactions R4.3 and R4.4 determine the sensing resistance with a presence of H_2, which is dependent on the amounts of reacted O_L. Thus, sensor resistance is quite low and weakly depended on P_{O2} as observed. With a high H_2 or low P_{O2}, the sensing process is dominated by R4.3 and R4.4 and the sensor resistance was completed independent of P_{O2} as shown in region (II) and (III) of Fig. 4-9.

It should be noted that at low concentration of H_2, the sensor response caused by the surface reduction of R3.3 and R3.4, should also exhibit a linear relationship with the square root of P_{H2} as presented in Fig. 3-11. Since in this redox reaction, one electron was released into the conduction band by one hydrogen molecule same as the reaction with adsorbed oxygen (O^-). However, when the surface reduction dominated the sensing response at a high concentration of H_2 or relatively poor oxygen containing atmosphere, the linear relationship of $(R_a/R_g)^2$ with P_{H2} was not valid. It was because that the linearity was based on the reaction with a high density of surface adsorbed oxygens [2-3]. This was could be one of the reasons for the degradation of the linearity observed in Fig. 3-11 and 3-12. Based on the above discussions, we would like to address that with Pd-loading; the surface redox process of WO_3 can occur and play a vital role in the sensing of H_2 even in air and control the sensing process in low P_{O2} region and high concentration of H_2.

Under a wet condition, the weak dependence of oxygen for Pd-WO_3 sensors was also observed. Figure 4-10 shows resistive response of sensors to P_{O2} with

different concentration of H_2 under 1 VOL.% humidity. With increasing H_2 concentration, the sensing resistance obviously decreased for neat WO_3. However, Pd-loaded WO_3 sensor kept a quite small resistance comparing with the neat one and slightly decreased with increasing concentration of H_2. Additionally, in all of concentrations, the sensor resistance raised with P_{O2} for neat WO_3. On the contrary, the sensing resistance of Pd-loaded WO_3 even slightly decreased with increasing P_{O2} as shown in Fig. 4-6 (c). This was quite similar with that observed under dry atmosphere.

As discussed in the last part, the surface reduction should be favored by decreasing P_{O2} in the presence of reducing gases. Under humid condition, the sensing response to oxygen was studied at a low concentration of P_{O2}. The small region of P_{O2} was obtained by mixing air and 1% oxygen with pure N_2. Figure 4-11 (b) shows the resistive response of oxygen at a low concentration region with the presence of 200 ppm H_2 under 1 VOL.% humidity. At the first glance, one can find that the sensor resistance is reduced by decreasing P_{O2} down to 10^{-3} atm level.

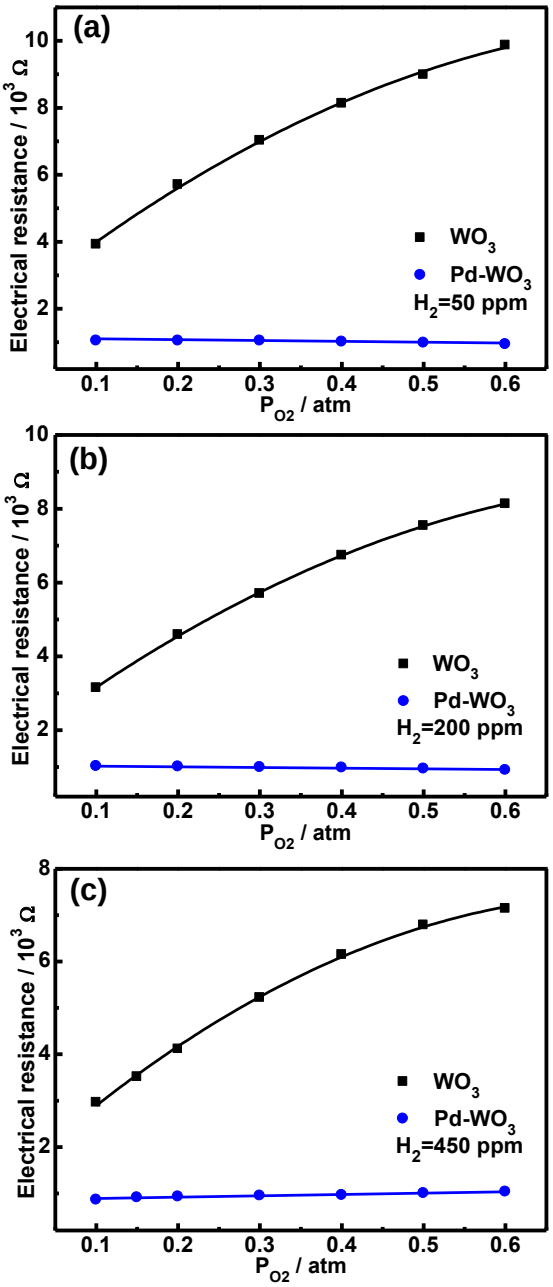

Figure 4-10 the dependence of sensor resistance on P_{O2} with (a) 50 ppm, (b) 200 ppm and (c) 450 ppm of H_2 under 1 VOL.% humidity at 350 ºC.

It was found that the sensor resistance was reduced by decreasing P_{O2} down to 10^{-2} atm level. It was found that the whole region of P_{O2}, sensing resistance of neat WO_3 demonstrated a strong dependence on oxygen indicating that oxygen adsorption was responsible for the sensing response. In contrast, sensor resistance of Pd-loaded WO_3 slightly increased with oxygen at high P_{O2} region.

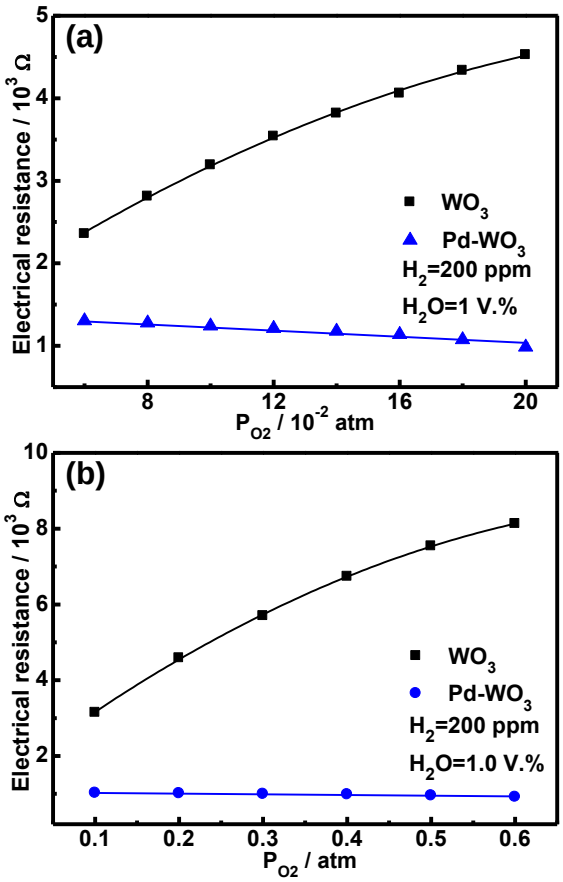

Figure 4-11 sensor resistance as function of P_{O2} at the region of (a) 6×10^{-3} to 0.02 atm and (b) 0.1 to 0.6 atm with presence of 200 ppm H_2 and 1 VOL.% humidity at 350 ºC.

However, the sensor resistance decreased with increasing P_{O2} and the reduction became more apparent at low partial pressure of oxygen. These results were highly consistent with that for dry conditions. Therefore, it can be claimed that the sensing mechanism of Pd-loaded WO_3 should be different from the neat one. The surface redox process described by equations (R4.3) and (R4.4) should be responsible for the sensing process of H_2 under both dry and wet conditions. It is believed that this surface redox is favored with presence of water vapor because oxygen adsorption on WO_3 is blocked by water.

By using the same method, the sensing mechanism and the role of adsorbed oxygen in the sensing process of CO and CH_4 were investigated. Figure 4-12

shows the resistive response to oxygen with presence of 200 ppm CO for neat and Pd-loaded WO_3 sensors with a range of 0.8×10^{-3} to 0.6 atm.

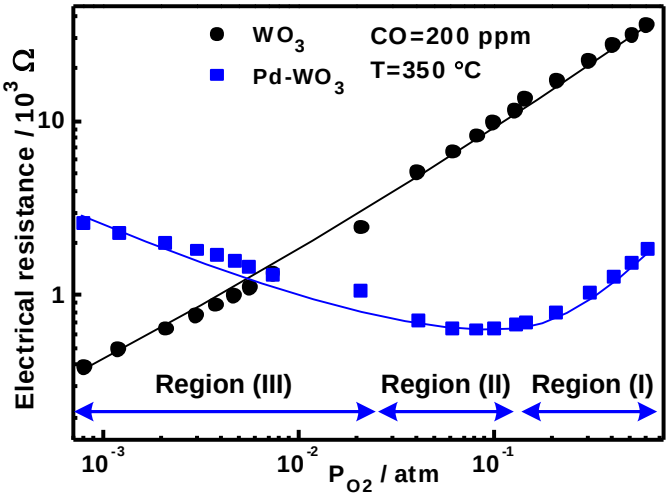

Figure 4-12 the dependence of sensing resistance on P_{O2} from 0.8×10^{-3} to 0.6 atm with a presence of 200 ppm CO at 350 ºC.

Similarly, neat and Pd-loaded WO_3 sensors demonstrated a quite different response to P_{O2} with the presence of CO and resistive response to oxygen could be also divided into three regions. Pd-loaded WO_3 showed a relatively weak dependence on oxygen at a high P_{O2}; however, sensing resistance of neat WO_3 sensor was strongly oxygen-dependent at the whole region of P_{O2}. With a very small P_{O2}, region (III), an opposite response to oxygen was also observed with presence of CO for Pd-loaded WO_3 sensor. Thus, this clearly indicated a different sensing mechanism of CO for neat and Pd-loaded WO_3 sensors.

These results were highly similar with that of H_2, indicating that the redox process is also involved for CO sensing with Pd-loading. At poor oxygen background, it was believed that the surface redox even dominated the sensing process. The surface reaction can be described by:

$$CO + O_L^{2-} + W^{6+} \longrightarrow CO_2 + W^{5+} + V_O^{\bullet} + e \quad \textbf{(R4.5)}$$

$$\frac{1}{2}O_2 + W^{5+} + V_O^{\bullet} + e \longrightarrow O_L^{2-} + W^{6+} \quad \textbf{(R4.6)}$$

It was proposed that Pd-loading also promoted the response of CO and changed the basic sensing process from the reaction of surface adsorbed oxygen into surface lattice oxygen.

The surface redox process was evidenced for Pd-loaded WO_3 sensors under wet condition through the quite weak response of oxygen in the presence of CO as demonstrated in Fig. 4-13. It was found that neat WO_3 was sensitive to P_{O2} and the sensor resistance increased with P_{O2}. In contrast, Pd-loaded WO_3 demonstrated a weak response to P_{O2} with presence CO, even the resistance was slightly decreased with P_{O2} at both low and high partial pressure. This was consistent with that of dry condition that surface redox is response for the sensing process of CO. However, the weak dependence on P_{O2} was evidenced for the whole region of P_{O2} under wet condition, which is only observed at low concentration of oxygen, below 10^{-2} atm as shown in Fig. 4-13. Thus, it is believed that the surface redox by CO is promoted by humidity.

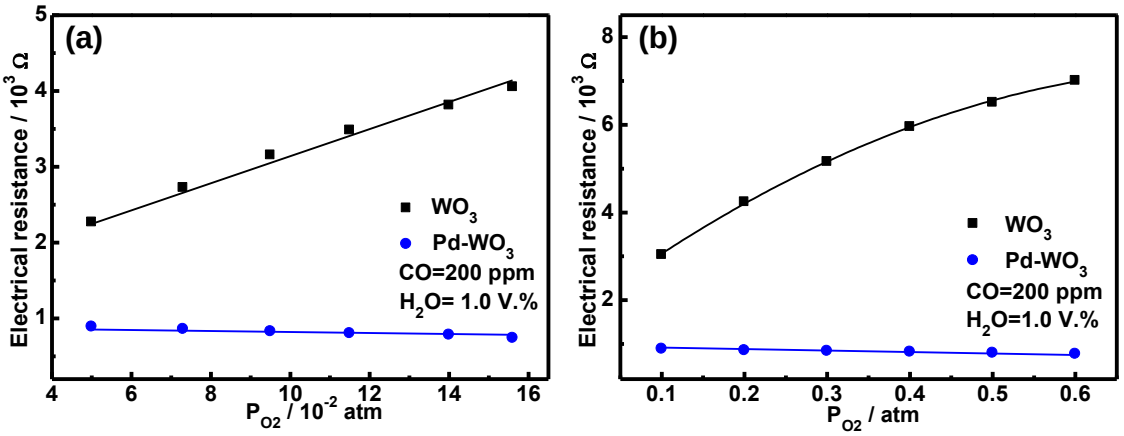

Figure 4-13 sensor resistance as a function of P_{O2} at a range of (a) 0.01 to 0.18 atm and (b) 0.1 to 0.6 atm with the presence of 200 ppm CO and 1 VOL.% humidity at 350 ºC.

It is known that methane has a stable molecules structure [13-14] and WO_3 is not sensitive for CH_4 as a MOS gas senor [15]. Therefore, it is proposed that the surface redox reaction should be hard to take part in the sensing process as

observed for the sensing of H_2 and CO. In order to confirm this proposal, oxygen resistive response in presence of CH_4 was firstly characterized as shown in Fig. 4-14. Firstly, it was observed that the sensor resistance with CH_4 was quite higher than that with presence of H_2 and CO at the same P_{O2}. In addition, the electrical resistance for Pd-loaded WO_3 sensor was comparable with neat WO_3 sensor and became sensitive to oxygen in the presence of CH_4 for both sensors. However, with a small region of P_{O2}, Pd-loaded WO_3 sensor showed a weak dependence on oxygen. Such observations were quite different from that with presence of H_2 and CO, indicating a different sensing mechanism. The surface process for sensing response is the oxidization of CH_4 molecules with surface adsorbed oxygen.

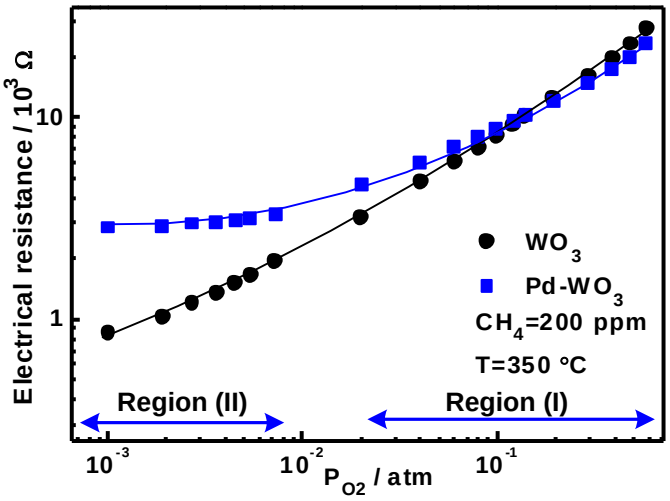

Figure 4-14 sensing resistance as a function of P_{O2} from 0.8×10^{-3} to 0.6 atm with a presence of 200 ppm CH_4 at 350 ºC.

Under wet condition, the resistive response of oxygen in the presence of CH_4 was also investigated. Figure 4-15 shows the sensor resistance with P_{O2} with the presence of 200 ppm CH_4 and 1 VOL.% humidity. The sensor resistance for both sensors increased with P_{O2}; nevertheless, the sensor resistance was quite smaller than that of dry condition, indicating a blocking of oxygen adsorption on the surface. Comparing with dry condition, the sensing resistance of Pd-WO_3

became more oxygen-dependent under wet condition. In addition, it was found that the sensor resistance was more closed for neat and Pd-loaded WO_3. These results revealed that Pd-loaded WO_3 had a different sensing mechanism towards CH_4 with that of H_2 and CO under both dry and wet conditions.

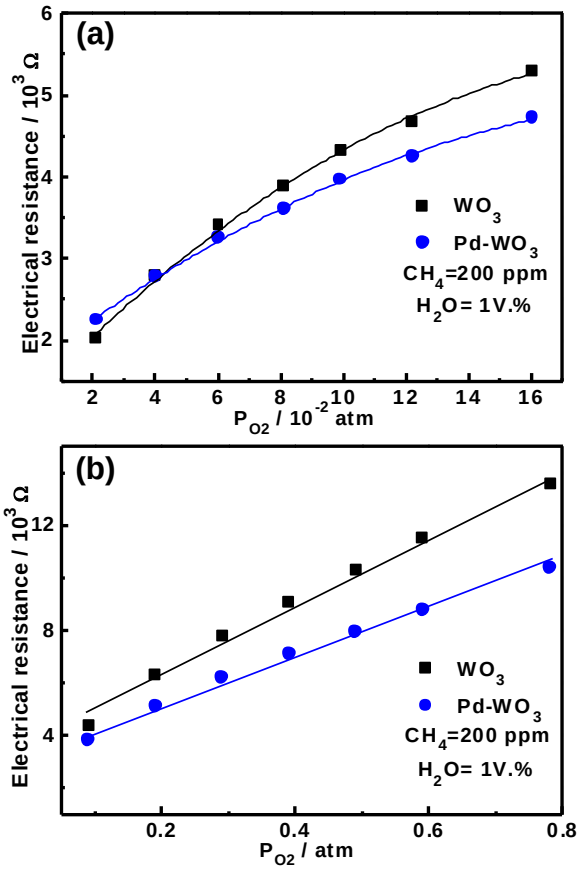

Figure 4-15 sensing resistance as a function of P_{O2} at (a) high and (b) low partial pressure with presence of 200 ppm CH_4 and 1 VOL.% humidity at 350 ºC.

4.4 Conclusions

In this chapter, the adsorption and interaction of oxygen with WO_3 has been investigated based on the resistive response and TPD measurements. The main results and conclusion of this chapter are recapitulated below.

- Oxygen adsorption results revealed that oxygen is difficult to be adsorbed on the surface of WO_3 and the adsorption was in O_2^- form for both neat and

Pd-loaded sensors. Pd-loading did not increase the adsorption amount but promote the electronic interaction of oxygen with WO_3, i.e. increasing the sensing response of oxygen.

- The enhanced electronic interaction of oxygen with the loading of Pd can be caused by the p-n junction. Additionally, with Pd-loading, the oxidization ability could be promoted resulting in an enhanced electronic interaction with WO_3 surface. Oxygen resistive response suggested that the adsorption of oxygen was significantly inhibited by the presence of water vapor for both neat and Pd-loaded WO_3 sensors.
- In the presence of H_2, the resistive response of oxygen was quite different for neat and Pd-loaded WO_3 sensors regardless of the humidity. For the neat WO_3 sensor, the sensing resistance was strongly oxygen-dependent with presence of H_2 or not. In contrast, Pd-loaded WO_3 sensor resistance demonstrated a really weak dependence on P_{O2} with presence of H_2. This became more apparent with increasing H_2 concentration or decreasing P_{O2}.
- In the presence of CO, the oxygen resistive response showed a similar result as that of H_2. The sensing process of CO was oxygen-dependent for neat WO_3; however, the sensing process of Pd-loaded WO_3 sensor demonstrated a weak dependence on oxygen.
- The oxygen resistive response with the presence of CH_4 was obviously different from that of H_2 and CO. It was found that the sensor resistance depended on P_{O2} for both neat and Pd-loaded WO_3 sensors regardless of the concentration of CH_4 and O_2.
- Experimental results suggested that Pd-loading not only promoted the sensing

response but also changed the sensing process of WO_3 to H_2 and CO. In the case of CH_4, the sensing mechanism was the reaction of CH_4 molecules with adsorbed oxygen regardless of Pd-loading and the sensing background.

References

[1] N. Yamazoe, K. Shimanoe, New perspectives of gas sensor technology, Sensors and Actuators B: Chemical 138 (2009): 100-107.

[2] N. Yamazoe, K. Shimanoe, Roles of shape and size of component crystals in semiconductor gas sensor. (1) Response to oxygen, J. Electrochem. Soc., 155 (4) (2008): J85–J92.

[3] N. Yamazoe, K. Shimanoe, Roles of shape and size of component crystals in semiconductor gas sensor. (2) Response to NO_2 and H_2, J. Electrochem. Soc., 155 (4) (2008): J93-J98.

[4] Z. Hua, M. Yuasa, T. Kida, N. Yamazoe, K. Shimanoe, H_2 sensing mechanism of Pd-loaded WO_3 nanoparticles gas sensors, Chemistry letters, 2014 (dx.doi.org/10.1246/cl.140396).

[5] M. Hübner, N. Bârsan, U. Weimar, Influences of Al, Pd and Pt additives on the conduction mechanism as well as the surface and bulk properties of SnO_2 based polycrystalline thick film gas sensors. Sensors and Actuators B: Chemical, 171 (2012): 172-180.

[6] V. Oison, L. Saadi, C. L. Mauriat, R. Hayn, Mechanism of CO and O_3 sensing on WO_3 surfaces: First principle study. Sensors and Actuators B: Chemical, 160(2011): 505-510.

[7] M. Hübner, C. E. Simion, A. Haensch, N. Barsan, U. Weimar, CO sensing mechanism with WO_3 based gas sensors. Sensors and Actuators B: Chemical, 151(2010): 103-106.

[8] S. Matsushima, Y. Teraoka, N. Miura, N. Yamazoe, Electronic Interaction between Metal Additives and Tin Dioxide in Tin Dioxide-Based Gas Sensors, Japanese Journal of Applied Physics, 27(1998): 1798-1802.

[9] N. Yamazoe, K. Shimanoe, Receptor function of small semiconductor crystals with clean and electron-traps dispersed surfaces, Thin Solid Films, 517 (2009): 6148-6155.

[10] Z. Hua, M. Yuasa, T. Kida, N. Yamazoe, K. Shimanoe, High sensitive gas sensor based on Pd-loaded WO_3 nanolamellae, Thin Solid Films, 548 (2013): 677-682.

[11] A. Gurlo, Interplay between O_2 and SnO_2: Oxygen Ionsorption and Spectroscopic Evidence for Adsorbed Oxygen, ChemPhysChem, 7 (2008): 2041-2052.

[12] M. Iwamoto, Y. Yoda, N. Yamazoe, T. Seiyama, Study of Metal Oxide Catalysts by Temperature Programmed Desorption. 4. Oxygen Adsorption on Various Metal Oxides, The Journal of Physical Chemistry, 82 (1978): 2564-2570.

[13] R. F. Hicks, H. Qi, M. L. Young, R. G. Lee, Structure Sensitivity of Methane

Oxidation over Platinum and Palladium, Journal of Catalysis 122 (1994): 280-294.

[14] F. H. Ribeiro, M. Chov, R. A. D. Betta, Kinetics of the Complete Oxidation of Methane over Supported Palladium Catalysts, Journal of Catalysis 122 (1994): 537-544.

[15] V. Lantto, P. Romppainen, S. Leppävuori, Response studies of some semiconductor gas sensors under different experimental conditions, Sensors and Actuators, 15 (1988) 347–357.

CHAPTER 5

5 The Redox Process of Neat and Pd-loaded WO_3 Sensors

In this chapter, the surface reducibility and the surface redox process were studied based on the TPR tests and resistive response of inflammable gases in the atmosphere absent of oxygen. The TPR and resistive response results clearly revealed a reduction behavior in the presence of H_2 and CO in the absence of oxygen for Pd-loaded WO_3 sensor. On the contrary, there was no reduction behavior for neat WO_3. Thus, it was concluded that Pd-loading promoted the reducibility of WO_3, leading to an increase of sensor response for H_2 and CO. However, in the case of CH_4, the reaction of adsorbed oxygen should be responsible for the sensing response regardless of Pd-loading or not.

5.1 Introduction

It is well accepted that WO_3 surface is ready to loss lattice oxygen forming oxygen vacancies (V_O), which are considered as the predominant defects on surface [1-4]. The formation enthalpy of oxygen vacancy decreases and becomes exothermic at atmosphere with very low oxygen or presence of reducing gases, such as CO [2-3, 5]. This can significantly affect the surface process of WO_3 as a semiconductor gas sensor. Therefore, it is suggested that in case of reducing gases sensing, the surface reduction of WO_3, a direct reaction of gas molecules with lattice oxygen should be taken into considerations even in normal air atmosphere [5-6]. In other words, the sensing response of WO_3, when upon exposing reducing gases, can be created by a surface reduction and oxidation process (Redox) besides for the oxidization of reducing gases with surface

adsorbed oxygen (O_2^-, O^- and O^{2-}). This has been confirmed by a revisable sensing response to CO in the absence of oxygen or at extremely poor oxygen atmosphere. Where the resistive responding and recovery speed were found to be relatively slow, which resulted from the surface reduction and oxidation process supported by the production of CO_2 proven by the catalytic conversion and DRIFTS measurements [5-6]. The resistive response of oxygen in chapter 4 with high concentration of H_2 and CO or low P_{O2} also suggested the surface redox process [7]. In addition, studies based on first principle demonstrated that CO was oxidized into CO_2 on WO_3 surface with increasing the concentration of oxygen vacancies [5].

It is accepted that noble metals can activate the surface reduction behavior of WO_3 [8-10]. Therefore, Pd-loading can promote the surface redox reaction and change the sensing process from adsorbed oxygen into surface lattice oxygen [7]. In this chapter, the surface reducibility was characterized by TPR (Temperature programmed reduction) and sensing response of inflammable gases in the absence of oxygen. This result supports our proposal that the surface redox processes take part in the sensing process and result in a direct interaction of inflammable gas molecules with the sensor surface rather than the chemically adsorbed oxygen for Pd-loaded WO_3 sensors.

5.2 Experimental Details

The interaction of inflammable gases and the surface redox process with WO_3 were investigated by the TPR and resistive response with non-oxygen containing background. H_2 and CO-TPR was performed in a flow of 1000 ppm H_2 or CO balanced with pure N_2 (50 mL min^{-1}) at a ramping rate of 10 ºC min^{-1}

(BEL-CAT, BEL Japan). The sample powders (0.1 g) were packed in a tubular quartz reactor and heat-treated at 400 ºC for 30 min in a flow of air. After cooling down to 50 ºC in air and the TCD (thermal conductivity detector) and mass spectrometer (MS, GDS30102 PFEIFFER VACUUM) were stabilized for 3 h in H_2 or CO before the TPR measurements. Figure 5-1 shows the procedure for the pretreatment and measurements of TPR.

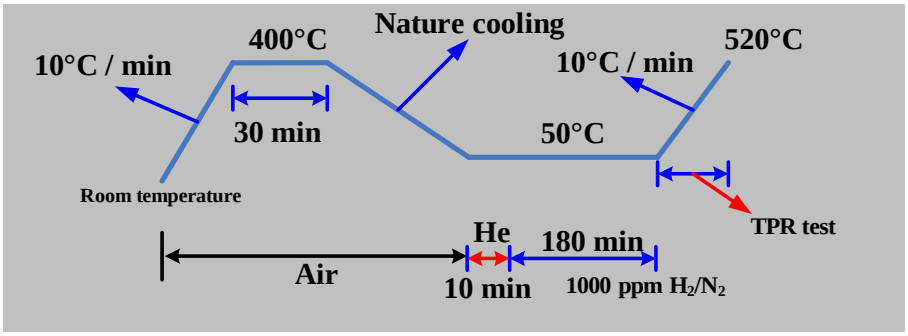

Figure 5-1 the procedure for pretreatment and measurement of TPR.

The sensing properties of inflammable gases were studied with the absence of oxygen under dry and wet atmosphere, respectively. It should be noted that the atmosphere absent from oxygen refers to the pure N_2 or H_2 balanced with N_2. Although, it has been mentioned that even in a highly pure N_2 atmosphere, there is an extremely low concentration of oxygen as the impurity. According to the home-made oxygen sensor, the impurity oxygen is around several ppm in pure N_2 background.

5.3 Results and Discussions

Based on the results of chapter 4, it can be concluded that Pd-loading not only enhances the sensing response of WO_3 but also significantly changes the basic sensing process. It was proposed that Pd-loading can promote the reducibility of WO_3 [8-10]. Therefore, sensing tests and TPR measurements were performed in the absence of O_2 to evaluate the reduction ability. Figure 5-2

shows the resistive response of neat and Pd-loaded WO_3 sensors to H_2 in the absence of oxygen under dry and wet condition, respectively. Here, the atmosphere absent from oxygen refers to the pure N_2 or H_2 balanced with N_2. However, the presence of oxygen at an extremely low concentration as the impurity is inevitable [6, 11-12].

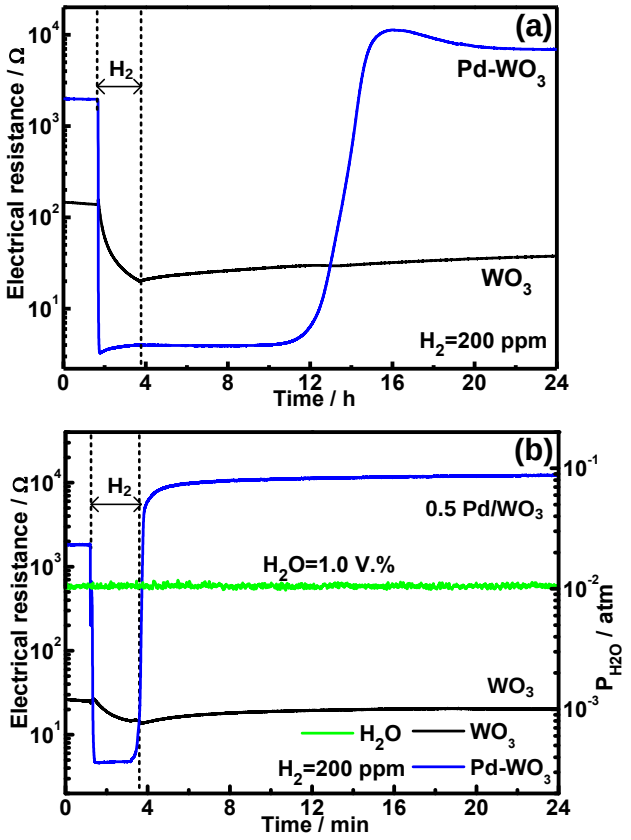

Figure 5-2 resistive response of neat and Pd-loaded WO_3 sensors to 200 ppm H_2 in the absence of oxygen under (a) dry and (b) wet condition at 350 ºC.

Apparently, Pd-loaded and neat WO_3 sensors demonstrated a rather different sensing behavior. The resistance of 0.5 Pd-WO_3 decreased quickly from around 1967 Ω to only 3 Ω, which was almost comparable to the resolution limitation of the electrical multi-meter in less than 3 min. Then a steady state of resistance was obtained or resistance value beyond the measurability of the electrical multi-meter.

In contrast, the sensor resistance of neat WO_3 went down very slowly from about 140 Ω to 21 Ω; nevertheless, the equilibrium state could not be observed even after several hours. When removing H_2 from the background, the sensing resistance fully recovered to the initial R_{N2} within 12 h for Pd-loaded WO_3 sensor. However, the sensor resistance of neat WO_3 gradually went up with time and could not totally be recovered even 2 days later. Such a slow responding and unrecovered response clearly indicated a surface reduction behavior of neat WO_3 as our expectation. It was worthy to note that the recovery of Pd-loaded WO_3 sensor was so slow at the very beginning stage of changing atmosphere from the H_2/N_2 to a pure N_2. In the first several hours, the sensor resistance was just increased from 4 Ω to 5 Ω. In addition, it was found that the sensor resistance continuously went up with time even after reaching the initial R_{N2}. A similar phenomenon was also observed in the sensing of CO [6]; however, the reason was not clear.

The sensor response defined by R_{N2}/R_g to 200 ppm H_2/N_2 was 506 and 7 for Pd-WO_3 sensor and the neat WO_3 sensor, respectively. Comparing with that in air atmosphere shown in Fig. 2-9 and Fig. 3-12, the sensor response was 578 and 55 for Pd-loaded and the neat WO_3 sensor, respectively. Therefore, it could be seen that in the absence of oxygen, Pd-loaded sensor showed a sensing response comparable with that in air background. On the contrary, neat WO_3 demonstrated a response based on surface redox was far smaller than that of surface adsorbed oxygen, revealing that the main sensing process could be ascribed to the chemically adsorbed oxygen. The resistive response of reducing gases in N_2 background clearly suggested an improved reduction ability of WO_3 by

Pd-loading. In addition, the fully recovery of sensing response for Pd-loaded WO_3 indicated that the oxidization ability was promoted by the loading of Pd comparing with the neat WO_3. This conclusion was in a good agreement with the above oxygen adsorption study that the electronic interaction was improved partially due to an enhanced oxidization with P_{O2} for Pd-loaded WO_3 sensor.

The interaction of H_2 with WO_3 surface in the absence of oxygen was also investigated by TPR measurements, which demonstrated an enhanced activity of surface lattice oxygen for Pd-loaded WO_3 nanoparticles. Figure 5-3 represents the mass spectra of H_2O desorption and H_2 consumption in the absence of oxygen.

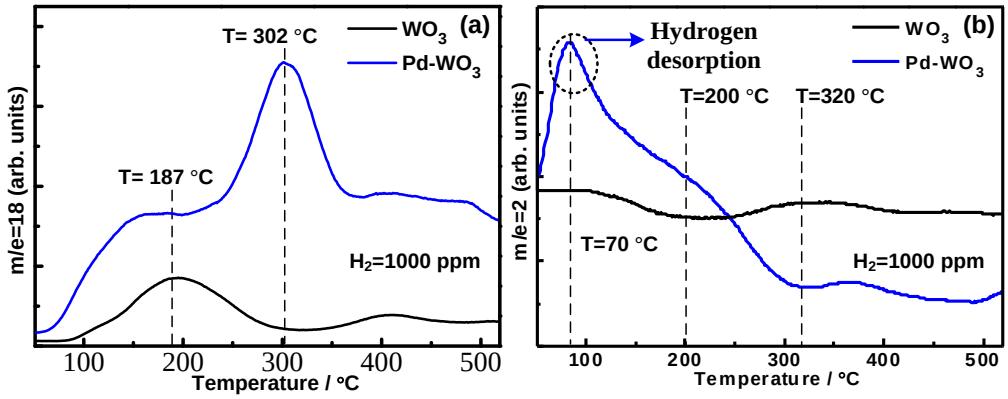

Figure 5-3 (a) H_2O desorption spectra and (b) H_2 consumption spectra of H_2-TPR for neat and Pd-loaded WO_3 nanoparticle powders in the absence of oxygen.

There are two main peaks of water desorption for neat WO_3 nanoparticle powders around 190 ºC and 405 ºC, respectively. Pd-loaded WO_3 sample also showed two main peaks of water spectra and the first peak was consistent with that of neat WO_3 powder. Thus, it was suggested that the peak at low temperature was mainly due to the physical desorption of water for both samples, which was in a good accordance with the H_2 consumption spectra shown in Fig 5-3 (b). Peaks at high temperatures were caused by the reaction of O_L with H_2 in the

absence of oxygen. A large desorption of water was observed for Pd-loaded WO_3 sensor indicating a strong activity of surface lattice oxygen. This was consistent with the results observed the resistive response in Fig 5-2. However, neat WO_3 sensor showed a poor activity of O_L as proved by the little water desorption and H_2 consumption. It was found that the amounts of H_2O desorption and H_2 consumption becomes much larger with a heavy Pd-loading, indicating a promoted reducibility with Pd amount. In addition, desorption of H_2 was observed at low temperature for Pd-loaded WO_3, revealing a dispersion of metallic Pd on the surface of WO_3.

The improved reduction of WO_3 surface by H_2 in the absence of oxygen was also proved by the XRD patterns. After H_2-TPR tests, sample powders were cooled down to room temperature and the reduction state was kept for XRD measurements. However, an oxidization of the samples could occur before and during the XRD characterization. Figure 5-4 shows the XRD spectra of neat and Pd-loaded WO_3 powders after TPR tests. Comparing with Fig. 2-4, there was no obvious difference in the phase structure for neat WO_3 after TPR tests.

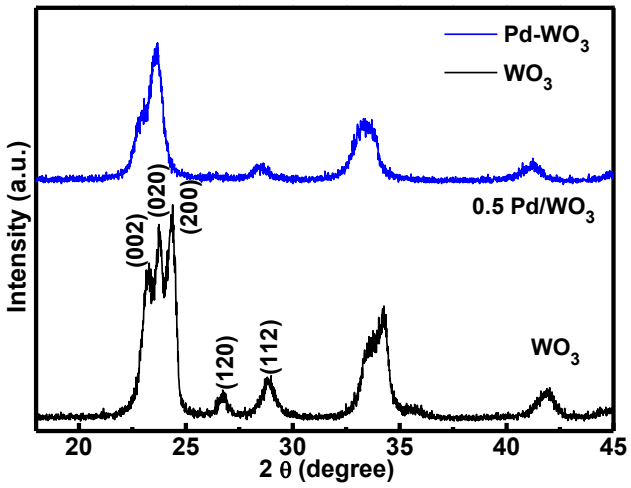

Figure 5-4 XRD patterns of neat and Pd-loaded WO_3 nanoparticle powders after H_2-TPR measurements.

In contrast, XRD patterns of Pd-loaded WO_3 was significantly changed after TPR tests, suggesting an irreversible interaction with H_2 in the absence of oxygen. However, it was quite difficult to distinguish the phase structure after TPR measurements.

The reduction behavior was also evaluated in the presence of CO balanced with pure N_2. Figure 5-5 shows the resistive response of CO in the background of N_2 under dry and humid conditions, respectively. In the absence of oxygen, both neat and Pd-loaded WO_3 sensors exhibited a response to CO.

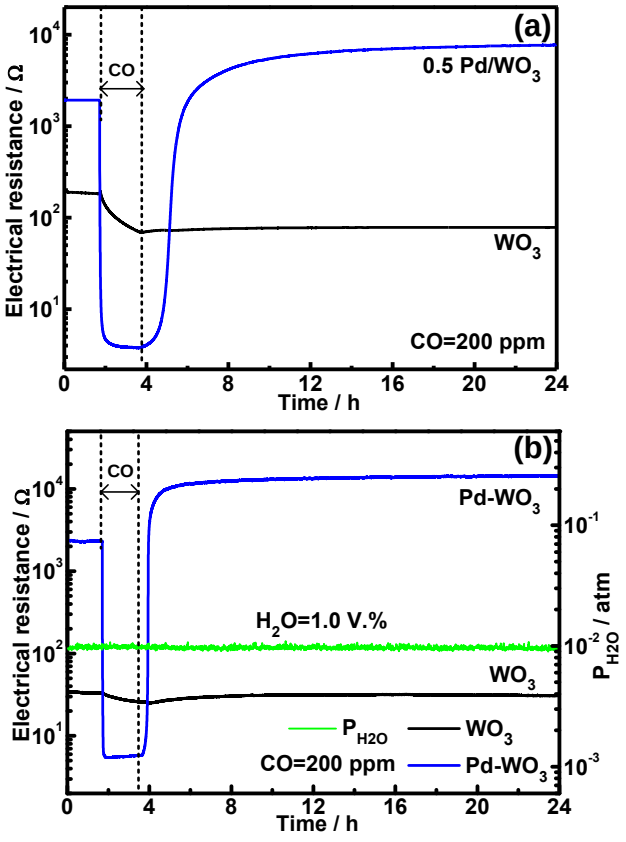

Figure 5-5 resistive response of neat and Pd-loaded WO_3 sensors to 200 ppm CO in the background of N_2 under (a) dry and (b) humid condition at 350 ºC.

It was found that the sensing resistance of neat WO_3 relatively slowly decreased and could not get equilibrium state even after 2 h. Moreover, the sensing resistance could not fully be recovered similar as that observed for H_2. This

clearly indicated a surface reduction behavior by CO. However, with Pd-loading, WO_3 demonstrated a significantly high response to CO and the sensing resistance quickly and fully went back in 6 h. The response defined by R_{N2}/R_g was 2.6 and 500 for neat and loaded WO_3, respectively. These results clearly showed that Pd-loading greatly promoted the reduction; nevertheless, the surface redox for neat WO_3 in CO was neglectable, even in the absence of oxygen.

The surface reduction behavior was also revealed by the CO-TPR measurements in the absence of oxygen. Figure 5-6 shows the mass spectra of CO_2 for neat and Pd-loaded WO_3 nanoparticle powders during the CO-TPR tests. It was quite clear that Pd-WO_3 demonstrated a reduction peak around 210 ºC. In contrast, the reduction peak of neat WO_3 was quite small and almost neglectable. This observation was similar with that of H_2. Therefore, it can be concluded that Pd-loading alters the sensing mechanism of CO due to the promoted reduction ability. The surface redox processes, which occur at extremely poor oxygen atmosphere for neat WO_3, have also been observed in a high oxygen concentration containing atmosphere with Pd-loading.

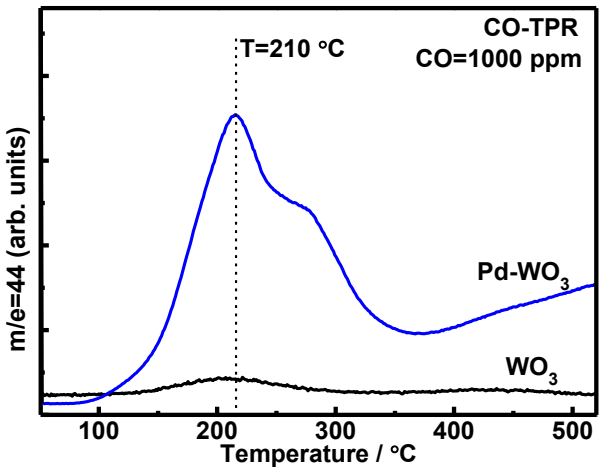

Figure 5-6 CO_2 mass spectroscopy of CO-TPR obtained on neat and Pd-loaded WO_3 nanoparticle powders in the absence of oxygen.

In addition, with presence of humidity, the based sensor resistance and response to H_2 and CO were decreased for neat and Pd-loaded WO_3 sensors, indicating a presence of oxygen in the background and took part in the sensing process.

In the chapter 4, it has been found that with presence of CH_4, the sensor resistance was large and highly dependent on P_{O2}, which was different from that of H_2 and CO. In addition, neat and Pd-loaded WO_3 demonstrated a much smaller response than H_2 and CO. Therefore, it is proposed that the surface redox reaction should be hard to take part in the sensing process of CH_4. To confirm this proposal, the reducibility of WO_3 surface in the presence of CH_4 was investigated by the resistive response in the background without oxygen as shown in Fig 5-7.

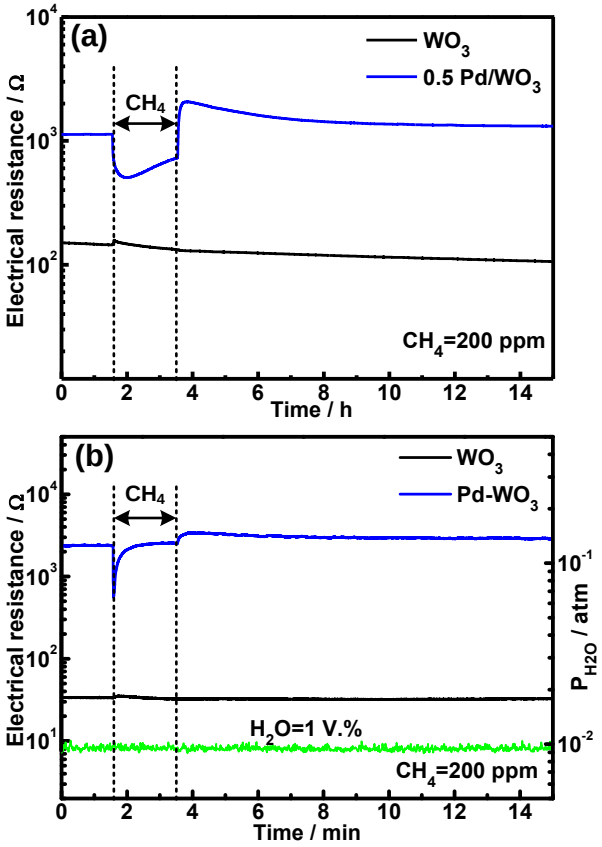

Figure 5-7 resistive response to 200 ppm CH_4 and (b) mass spectra of CH_4-TPR obtained on neat and Pd-loaded WO_3.

Surprisely, it was found that there was completely no resistive response to CH_4 in none oxygen containing condition for neat WO_3 sensor, indicating no reduction behavior. In the case of Pd-loaded WO_3, the sensor response to 200 ppm CH_4 was less than 3, much smaller than that of H_2 and CO (506 and 500, respectively) in the same concentration. This small response of CH_4 suggested a slight reduction behavior for Pd-loaded WO_3 sensor under dry condition. However, with presence of humidity, there was almost no sensing response of CH_4 for Pd-loaded WO_3 sensor. Therefore, it was believed that the sensing response under dry condition could be caused due to the trace amount of oxygen rather than the surface adsorbed oxygen. In case of neat WO_3 sensor, there was completely no response to CH_4 in the absence of oxygen under both dry and wet condition.

The results of CH_4-TPR also demonstrated a relatively weak reduction behavior for Pd-loaded WO_3. Figure 5-8 shows the mass spectroscopy of CO_2 during the CH_4-TPR measurements.

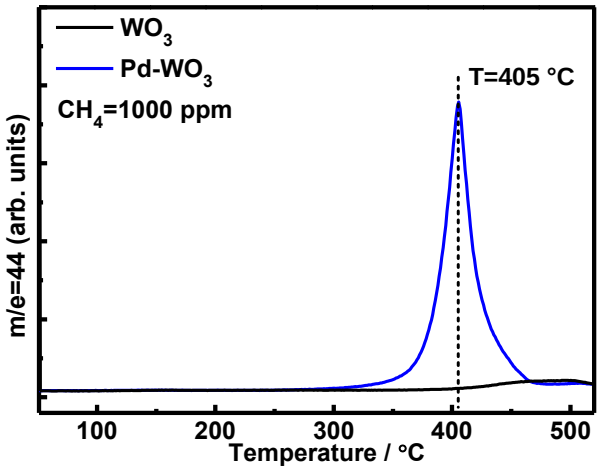

Figure 5-8 mass spectra of CH_4-TPR obtained on neat and Pd-loaded WO_3 nanoparticles powders.

The mass spectroscopy only exhibited a very slight emission of CO_2 above 400 ºC, higher than the sensing temperature at 350 ºC for neat WO_3. Thus, it can be safely concluded that adsorbed oxygens on the surface is the only origin of

sensing response of CH_4 for neat WO_3 sensors regardless of the presence or partial pressure of oxygen. This was quite different from the cases of H_2 and CO. As for Pd-loaded WO_3 sensor, there was an emission peak of CO_2 at 405 ºC, much higher than the sensing temperature. Therefore, the reduction behavior was quite difficult at working temperature of sensing (350 ºC) for Pd-loaded WO_3, even without the presence of oxygen. This was in a good agreement of observations of sensing response in the absence of oxygen, which demonstrated a quite weak response.

As shown in Fig 5-8, under non-oxygen background, surface lattice oxygen demonstrated an activity to CH_4 only at high temperature around 405 ºC. In order to evaluate the activity of surface lattice oxygen in the sensing process with presence of oxygen, the sensing response was investigated at 400 ºC. Fig 5-9 (a) shows the sensor response to CH_4 at high temperature under air atmosphere. The sensor response for neat WO_3 sensor was increased by around 2 times at 400 ºC. However, the sensor response was just slightly improved for Pd-loaded WO_3 sensor. Fig 5-9 (b) shows the resistive response to oxygen with presence of CH_4 at high temperature. It was observed that Pd-loaded WO_3 sensor showed strong oxygen dependence as that of neat WO_3 sensor in the presence of CH_4 at 400 ºC. Thus, the enhanced response could be caused by a promoted reaction with surface adsorbed oxygen with increasing temperature. Although Pd-loading promotes the activity of surface lattice oxygen to CH_4 in the absence of oxygen, the activity should be very low under a high P_{O2} such as air even at a high temperature. The sensing process of CH_4 should be dominated by the reactions with surface adsorbed oxygen with presence of oxygen even at a high

temperature.

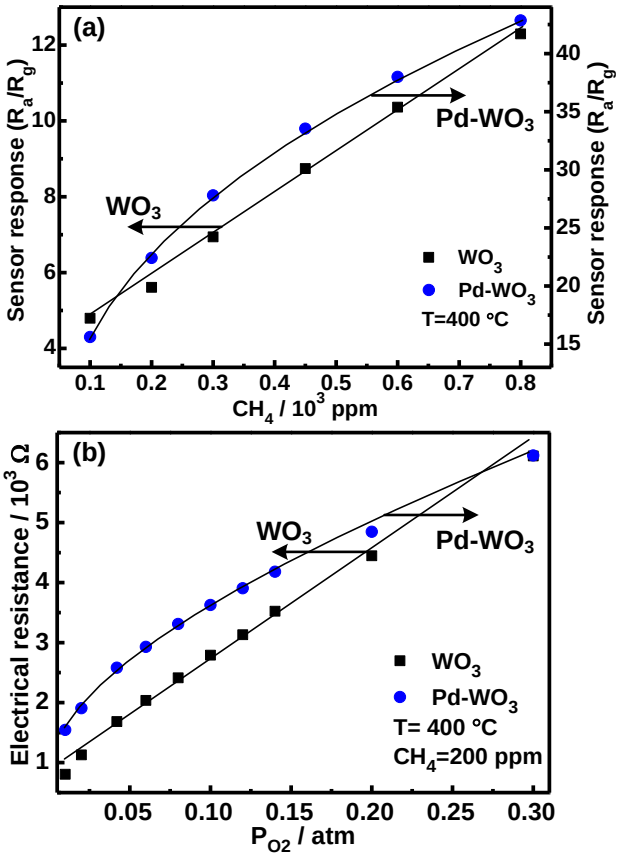

Figure 5-9 (a) sensor response as a function of CH_4 concentration at 400 ºC, (b) resistive response to P_{O2} with presence of 200 ppm CH_4 at 400 ºC.

5.4 Conclusions

The main conclusions drawn from the interaction of inflammable gases with WO_3 in are listed below.

- The resistive response and TPR measurements of H_2 in the absence of oxygen revealed that Pd-loading significantly promoted the surface reducibility of WO_3. The reduction behavior of neat WO_3 was not obvious compared with the Pd-loaded WO_3. The resistive response could not be repeatable for WO_3 in the absence of oxygen; however, it could be fully recovered with Pd-loading.
- Neat and Pd-loaded WO_3 sensors demonstrated similar results of the resistive response properties and TPR to CO with that of H_2 in non-oxygen containing

atmosphere under both dry and wet conditions.

- In the case of CH_4, there was no surface reduction behavior for neat WO_3 up to 400 ºC in the absence of oxygen. On the contrary, Pd-loaded WO_3 exhibited a reduction peak around 405 ºC, which was much higher than the sensor operation temperature at 350 ºC. Under non-oxygen background, there was no sensing response to CH_4 for neat WO_3 and the sensing response was just 2.5 for Pd-loaded WO_3 sensor, which was far smaller that of H_2 and CO. With presence of humidity, the small response of Pd-loaded WO_3 was almost disappeared.

References

[1] E. I. Altman, U. D. Schwarz, Mechanisms, Kinetics and Dynamics of Oxidation and Reactions on Oxide Surfaces Investigated by Scanning Probe Microscopy, Advanced Materials 22 (2010) 2854-2869.

[2] C. L. Mauriat, V. Oison, L. Saadi, K. Aguir, Ab initio study of oxygen point defects on tungsten trioxide surface, Surface Science 606 (2012) 40-45.

[3] P.M. Oliver, S.C. Parker, R. G. Egdell, F. H. Jones, Computer simulation of the surface structures of WO_3, J. Chem. Soc., Faraday Trans., 92 (12) (1996), 2049-2056.

[4] R.A. Dixon, J.J. Williams, D. Morris, et. al, Electronic states at oxygen deficient WO_3 (001) surface: a study by resonant photoemission, Surface science 399 (1998) 199-211.

[5] V. Oison, L. Saadi, C. L. Mauriat, R. Hayn, Mechanism of CO and O_3 sensing on WO_3 surfaces: First principle study, Sensors and Actuators B: Chemical 160 (2011) 505-510.

[6] M. Hübner, C.E. Simion, A. Haensch, N. Bârsan, U. Weimar. CO sensing mechanism with based gas sensors, Sensors and Actuators B: Chemical 151(2010) 103-106.

[7] Z. Hua, M. Yuasa, T. Kida, N. Yamazoe, K. Shimanoe, H_2 sensing mechanism of Pd-loaded WO_3 nanoparticles gas sensors, Chemistry letters, 2014 (dx.doi.org/10.1246/cl.140396).

[8] C. Bigey, L. Hilaire, G. Maire, Catalysis on Pd/WO_3 and Pd/WO_2: Effect of the Modifications of the Surface States Due to Redox Treatments on the Skeletal Rearrangement of Hydrocarbons, J. Catal. 184 (1999) 406-420.

[9] S. Triwahyono, T. Yamada, H. Hattori, Kinetic study of hydrogen adsorption on Pt/WO_3-ZrO_2 and WO_3-ZrO_2, Appl. Catal. A: Gen. 250 (2003) 65-73

[10] C. Bigey, G. Maire, Catalysis on Pd/WO_3 and Pd/WO_2, J. Catal. 184 (2000) 224-240.

[11] M. Hübner, N. Barsan, U. Weimar, Influences of Al, Pd and Pt additives on the conduction mechanism as well as the surface and bulk properties of SnO_2 based polycrystalline thick film gas sensors, Sensors and Actuators B: Chemical 171-172 (2012) 172-180.

CHAPTER 6

6 Conclusions and Future Research

The microstructure, sensing properties and mechanism for neat and Pd-loaded WO_3 nanoparticle gas sensors have been studied through four main parts. The followings are the brief summaries and some suggestions for the further research envisioned from the present study.

6.1 Conclusions

1. Microstructure

The microstructural properties of the nanoparticles and sensor devices were investigated in Chapter 2 and 3 for a basic understanding on the sensing mechanism. The prepared WO_3 nanoparticles have a 2-demisional structure with a very small thickness *c.a.* 10 nm, which is less than the width of depletion layer of WO_3 in air atmosphere (16 nm). Thus, the volume depletion theory is valid for the sensing process. The presence of Pd on the surface of WO_3 nanoparticles demonstrates the effectiveness of the modified impregnation loading process. The dispersion of Pd is very fine; nevertheless, the loading amount is quite low due to a small surface area of support. Pd-loading has no effects on the size and shape of WO_3 nanoparticles. The fabricated sensor devices have a mesoporous structure with a good distribution of porosity on the surface. Both the morphology of nanoparticles and sensor surface has showed a good stability during the heating treatments and sensing processes.

2. Sensing Properties

The static sensing properties of neat and Pd-loaded WO_3 sensors were

characterized by their resistive response to oxygen and inflammable gases (H_2, CO and CH_4) under dry and humid condition, respectively. As expected, neat WO_3 sensor demonstrated a small response to the inflammable gases in a sequence of H_2, CO and CH_4. With the presence of humidity, the sensor response was within 2 for all of three kinds of inflammable gases with concentrations up to 1000 ppm. Pd-loading significantly promoted the sensing response of inflammable gases in a sequence of H_2, CO and CH_4. For H_2 and CO, the sensor response of Pd-loaded WO_3 was more than 2 orders higher than that of neat WO_3. However, the promotion effect was quite moderate for CH_4; the sensor response was just increased by several times with Pd-loading. The sensor response of Pd-loaded WO_3 was also greatly decreased by water vapor. With 0.5 VOL.% humidity, the sensor response was reduced by more than one order. Under humid condition, the sensor response was above one order larger than that of neat WO_3 for H_2 and CO. However, the sensor response of CH_4 was very small just less than 2 up to 1000 ppm for neat and Pd-loaded WO_3 sensors under wet condition.

3. Sensing Mechanism

The interpretations of sensing mechanism for WO_3 gas sensor to inflammable gases were based on the results of oxygen adsorption and interaction with WO_3 in Chapter 4 and the interaction of inflammable gases with surface lattice oxygen for WO_3 in Chapter 5. The adsorption amount of oxygen was relatively low, around 10^{-5} mol g^{-1} for both neat and Pd-loaded WO_3. The adsorption form was in O_2^- characterized by the resistive response and TPD measurements. Pd-loading greatly enhanced the electronic interaction of oxygen with WO_3 sensors. This enhanced electronic interaction was caused by the P-N

junction effect and a promoted oxidization ability of WO_3 with Pd-loading. The oxygen resistive response with the presence of H_2 and CO was quite different between neat and Pd-loaded WO_3 sensors. The sensor response was really low for neat WO_3 and the sensing process was highly oxygen-dependent. In contrast, the sensor response for Pd-loaded WO_3 sensor was very high and the sensing process weakly depended on P_{O2} for Pd-loaded WO_3 sensors. This clearly suggested that Pd-loading not only promoted the sensing response but also changed the basic sensing mechanism. The interaction of H_2 and CO with neat WO_3 in the absence of oxygen was also significantly different with Pd-loaded WO_3 sensor. According to these results, it was proposed that the surface lattice oxygen has a high activity and redox involved the sensing process of H_2 and CO for Pd-loaded WO_3 sensors. At low oxygen or non-oxygen atmosphere, reaction of lattice oxygen dominates the sensing processes for Pd-loaded WO_3 sensor. The sensing process of H_2 and CO with different P_{O2} is schematically shown in Fig. 6-1. The sensing mechanism is same for H_2 and CO; however, for simplicity, only the process of H_2 sensing is demonstrated. The surface lattice oxygen involves the sensing process to H_2 and CO for Pd-loaded WO_3 sensor even with a high P_{O2}. This is responsible for the highly sensitive response and weak oxygen dependence for Pd-loaded WO_3 sensor.

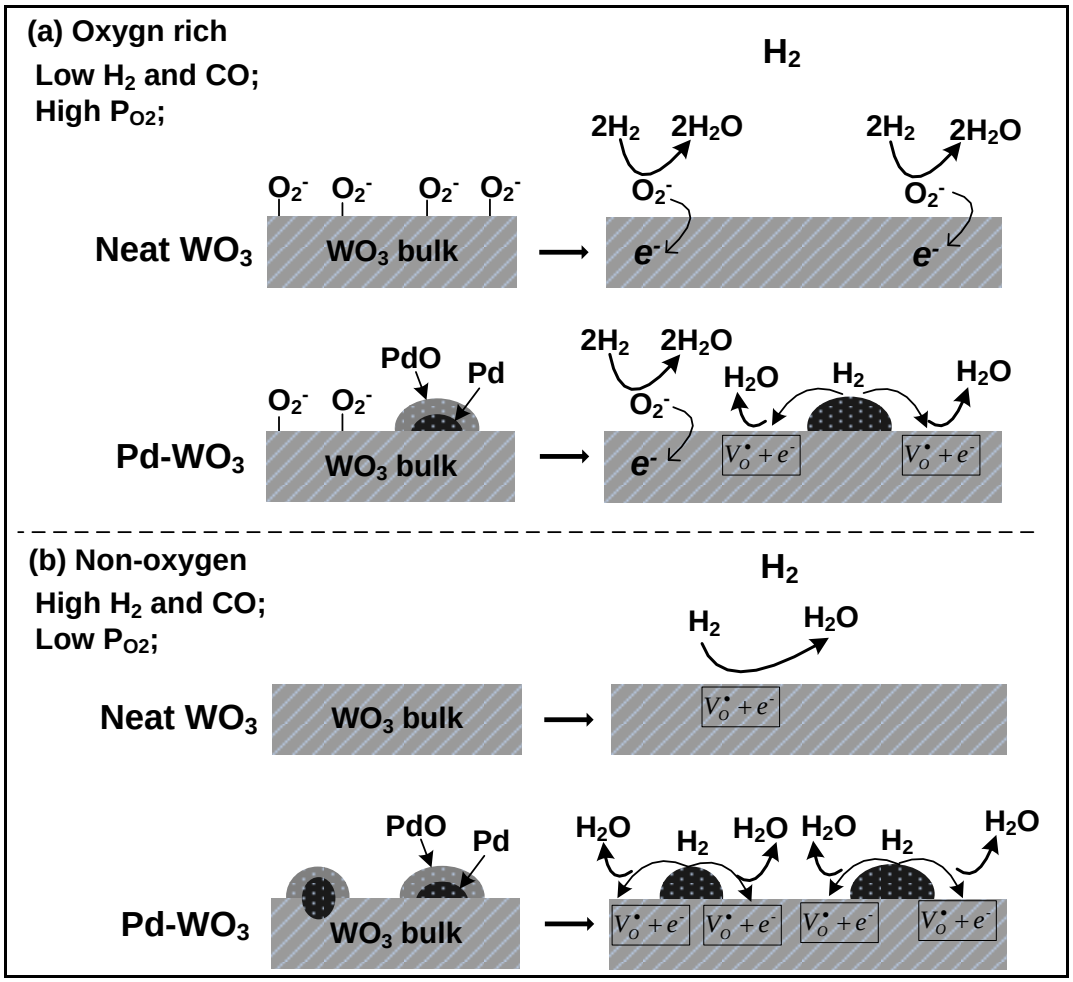

Figure 6-1 a schematically drawing of sensing mechanism for neat and Pd-loaded WO_3 sensor to H_2 with different oxygen concentration.

In the case of CH_4, the sensing mechanism is different from that of H_2 and CO. The sensor response is poor for both neat and Pd-loaded WO_3 sensors; however, the sensing process is obviously oxygen-dependent for both sensors. In the absence of oxygen, the resistive response and TPR measurements indicate that surface lattice oxygen has no activity to CH_4 for neat WO_3 and a very poor activity for Pd-loaded WO_3 sensor at high temperature. Therefore, the basic sensing mechanism of CH_4 sensing is based on the conventional process that the oxidization of CH_4 molecules with the surface adsorbed oxygen for both neat and Pd-loaded WO_3 sensors. This is contributed to the poor response and oxygen-dependent sensing process of CH_4. Under extremely poor oxygen or non-oxygen atmosphere, CH_4 can react weakly with surface lattice oxygen through Pd particles on surface as shown in Fig. 6-2. However, there is no reaction of surface lattice oxygen with CH_4 molecules for neat WO_3 sensor even under non-oxygen background at high temperature.

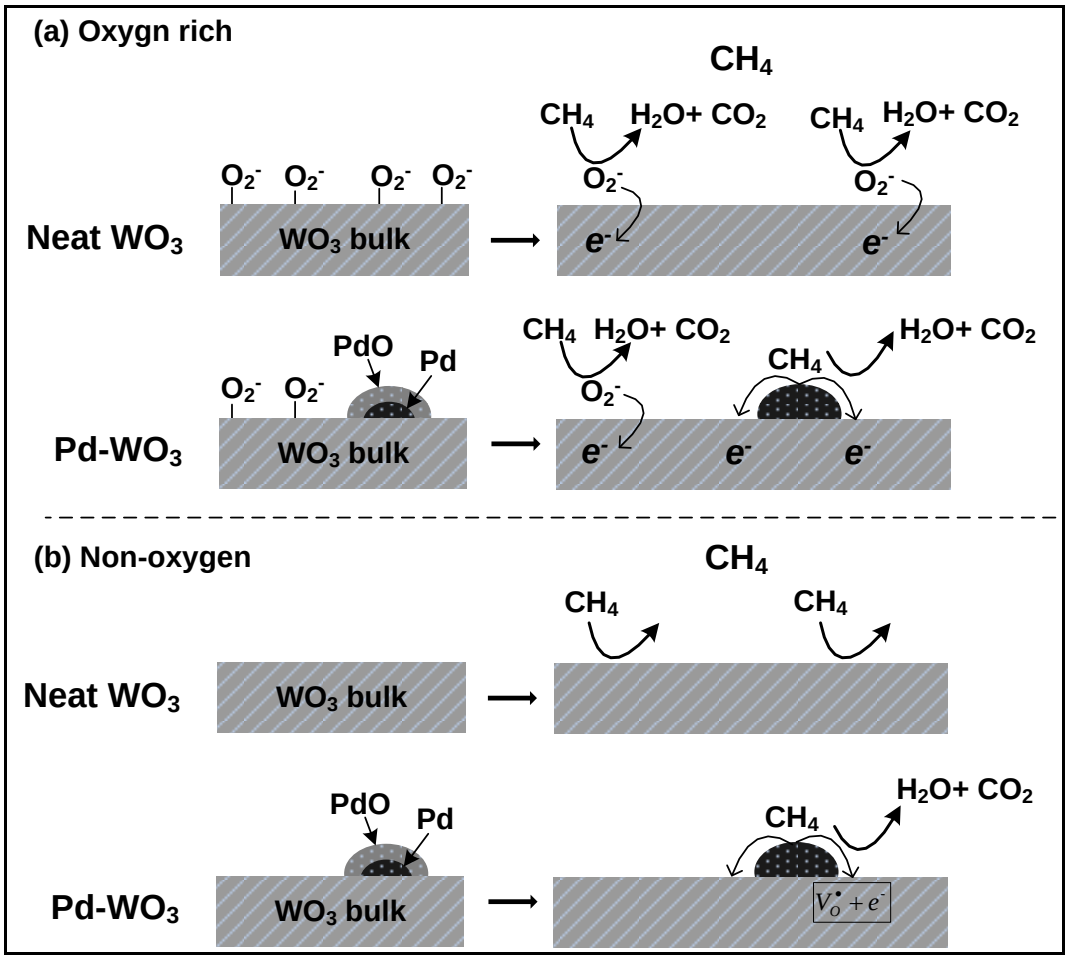

Figure 6-2 a schematically drawing of sensing mechanism of CH_4 for neat and Pd-loaded WO_3 sensor with different oxygen concentration.

6.2 Future Research

The present study has demonstrated that the sensing process of WO_3 to inflammable gases was different from the traditional theory. Pd has an electronic and chemical effect on the sensing process of WO_3. The surface lattice oxygen was activated by Pd dispersed on the surface and reacted with inflammable gases. This study is beneficial for a better understanding on the basic mechanism of MOS gas sensors and the role of additives. To further clarify the surface process of gas sensing and promote the sensing performance of MOS gas sensors, the following aspects are proposed based on the present thesis for a future research.

1. The investigation on the sensing mechanism and the role of Pd are mainly based on the resistive response of oxygen and inflammable gases under different designed atmospheres. The present method allows us an effective approach to study the sensing process and can be applied for different additives such as Au and Pt, and different support (SnO_2 and In_2O_3). A systemic study on the mechanism of noble metal additives (Au, Pd and Pt) can be conducted through the proposed simple method. This is good for the clarification of the role of additives in gas sensing, which is one of the most important subjects in MOS gas sensors.
2. The reaction of lattice oxygen with H_2 and CO molecules was derived from the resistive response of oxygen and sensing response in the absence of oxygen. Therefore, the reaction of lattice oxygen under oxygen containing atmosphere is indirectly derived from the resistive response and directly observed in the absence of oxygen. However, with presence of oxygen, namely in air background, the reaction of H_2 and CO with surface lattice

oxygen should be different from that of non-oxygen containing atmosphere and difficult to occur. Therefore, other analysis techniques such as oxygen isotopic labeling, which can allows us a direct observation of reaction of lattice oxygen with presence of oxygen, are highly required.

LIST OF PUBLICATIONS & PRESENTATIONS

Research works related to the present thesis has been presented at several conferences and publications. Some of them are listed below.

PUBLICATIONS

1. Z.Q. Hua, M. Yuasa, T. Kida, N.Yamazoe, K.Shimanoe; High sensitive gas sensor based on Pd-loaded WO_3 nanolamellae, Thin solid film, 2013 (548) 677-682.
2. Z.Q. Hua, M. Yuasa, T. Kida, N.Yamazoe, K.Shimanoe; H_2 sensing mechanism of Pd-loaded WO_3 nanoparticles gas sensors, Chemistry letters, 2014 (dx.doi.org/10.1246/cl.140396).
3. Z.Q Hua, M. Yuasa, T. Kida, N. Yamazoe, K. Shimanoe, Sensing mechanism of reducing gases with neat and Pd-loaded WO_3 gas sensors, Sensors and Actuators B: Chemical, (To be published).

PRESENTATIONS

1. Z.Q Hua, M. Yuasa, T. Kida, N. Yamazoe, K. Shimanoe, Preparation of Pd-loaded Lamellar WO_3 particles for VOC Gas sensing, Japan Electrochemical Society (Kida Kyushu, Japan), 2012.
2. Z.Q Hua, M. Yuasa, T. Kida, N. Yamazoe, K. Shimanoe, High sensitive gas sensor based on Pd-loaded WO_3 nanolamellae, VIII International Workshop on Semiconductor Gas Sensors (Cracow, Poland), 2012, p37.
3. Z.Q Hua, M. Yuasa, T. Kida, N. Yamazoe, K. Shimanoe, Pd loaded lamellar WO_3 nanoparticles and their enhanced gas sensing performances to toluene and ethanol, 25^{th} Fall Meeting of The Ceramic Society of Japan (Nagoya, Japan), 2012, p32.
4. Z.Q Hua, M. Yuasa, T. Kida, N. Yamazoe, K. Shimanoe, Gas sensing properties of WO_3 in the volume depletion state, 5^{th} GOSPEL workshop (Oita, Japan), 2013, 32.
5. Z.Q Hua, M. Yuasa, T. Kida, N. Yamazoe, K. Shimanoe, Material design of semiconductor gas sensors. [4] Gas adsorption behavior on Pd-loaded WO_3 nanoparticles gas sensor, 26^{th} Fall Meeting of The Ceramic Society of Japan (Nagano, Japan), 2013, p22.
6. Z.Q Hua, M. Yuasa, T. Kida, N. Yamazoe, K. Shimanoe, Gas adsorption behavior on Pd-loaded WO_3 nanoparticles gas sensor, The 6^{th} KU-KU Joint Workshop on Functional Materials (Yamaguchi, Japan), 2013, p8.
7. Z.Q Hua, M. Yuasa, T. Kida, N. Yamazoe, K. Shimanoe, Oxygen adsorption

behavior on Pd-loaded lamellar WO_3 nanoparticles, The 10th Asian Conference on Chemical Sensors, (Chiangmai, Thailand) 2013, p150.

8. Z.Q Hua, M. Yuasa, T. Kida, N. Yamazoe, K. Shimanoe, Reducing gas sensing mechanism of Pd-loaded WO_3 gas sensors, 27th Fall Meeting of The Ceramic Society of Japan (Kagoshima, Japan), 2014.
9. Z.Q Hua, M. Yuasa, T. Kida, N. Yamazoe, K. Shimanoe, Sensing behavior and mechanism of Pd-loaded WO_3 sensors to reducing gases, The 57th Chemical sensors (Hokkaido, Japan), 2014.

ACKNOWLEGMENT

I am indebted to many for their help and generosity during my doctoral study at Kyushu University at Japan.

Words are not enough to express my deep gratitude to my advisor, Prof. Kengo Shimanoe. Without his guidance, patience and encouragement, this dissertation would not have been finished. I would like to express my sincere appreciation to the vice-supervisors, Prof. Masaharu Tsuji and Prof. Maiko Nishibori, for their kind work on the dissertation and defense. I would like to extend my sincere gratitude to Prof. Noboru Yamazoe and Prof. Tetsuya Kida for many beneficial discussions and advices on the development of this dissertation. I am very grateful to Dr. Yuasa and Dr. Suematsu for their kind support and friendship.

I would like to thank former and present members of our research group: Mr. Tachibana, Mr. Choi, Miss. Shin, Miss Ma, Mr. Hori, Mr. Yamasaki, Mr. Kodama, Mr. Shimada, Mr. Kato, Mr. Ishado and all friends in Shimanoe research group for their support during my stay in Japan. I would like to thank Dr. Gao Hongye and Mr. Uchiyama in Kyushu University for their patient guidance and help on many of experiments. I am also thankful for China Scholarship Council (CSC) for the financial support, which enable me to complete the doctoral study.

Finally, I am particularly indebted to my loving family for their financial support and constant encouragement, but primarily for their love. I would like to thank my wife, Song Min for her love and continuous support throughout my study.